CHEMICAL AND BIOMOLECULAR FUNCTIONALIZATION OF SILICON SURFACES FOR BIOSENSING APPLICATIONS

by

NORMAN A. LAPIN

A dissertation submitted to the

Graduate School-New Brunswick

Rutgers, The State University of New Jersey

and

The Graduate School of Biomedical Sciences

University of Medicine and Dentistry of New Jersey

In partial fulfillment of the requirements

For the degree of

Doctor of Philosophy

Graduate Program in Biomedical Engineering

Written under the direction of

Professor Yves J. Chabal

And approved by

Y Chabal

Martin

Richard

New Brunswick, New Jersey

May 2009

ABSTRACT OF THE DISSERTATION

Chemical and Biomolecular Functionalization of Silicon Surfaces for Biosensing Applications

By NORMAN A. LAPIN

Dissertation Director:
Professor Yves J. Chabal

The reliable functioning of biosensors and bioassays is dependent on the robust attachment of active biomolecules to device substrates, such that the structural integrity, organization and appropriate orientation of these molecules at the surface is maintained. To a significant extent, the underlying surface chemistry and molecular organization that these biomolecules come in contact with and attach to affect the properties of the functional overlayer that they compose. In this work, primarily through the use of infrared spectroscopy, we characterize two main types of biosensor platforms including biotin-streptavidin linkage and surface attachment and covalent attachment of protein to sensor surfaces via amines and sulfhydryls. We further observe the effects of several variations in processing conditions on these platforms including initial atmospheric humidity, use of anhydrous versus aqueous solvents in molecular adsorption and the effect of primary molecular layer stability on the organization and characteristics of subsequently adsorbed biolayers.

With infrared spectroscopy, not only do we identify the formation and breaking of chemical bonds in each of the attachment steps, we also monitor changes in the moieties of each layer with changing environmental conditions. We find that changes in ureido moiety vibrational modes of the biotinylated surface occur near 1250 and 1700 cm^{-1} dependent on the stability of an underlying layer of aminopropyltriethoxysiloxane, on the type of solvent used in biotinylation itself, and on subsequent protein adsorption to and/or rinsing of the biotinylated surface. In covalent attachment studies, we use small molecules in lieu of protein to characterize amine and sulfhydryl chemical bonding to maleimide-terminated surfaces and using infrared polarization techniques, we find that molecular orientation may be restricted upon covalent attachment. Ellipsometry is used in conjuction with infrared absorption area measurements to determine the relative composition of silane and maleimide prior to attachment of protein.

Additionally, fluorescence measurements of labeled protein are used to quantify protein desorption by surface acoustic wave streaming (SAWS). These measurements are correlated with power dose of SAWS operation. In all, these surface characterization methods are found to successfully monitor chemical and biomolecular layer formation and change under a variety of conditions.

Dedication

This thesis is dedicated to my family,

whose love and support made this work possible.

Acknowledgements

I would like to thank my research advisor, Professor Yves Chabal for the opportunity to work in his laboratory and learn from him over the years and for going beyond what would normally be expected to help and support me in my research and in my life. Many thanks to Sandrine Rivillon-Amy for her insight and coaching, providing valuable input into the content of my work. I'd also like to thank Robert Pasternack and Eric Yang for helpful discussion and important input into my work as well. Thank you to my labmates Melissa Stokes, Meng Li and Ming Tsung Ho for insightful discussions and friendship.

I'd like to thank Professor Martin Yarmush for his co-advisement over the years, providing helpful suggestions and insight that brought my work to a higher level. I'd like to thank Dr. Sobin Kim and Professor Richard Ludescher for helpful advice and input with my research. I'd like to thank the members of the Physics machine shop (in particular, Ernie Erskine, Billy Schneider, Arvid Knudsen, Eric Paduch and Val Myrnyj) for their assistance in the design of several pieces used in my research as well as guidance in using the student machine shop and friendly conversation. I would also like to acknowledge my funding sources: the Ruth L. Kirschstein National Research Service Award No. 5-T32-GM008339-18 and the Rutgers University GAANN Fellowship.

Finally, I would like to thank my parents for their continuous love and support (I am especially touched by my father, who tirelessly read significant parts of my work) and my Aunt Fay, my sister, my grandparents and others family members for their confidence in my abilities and continuous encouragement.

Please note that Chapter 2 and Chapter 6 are published elsewhere as indicated at the beginning of those chapters.

Table of Contents

Abstract of the Dissertation……………………………………………………………………ii
Dedication……………………………………………………..……………………………..iv
Acknowledgements…………………………………………..……………………………..…v
Table of Contents vii
List of Tables xi
List of Figures xi
List of Schemes xiii

CHAPTER 1: INTRODUCTION 1

1.1 Motivation 1
1.2 Thesis overview 2
1.3 Background 3
  1.3.1 General Background on Biosensors 3
  1.3.2 A Biosensor Frontier – The Protein Microarray 6
  1.3.3 Methods of Biomolecule Attachment to Surfaces 8
  1.3.4 Characterizing biomolecule attachment to surfaces 11
  1.3.4.1 Limitations 12
  1.3.5 Infrared Studies of Biosensor Surfaces 13
1.4 Techniques for characterizing surfaces 15
  1.4.1 Fourier Transform Infrared Spectroscopy (FTIR) 15
  1.4.2 Fluorescence Measurements (for Chapter 5) 31
  1.4.3 Ellipsometry Measurements (Chapters 4 and 5) 39
1.5 References 42

CHAPTER 2: INFRARED CHARACTERIZATION OF BIOTINYLATED SILICON OXIDE SURFACES, SURFACE STABILITY AND SPECIFIC ATTACHMENT OF STREPTAVIDIN 46

2.1 Abstract 46
2.2 Introduction 47
2.3 Experimental Methods 51
2.4 Results 54
  2.4.1 Step 1: Aminosilanization: Characterization of amine-derivatized silicon oxide surfaces; observation and control of silane growth and stability.. 54
  2.4.2 Step 2: Biotinylation: Surface Characterization and the Effects of Sonication 58
  2.4.3 Step 3: SA Adsorption: Effect of SA attachment and rinse steps on the biotinylated surface 60
2.5 Discussion 66
  2.5.1 Step 1: Aminosilanization: Dependence of APS film growth and degradation on pre-silanization atmospheric moisture content. 66
  2.5.2 Step 2: Biotinylation: Distinguishing chemisorbed from physisorbed biotin-NHS and the effects of sonication. 69

2.5.3 Step 3: SA Adsorption: Change in the biotinylated surface upon SA adsorption. 71
2.6 Conclusions 72
2.7 Acknowledgements 73
2.8 References 74
2.9 Appendix 76
2.9.1 Supplement to Experimental Methods 76
2.9.2 Supplement to Results 77
2.9.3 Supplement to Discussion 81
2.9.4 References 89

CHAPTER 3: FURTHER INVESTIGATION OF IR FEATURES OF THE BIOTINYLATED SURFACE AND BIOTIN-SA SPECIFIC ATTACHMENT 91

3.1 Abstract 91
3.2 Introduction 92
3.3 Experimental Methods 94
3.3.1 Reagents (differing from those in Chapter 2). 94
3.3.2 Sample Preparation. 94
3.3.3 Data Analysis. 95
3.4 Results 96
3.4.1 Relationship between biotin ureido IR bands 96
3.4.2 Streptavidin adsorption to biotinylated surface: Investigation of “dip” feature 99
3.5 Discussion 104
3.5.1 Relationship between biotin ureido IR bands 104
3.5.2 Streptavidin adsorption to biotinylated surface: Investigation of dip feature 105
3.5.3 Fitting the dip to the biotin ureido shift 108
3.6 Conclusions 111
3.7 References 113

CHAPTER 4: DIRECT ATTACHMENT OF PROTEIN TO SILICON SURFACES . 114

4.1 Abstract 114
4.2 Introduction 115
4.2.1 Surface Characterization 116
4.3 Experimental Methods 118
4.4 Results 122
4.4.1 PMPI attachment to the amine-terminated surface 123
4.4.2 Test molecule (MPS) chemical attachment to the maleimide-terminated surface 128
4.4.3 Polarization dependence of MPS chemical attachment 130
4.4.4 Test molecule (APTES) chemical attachment to the maleimide-terminated surface 132
4.5 Discussion 136
4.5.1 PMPI attachment to the amine-terminated surface 136
4.5.2 Ellipsometry of maleimide-terminated films 137

4.5.3 Test molecule (MPS) chemical attachment to the maleimide-terminated surface ... 137
4.5.4 Polarization dependence of MPS chemical attachment ... 139
4.5.5 Test molecule (APTES) chemical attachment to the maleimide-terminated surface ... 140
4.5.6 Protein fragment adsorption to the maleimide-terminated surface ... 141
4.5.7 Identification of shift in the maleimide carbonyl band: comparison with biotin ureido carbonyl shift ... 143
4.6 Conclusions ... 144
4.7 References ... 146

CHAPTER 5: SURFACE ACOUSTIC WAVE STREAMING REMOVAL OF NON-SPECIFICALLY BOUND PROTEIN ON PROTEIN MICROARRAY SURFACES .. 148

5.1 Abstract ... 148
5.2 Introduction ... 149
5.3 Experimental Methods ... 153
5.3.1 Surface preparation ... 153
5.3.2 Fluorescent Labeling of Proteins ... 154
5.3.3 Protein patterning of the surface for formation of antigen arrays ... 155
5.3.4 Protein adsorption to antigen array surfaces ... 157
5.3.5 Verification of Film Thickness ... 158
5.3.6 Microfluidic Setup ... 158
5.3.7 SAWS Device Design and Integration with Microfluidic Channel ... 160
5.3.8 Imaging ... 161
5.3.9 Image Data Processing ... 162
5.4 Results ... 164
5.4.1 Definitions for device characterization and evaluation of device efficacy 164
5.4.2 Removal of non-specifically bound antibody from antigen-patterned surfaces ... 165
5.4.3 Control Experiment: Removal of general protein fouling from the microarray surface ... 169
5.4.4 Control Experiment: Acoustic cleaning on covalently bound protein . 170
5.5 Discussion ... 171
5.5.1 Removal of non-specifically bound antibody from antigen-patterned surfaces ... 171
5.5.2 Control Experiment: Removal of general protein fouling from the microarray surface ... 173
5.5.3 Ceiling on protein removal for this setup ... 174
5.6 Conclusions ... 175
5.7 References ... 176

CHAPTER 6: INFRARED SPECTROSCOPIC CHARACTERIZATION OF GENIPIN-INDUCED CHANGES IN COLLAGEN GELS 177

6.1 Abstract 177
6.2 Introduction 177
6.3 Materials and Methods 179
6.4 Results 181
6.5 Discussion 184
6.6 Conclusions 185
6.7 References 187

CHAPTER 7: CONCLUSIONS 189

Curriculum Vita 192

List of Tables

Table 2.1. IR band assignments for molecules present at each surface modification step. 65
Table 4.1. Values for APS and PMPI absorbance areas, total film thickness and estimated number of monolayers. 125

List of Figures

Figure 1.1 Explanation of specific binding. 6
Figure 1.2. Explanation of non-specific binding. 6
Figure 1.3. Protein microarray spotter deposits micro-spots of protein (antibody) on microarray surface. 7
Figure 1.4. The electromagnetic spectrum. 16
Figure 1.5. Potential well and energy levels for a harmonic oscillator 19
Figure 1.6. Vibrational modes of the CH_2 moiety. 21
Figure 1.7. Schematic of a Michelson interferometer. 24
Figure 1.8. Examples of spectra and their corresponding interferograms. 26
Figure 1.9. Single beam spectrum. 28
Figure 1.10. Absorbance spectrum. 29
Figure 1.11. Transmission geometry 31
Figure 1.12. ATR geometry. 31
Figure 1.13. Electronic transitions diagram demonstrating fluorescence. 34
Figure 1.14. Absorption and fluorescence spectra of anthracene in ethanol. 35
Figure 1.15. Inverted epi-fluorescence (Olympus® IX-70) microscope. 37
Figure 1.16. Ellipsometer. 39
Figure 1.17. Orientation of linearly and elliptically polarized light relative to the surface. 40
Figure 2.1. Representative FTIR spectra of APTES chemically attached and referenced to silicon dioxide surfaces in winter and summer. The Si-O-Si band area increase from winter to summer indicates that more APS is adsorbed at the surface in summer due to greater humidity. 55
Figure 2.2 Amount of APS adsorbed to silicon oxide surface 56
Figure 2.3. APS Si-O-Si band area percentage loss 57
Figure 2.4. Representative FTIR spectra of biotin-NHS chemisorption and sonication. 58
Figure 2.5. Representative FTIR spectra of biotinylated surfaces exposed to SA or rinse. 61
Figure 2.6. FTIR spectra of an APS surface exposed to biotin-NHS and rinse step. 62
Figure 2.7. Loss of biotin band absorbance area with loss of APS absorbance area. 64
Figure 2.9.1. FTIR spectra of biotin-NHS and NHS-terminated surface. 78
Figure 2.9.2. IR absorption band area correlation 79
Figure 2.9.3. Loss of biotin band absorbance area vs initial band area. 80
Figure 2.9.4. Biotin band absorbance area vs percent APS band area loss. 80

Figure 3.1. Change in biotin ~1250 cm^{-1} band area vs biotin ureido carbonyl frequency. 97
Figure 3.2. Selected spectra of biotinylated surfaces corresponding to data of Figure 3.1 98
Figure 3.3. Spectra of biotinylated surfaces before and after rinse step. 99
Figure 3.4. Spectra of protein adsorbed and referenced to biotinylated surfaces. 100
Figure 3.5. Comparison of spectra with and without "dip" at 1716 cm^{-1}. 101
Figure 3.6. Spectra of SA adsorbed and referenced to biotinylated surfaces. 102
Figure 3.7. Depth of dip at 1716 cm^{-1} vs SA incubation time. 103
Figure 3.8. Spectra of protein adsorbed to biotinylated and APS surfaces. 103
Figure 3.9. Deconvolution of biotinylated surface referenced to APS surface 109
Figure 3.10. Manual generation of "dip" feature at ~1716 cm^{-1}. 110
Figure 3.11. Demonstration of spectral fit to "dip" feature. 111
Figure 4.1. FTIR spectra of maleimide attachment to the APS surface 124
Figure 4.2. Total film thickness in nm vs APS ($R^2 = 0.85$) and PMPI ($R^2 = 0.92$) adsorption times. 126
Figure 4.3. IR absorbance areas of APS and PMPI bands vs total film thickness. 126
Figure 4.4. Fold increase over minimum (IR absorbance areas vs total film thickness). 127
Figure 4.5. Spectra of sulfhydryl-linkage test molecule (MPS) to maleimide surface. 129
Figure 4.6. Polarization study of chemisorption of MPS to a maleimide surface. 131
Figure 4.7. Comparison of amine (APTES) and sulfhydryl (MPS) chemical attachment to the maleimide surface. 133
Figure 4.8. Comparison of protein fragment and amine-terminated small molecule (APTES) attachment to maleimide-terminated surfaces 135
Figure 5.1. Fluorescence intensity of Alexa Fluor 488-labeled antibody (normalized to maximum initial intensity of all regions per trial) vs acoustic cleaning power dose 167
Figure 5.2. Representative fluorescence intensity image of labeled-antibody adsorption. 167
Figure 5.3. Representative thresholded image of fluorescent intensity of antibody adsorbed to antigen array prior to acoustic desorption, corresponding to Figure 5.1**a**. 168
Figure 5.4. Representative thresholded image of fluorescent intensity of antibody adsorbed to antigen array at final acoustic desorption power dose, corresponding to Figure 5.1**b**. 168
Figure 5.5. Representative thresholded image of fluorescent intensity of antibody adsorbed to antigen array corresponding to Figure 5.1**c**. 168
Figure 5.6. Fluorescence intensity of nonspecifically bound protein 170
Figure 5.7. Fluorescence intensity of covalently attached antigen (Alexa Fluor 594-labeled mouse IgG) vs SAWS device power dose (mW*s). Fluorescence intensity does not decrease with acoustic power dose delivered to surface. Due to minimization of photobleaching, photobleaching correction was not applied. 171
Figure 6.1. ATR setup showing genipin deposition for time-resolved study. 180
Figure 6.2. IR absorbance spectra of genipin and genipin-crosslinked collagen. 182
Figure 6.3. Changes in absorbance band areas versus crosslinking time 183
Figure 6.4. Description of the modes marked in the spectra of Figure 6.2. 186

List of Schemes

Scheme 2.1. Steps to attach biomolecules to silicon oxide surfaces. 48
Scheme 4.1. Antibody attachment to the silicon oxide surface.................................... 123
Scheme 4.2. Polarization dependence. 132
Scheme 5.1. Bi-directional acoustic horn IDT SAWS device...................................... 153
Scheme 5.2. Reaction of GPTMS with the lithium niobate surface............................. 154
Scheme 5.3. Reaction of primary amines of lysine and arginine residues of protein (antigen) with surface-bound GPTMS. 157
Scheme 5.4. Integrated Microfluidic-SAWS device setup... 160

CHAPTER 1: INTRODUCTION

1.1 Motivation

The continuing development of biosensors and bioassays is critical to a wide variety of research areas and applications. Bioassays are used as diagnostics in early stage disease detection. Protein microarrays are critical to drug discovery and biomedical research in the understanding of drug-protein and protein-protein interactions. Biosensors are important to homeland security and environmental monitoring in the early detection of bioweapons such as anthrax and environmental pathogens.

Robust attachment of biomolecules to surfaces is critical to the reliable function of such bioassays and biosensors. If biomolecules are denatured, non-uniformly distributed or disordered at the surface, device quality at such small scales may be compromised [1-4]. Undesirable events include non-specific binding of target molecules leading to false positive readings, denaturation of capture molecules causing false negative readings and cross-binding events that produce both false positive and negative results. As bioassays and biosensors are progressively scaled down to meet increasingly high throughput, small quantity and rapid scan requirements, the accuracy and sensitivity of these devices become increasingly important. The underlying surface chemistry and intermediate biolayers can significantly affect the organization and function of these biomolecules [3, 5]. Hence, control of these attachment steps to device substrates is important for device performance.

By identifying chemical and biochemical features associated with the attachment and behavior of molecules at the biosensor surface, a first step is taken towards understanding and controlling biosensor properties. The scope of this study is the investigation of the chemical and biochemical layers between proteins and the surface as well as the attachment of proteins to these layers. The main tool used in this investigation, Fourier Transform Infrared Spectroscopy (FTIR), provides a means of investigating initial stages of chemical and biomolecule attachment to sensor substrates, not possible with other methods, such as fluorescence and Surface Plasmon Resonance. Unlike other techniques, FTIR is specific in elucidating the chemical nature of binding of various molecules to the biosensor surface.

1.2 Thesis overview

The goal of this thesis is to determine various features that indicate surface characteristics and surface attachment to assess the surface quality of biosensor platforms. The first chapter introduces various types of biosensors and bioassays, and discusses common methods of biomolecule attachment to inorganic surfaces and methods used to probe these surfaces. In the chapters that follow, surface features are identified primarily through infrared (IR) spectroscopy. Biosensor platforms investigated in this thesis are the biotin/streptavidin system for linking biomolecules to surfaces, Chapters 2 and 3, and direct attachment of proteins to surfaces through maleimide crosslinking, Chapter 4. Specifically, Chapter 2 deals with stability and characteristics of biotinylated surfaces fabricated under humidity conditions varying prior to chemical modification. Chapter 3 further explores the characteristics of biotinylated surfaces and investigates features of the biotin-streptavidin interaction. Chapter 4 explores the idea of “test molecules”, where small molecules with reactive moieties similar to those on proteins are attached to the surface in place of their larger counterparts (proteins) in order to observe chemical binding events in the absence of interference from the protein molecules. Ellipsometry and IR polarization techniques are employed to characterize these surfaces as well. In contrast to the attachment techniques of Chapters 2-4, Chapter 5 explores a method of removing non-specifically bound protein from protein microarray surfaces using Surface Acoustic Wave Streaming. Chapter 6 tracks collagen crosslinking, examining biomolecule to biomolecule interaction rather than biomolecule to silicon surface interaction. Finally, conclusions about the utility of IR-based and other features are drawn in Chapter 7.

1.3 Background

1.3.1 General Background on Biosensors

Perhaps due to the relative newness of the field and the breadth of biosensor application, there is some variability in the definition of the biosensor. A relatively early definition describes a biosensor as a device that converts a biochemical event into a measurable signal using a transducer to produce a voltage or current [6]. A broader definition by the International Union of Pure and Applied Chemistry (IUPAC) states that a biosensor is a device that detects chemical compounds using biochemical reactions mediated by any of a number of different types of biomolecules including antibodies, organelles, whole cells and tissues. The biosensor signal can then be transduced by electrical, thermal or optical signals [7]. A narrower definition relating more closely to the investigations performed here would be a device used to detect chemical or biological molecules (target agents, such as proteins or DNA) in the air or in solution by using complementary biomolecules (capture agents, such as antibodies or complementary DNA strands) immobilized on a solid support.

Applications of biosensors are quite broad. One of the most common biosensors is the glucose sensor, often used to monitor the blood sugar levels of patients with diabetes. It uses the enzyme glucose oxidase to produce hydrogen peroxide from glucose, which is then oxidized at an electrode and the current measured, which is proportional to the concentration of glucose present. Biosensors are also used in diagnostics, drug discovery, biomedical research and even homeland security. As a diagnostic tool, a blood or saliva sample may be placed on a biosensor that detects early stage markers of a disease. In drug discovery, different proteins may be arrayed on a surface (as in a protein microarray) which is then exposed to drugs that may potentially react with one or a number of these proteins. Biomedical researchers may use protein microarrays in a similar way to understand protein-protein or protein-ligand interactions [4, 8]. Biosensor use in homeland security involve the early detection of bioweapons such as anthrax spores and other toxins present in the environment at ng/ml or ng/cm^2 levels [9, 10].

1.3.1.1 Capture and Target Agents

The biorecognition element of the biosensor, the capture agent, binds to a molecule called the target agent. This pair of biomolecules have complementary binding sites where recognition takes place. The capture agent is affixed to a solid support and the target agent in the air or solution comes in contact with the support and can thus bind to the capture agent. A variety of examples of biorecognition pairs exist in nature.

Complementarity determining regions (CDRs) on antibodies bind to specific sites on proteins called epitopes, with complementary shapes and patterns of charges. DNA strands in solution can bind to complementary coded strands bound to a surface. Enzymatic reactions may also take place at the sensor surface between enzymes bound to the surface and “substrates”, molecules with parts that fit into the enzyme’s active sites and are subsequently modified chemically. Receptor-ligand complexes may also make up a capture-target pair with one or the other biomolecule bound to the solid support.

1.3.1.2 Specific and Non-specific Binding

Specific binding is the interaction between biomolecules that have a morphological, electrostatic and/or hydrogen-bonded fit at specific sites on each respective molecule (Figure 1.1). Non-specific binding occurs when protein or other biomolecules adhere to incorrect binding sites (cross-binding) or to locations at the surface where no binding partner is present (Figure 1.2). Non-specifically bound proteins can attach to one another or to the interface with weak interactions at non-site specific locations. Non-specific binding of protein to assay surfaces can manifest as cross reactivity, increasing the rate of false positive readings [11]. Biofouling is a more generalized accumulation of proteins and biological materials on surfaces and can block binding sites causing false negatives.

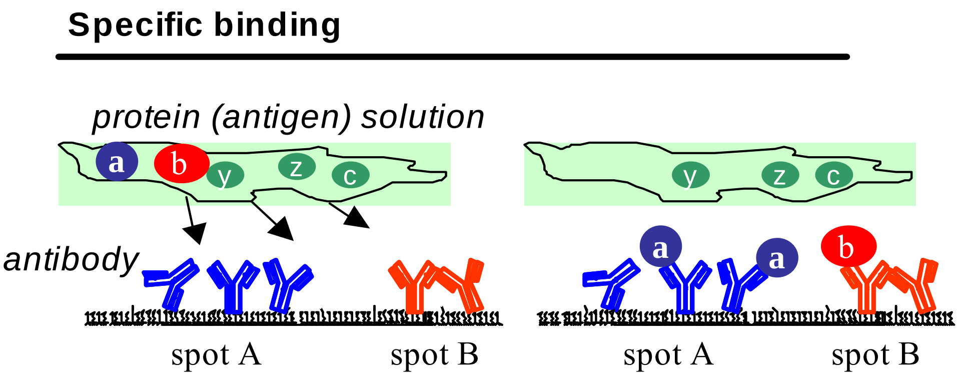
Specific binding
protein (antigen) solution
a
b
y
z
c
antibody
spot A
spot B
y
z
c
a
a
b
spot A
spot B

Figure 1.1 Explanation of specific binding.
Specific binding is a biologically pre-defined 3-D conformational fit between conjugate biomolecules. E.g., Antigen binding region (epitope) and antibody binding region (paratope). The specific interaction at this interface largely consists of hydrogen bonding between protein resides and through interstitial water molecules.

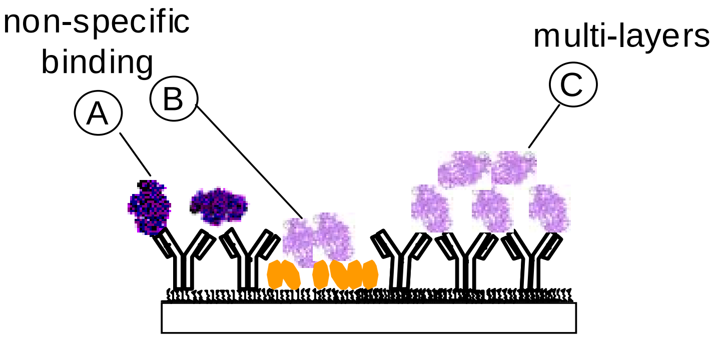
non-specific binding
A
B
multi-layers
C

Figure 1.2. Explanation of non-specific binding.
Any non-intended attachment between biomolecules, such as cross-binding (incorrect match) (A), binding to the surface (B), or multi-layer formation (C) is non-specific binding.

1.3.2 A Biosensor Frontier – The Protein Microarray

Of the various types of biosensors, protein microarrays present amongst the most challenges to successful implementation. For these biosensors, greater understanding of behavior at the molecular level has the potential to bring about significant improvements in the technology.

Protein microarrays are composed of micro-spots of capture agents (proteins or protein-interacting molecules) patterned on a solid support by a spotting robot (Figure 1.3). When the surface is exposed to a solution of multiple target proteins, the proteins in solution will bind specifically at cognate locations with complementary active sites. The high density of spots that can be arrayed on a single chip (100 μm spot diameter, ArrayIt®) gives protein microarrays the ability to manage a great magnitude of protein interactions.

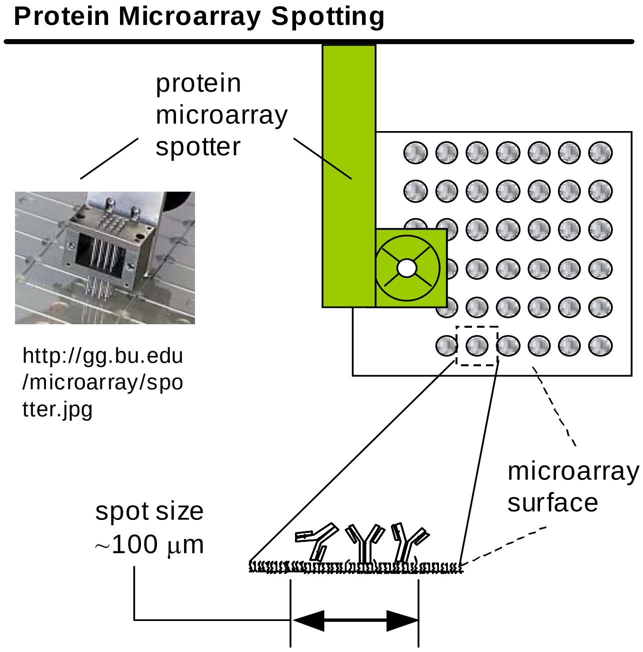
Protein Microarray Spotting
protein
microarray
spotter
http://gg.bu.edu
/microarray/spo
tter.jpg
microarray
surface
spot size
~100 μm

Figure 1.3. Protein microarray spotter deposits micro-spots of protein (antibody) on microarray surface.

Antibody microarrays are one of the more common types of protein microarray. In an antibody microarray, antibodies are often covalently bound to the surface and bind only to specific antigens when exposed to a multiplexed solution of antigens. In antigen microarrays the components are reversed with antigen bound at the surface and antibodies in solution.

There are myriad challenges in the successful production of protein microarrays. The surface chemistry must allow for a wide variety of different proteins to be immobilized on the same chip while retaining their structure and hence, biological activity [11]. It is also difficult to procure the wide variety of proteins and antibodies needed to populate a single protein array [8]. Diversity in protein structure makes it difficult to label a variety of different proteins uniformly, making it difficult to make the microarray quantitative [8]. For the great diversity in protein structure and function that exists, the diversity in protein sensitivities to their environment may make it difficult to maintain the integrity of many different proteins on the same surface under the same conditions. Additionally, in order to bind properly to target molecules, the proper orientation of antibodies or other capture molecules on the surface is important [4].

Physiological concentration levels of clinically important proteins are often near 1 μg/ml and can be as low as 10 ng/ml. For example, Prostate Specific Antigen (PSA), used to detect prostate cancer, is present from 10-20 ng/ml [12] as are concentrations of antibodies in certain immune responses [13]. Haab et al. [14], tested 115 different antibody-antigen pairs. Although the best results presented were detectable in this range, the majority of antibody arrays and half of antigen arrays tested could not detect concentrations of target proteins near 1 μg/ml. While the results of these studies are promising, there is still quite a bit of room for improvement.

1.3.3 Methods of Biomolecule Attachment to Surfaces

The scope of the investigations here is limited to attachment of biomolecules, mainly proteins, to modified surfaces and for the most part does not delve into protein modification. Procedures requiring protein modification may not be practical, since additional processing steps can lead to loss of protein activity [2]. Therefore, simple attachment processes are likely best for immobilizing proteins, especially in the case of protein microarrays requiring many unique protein types in small volume on the same surface [2]. Here introduced are the processes of physisorption, chemisorption and a widely used biological system of attachment, the biotin-(strept)avidin system.

1.3.3.1 Physisorption

Physisorption is the process of attaching molecules to surfaces via electrostatic and van der Waals forces. This method of attaching biomolecules to surfaces is the easiest, as such molecules are readily applied via solution deposition and require no chemical reaction to take place. However, this type of adsorption is the weakest form of attachment, as physisorbed molecules can be easily removed upon rinsing. Futhermore, macromolecules bound to surfaces via van der Waals and electrostatic forces may be denatured by these forces, degrading their integrity and function. Sheiko et al. have observed that highly branched polymers undergo carbon-carbon backbone scission as a result of mechanical strain due to spreading of the polymers at surfaces and expected similar results for brush structures and dendrimers, macromolecules similar in size and shape to proteins [15]. Denaturation of biomacromolecules may leave hydrophobic or charged sites exposed that may cause subsequent non-specific binding of target molecules. However, in one study, antibody physisorbed to gold surfaces was better at recognizing bacteria than antibody conjugated to self-assembled monolayer coated surfaces [16].

1.3.3.2 Chemisorption

Chemisorption or covalent attachment constrains biomolecules to fixed positions at the surface and increases specificity of attachment with pre-defined chemical reactions. Chemical attachment allows for extensive rinsing that can reduce multilayer formation and non-specific binding of target molecules. Since all protein types have amines on their surface (from lysine or arginine residues) covalent attachment via this moiety is quite convenient and common. Specific sites on biomolecules may be targeted for covalent attachment to the surface, such as the carbohydrate region of antibodies [17, 18] or sulfhydryls [2, 19, 20], freed by breaking antibody disulfide bonds. However, side reactions may occur undermining the attempt to control the attachment site. In general, covalent binding does not prevent disorganization of biomolecules at the surface, since random orientation of active sites and blocking by adjacent molecules is still possible.

1.3.3.3 Biotin-streptavidin linkage [21, 22]

The biotin-(strept)avidin system is widely used in biotechnology as a means of linking biomolecules to each other and to surfaces. Avidin is a protein found in egg white that was discovered to be anti-bacterial, binding tightly to the vitamin biotin, a small molecule (244.3 g/mol) attached to enzymes in certain bacteria. The affinity between biotin and avidin is the highest of all biological couples at 10^{15} M^{-1}. An analog of avidin, streptavidin, was isolated as a product of Streptomyces avidinii and has an affinity to biotin of about 10^{13} M^{-1}. Both avidin and streptavidin have four binding sites for biotin binding.

Biotin-(strept)avidin specific attachment eliminates the possibility of side reactions, suggesting that specific binding may be more reliable than chemical attachment. When biotin is bound to (strept)avidin the stability of the couple is found to be greater than that of unbound (strept)avidin [23-25]. Molecules bound to a surface via biotin-(strept)avidin linkage have the advantage that this linkage system is highly resistant to changes in pH, temperature and other environmental conditions. A variety of biomolecules can typically be chemically modified with biotin and bound to (strept)avidin coated surfaces.

1.3.4 Characterizing biomolecule attachment to surfaces

Attachment of biomolecules to biosensor surfaces may be monitored and characterized with a number of techniques. Labeling proteins and other biomolecules with fluorescent tags is one of the most commonly used ways to keep track of the quantity of biomolecules at a surface. Fluorescent intensity of labeled protein is proportional to the concentration of protein adsorbed to the surface. MacBeath et al. printed small molecules on the surface of glass slides and detected them with fluorescently-labeled proteins [26].

Surface Plasmon Resonance (SPR) is useful for observing small changes in mass, such as when target biomolecules bind to capture molecules at the surface [27]. Such changes are detected based on changes in the local refractive index of the surface upon adsorption of these molecules. Antibody and antigen surfaces coverages can be calculated from SPR measurements using theoretical calculations [28]. Quartz crystal microbalance (QCM) can also measure small changes in the quantity of biomolecule mass adsorbed at a surface. In this technique, the natural resonance frequency of a piezoelectric crystal changes in direct proportion to the mass of biomolecules added to the surface.

In addition to the above techniques, researchers have used other methods to characterize biomolecule attachment to inorganic oxide surfaces. Atomic force microscopy (AFM) was used in conjunction with enzyme immunoassay (EIA) to assess binding under a variety of solution conditions [29]. Other techniques include XPS for determination of surface elemental composition and ellipsometry to measure film thickness.

1.3.4.1 Limitations

The above techniques provide information about a variety of surface properties, from the mass of protein at the surface to the elemental composition of the surface beneath the protein. However, information about the chemistry of attachment of these molecules to the surface is limited. Antigen-binding assays can be used to indirectly monitor the effect of chemical preparation on antibody surface coverage and orientation, based on the fluorescent intensity of bound antigen [2, 3, 26, 30-32]. The quantity of biomolecules removed through extensive rinsing may suggest how tightly these molecules are bound to the surface and whether they are chemisorbed or physisorbed, but more detailed information about the molecular attachment may not be possible to obtain. Using infrared (IR) spectroscopy, direct observation of molecular binding to surfaces is possible and may be used to characterize biosensor surface properties, behavior and quality at this level.

1.3.5 Infrared Studies of Biosensor Surfaces

To directly determine the type of attachment of biomolecules to the biosensor surface, IR spectroscopy can be employed. This technique senses the presence of chemical bonds based on the absorption of IR radiation by these bonds. Hence, it is possible to determine whether chemical bonds have been formed or broken indicating chemisorption, or if reactive moieties remain unchanged after adsorption, suggesting physisorption to the surface. Furthermore, the IR signature of the surface can be tracked after each of a series of processing steps, such that it is possible to monitor the effect of molecular changes on the structure and stability of the biosensor platform.

One of the most common methods of protein immobilization to inorganic surfaces is through covalent attachment of proteins to an N-hydroxysuccinimide (NHS) terminated surface. Several studies have used IR spectroscopy to track the formation of NHS and the presence of protein or peptide in subsequent reaction with the surface [33-37]. Some studies have also tracked NHS removal in the reaction with protein or NHS degradation under various conditions [33, 34, 37]. The position of the CH_2 band has also been used to determine the organization of the carbon chains at the surface to which NHS is attached. Lower CH_2 stretching frequency (~2920 cm^{-1} compared with 2930 cm^{-1}) indicates tighter packing and greater chain organization [36].

Other biomolecule attachment systems have also been investigated with IR spectroscopy. Nucleic acids were immobilized on solid silica supports modified with aminosilane and terminated in maleimide crosslinkers. Degradation of the maleimide ring in buffer was tracked with IR spectroscopy via ring CH stretch bands at ~3100cm^{-1}. Using the integrated area under various regions of the spectra (initially calibrated by elemental analysis) surface coverage of various adsorbed species was determined as well [19, 38, 39]. Peptide attachment to titanium oxide surfaces via maleimide crosslinker was also characterized by infrared reflection absorption (IRAS) spectroscopy [40]. IR spectroscopy was further used to track oxygen plasma modification of self-assembled monolayers with subsequent antibody attachment [41] and electrostatic adsorption of enzymes on polymer coated gold surfaces [42].

In other studies, IRAS was used to characterize each step in the attachment of biotin and avidin to gold or silicon oxide surfaces terminated with several different chemistries. Avidin coverage was quantified with a cobalt-carbonyl label by using the integrated area of the label's alkyne carbonyl vibrations near 2050 cm^{-1} [43-46].

In the majority of studies where IR spectroscopy is used to investigate biosensor surfaces, only the presence of molecular and protein layers at the surface are characterized and not the bonding between layers. The lack of interfacial information may be due to far fewer bonds linking the layers together than exist in the layers themselves. For example, large protein amide band absorptions from the protein backbone may obscure bonds that link proteins to the surface in the same spectral region. This issue will be addressed in Chapter 4. There is also little discussion about physisorption that takes place along with chemisorption, when molecules fail to react with the surface. In the following investigations presented here, a number of these issues are addressed. By physisorbing molecules to surfaces in initial experiments, these IR features can be recognized in subsequent chemisorption experiments. Furthermore, data are often limited in several ways due to equipment setup. Attenuated total reflection (ATR) geometry does not permit observation of spectra below ~1500 cm^{-1}. Often used powder surfaces provide high surface area for increased absorption of IR in transmission, but lack the sensitivity of using planar surfaces, especially with IR incidence at the Brewster angle where transmission of IR radiation is maximized. In the following chapters, several different systems of biomolecule attachment to surfaces are investigated and various techniques to enhance spectra are employed. First, a detailed background on infrared spectroscopy is presented.

1.4 Techniques for characterizing surfaces

The main technique in the investigations here for characterizing surface modification and bonding between surface layers is Fourier Transform Infrared spectroscopy and is discussed here in detail. Fluorescence and ellipsometry are employed in Chapter 5 and are discussed briefly following FTIR.

1.4.1 Fourier Transform Infrared Spectroscopy (FTIR) [47-50]

IR spectroscopy is a highly popular and effective method of identifying the chemical makeup of materials. The main use of IR spectroscopy in this work is to identify the chemical structure of thin organic and biomolecular films adsorbed at inorganic surfaces, namely silicon and silicon oxide, as well as to identify the type of interaction that these materials have with the surface.

Molecular bonds can absorb radiation in the infrared region of the electromagnetic spectrum. When infrared radiation is transmitted to a detector, a sample in the path of the radiation beam absorbs some of the radiation, reducing the amount of light transmitted. The reduction in transmitted radiation at various frequencies sensed by the detector indicates that the chemical bonds of the sample material absorbed some of the radiation and these bonds can be identified based on the frequency of absorption. Following is a brief introduction to the nature of radiation and the interaction of molecules with this radiation.

1.4.1.1 Electromagnetic Spectrum

The electromagnetic spectrum is a continuum of energies ranging from high energy, short wavelength radiation such as gamma rays and X-rays to low energy, long wavelength radiation, including microwaves and radio waves (Figure 1.4).

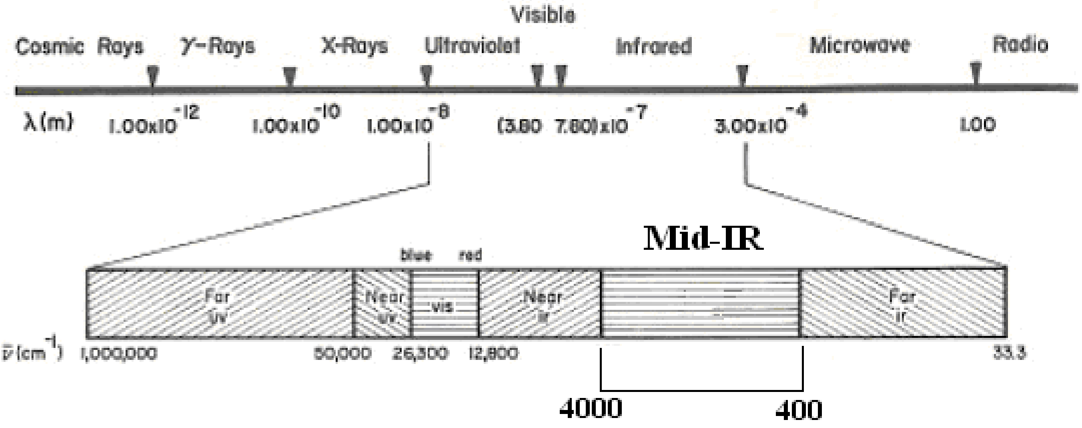
Visible
Cosmic Rays
γ-Rays
X-Rays
Ultraviolet
Infrared
Microwave
Radio
λ(m)
1.00x10^{-12}
1.00x10^{-10}
1.00x10^{-8}
(3.80 7.80)x10^{-7}
3.00x10^{-4}
1.00
Mid-IR
blue
red
Far uv
Near uv
vis
Near ir
Far ir
$\tilde{\nu}$(cm^{-1})
1,000,000
50,000
26,300
12,800
33.3
4000
400

Figure 1.4. The electromagnetic spectrum.
Wavelengths, λ, are stated in meters. The infrared region is stated in wavenumbers, $\tilde{\nu}$ (cm^{-1}). Taken from [49] and modified.

The various frequencies of electromagnetic radiation interact differently with atoms and molecules. While absorption of radiation such as ultraviolet light can break chemical bonds, radiation (of lower energy) in the infrared region of the spectrum causes molecules to vibrate.

Electromagnetic energy behaves as both a particle and a wave. In the wave representation, this energy can be classified in terms of its frequency. All electromagnetic radiation propagates at a constant speed, $c = 3.0 \times 10^8$ m/s, relating the wavelength, λ and frequency, ν of the radiation, such that $c = \lambda\nu$. In infrared spectroscopy it is convenient to use the reciprocal of the wavelength to express frequency in units of "wavenumbers", $\tilde{\nu}$ (cm^{-1}), increasing in the same direction as frequency.

$$\tilde{\nu} = \frac{1}{\lambda} = \frac{\nu}{c} \qquad \text{(eqn. 1.1)}$$

Within the infrared region of the electromagnetic spectrum, the radiation that is absorbed by most molecules is in the mid-infrared region, ranging from 2.5 to 25 μm in wavelength or 4000 –400 cm^{-1} in frequency (Figure 1.4).In the particle representation of electromagnetic energy, energy can be thought of as particles called photons. The frequency of the photon is related to its energy by the Planck constant, $h = 6.626 \times 10^{-34}$ J s.

$$E = h\nu \qquad \text{(eqn. 1.2)}$$

This representation of electromagnetic energy will be important for understanding how radiation interacts with molecules.

1.4.1.2 Molecular Vibrations

To a close approximation, molecules can be thought of as masses (atoms) connected by springs (the bonds between the atoms). In the simplest case, a diatomic molecule can be approximated by a harmonic oscillator, whose restoring force is given by Hooke's Law.

$$f = -kq \qquad \text{(eqn. 1.3)}$$

Here, the restoring force is f, due to spring constant, k and vibrational coordinate, $q = (r - r_e)$, where r is the displacement from the equilibrium position r_e, of the atomic nuclei. The vibrational frequency of the bond is related to this spring constant and to the masses of the atoms.

$$\nu = \frac{1}{2\pi}\sqrt{\frac{k}{m}} \qquad \text{(eqn. 1.4)}$$

For units in wavenumbers, $\tilde{\nu}$, equation 1.1 can be applied to this expression:

$$\tilde{\nu} = \frac{1}{2\pi c}\sqrt{\frac{k}{m}} \qquad \text{(eqn. 1.5)}$$

The quantity, m, called the reduced mass is a combination of the masses of the atoms, m_1 and m_2 on either side of the spring, as shown here.

$$\frac{1}{m} = \frac{1}{m_1} + \frac{1}{m_2} \qquad \text{(eqn. 1.6)}$$

Applying quantum mechanics to the harmonic oscillator, the molecular bond can have discrete energy levels, characterized by quantum number, n, such that

$$E_n = (n + \tfrac{1}{2})\, h\nu \qquad \text{(eqn. 1.7).}$$

These energy levels exist in a potential well, where energy is related to the vibrational coordinate, or displacement of the atoms from their equilibrium position, r_e (Figure 1.5).

When molecular bonds absorb photons with frequencies, ν in the infrared region, their vibrational energy is raised by photon energy, $h\tilde{\nu}$. This absorption causes a transition between vibrational energy levels. Most vibrational transitions occur between E_0 and E_1, called fundamental transitions. Absorptions raising the vibrational energy to higher levels for the same molecular bond are called overtones.

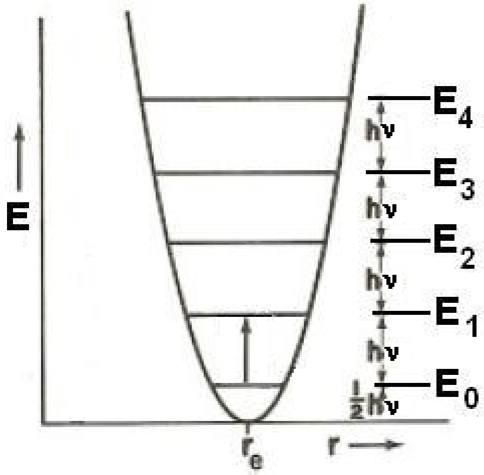

Figure 1.5. Potential well and energy levels for a harmonic oscillator for diatomic molecules. Taken from [49] and modified.

Another aspect of the bond that must be considered is its dipole moment. A bond has a permanent dipole moment when the electrons of the covalent bond are not evenly distributed between the atoms. Such a distribution occurs for heteronuclear molecules, where the atoms' electronegativities, the ability of each atom to attract valence electrons to itself, are different.

As the molecular bond vibrates, the oscillating dipole can absorb energy from an oscillating electric field of precisely the same frequency. Such resonance energy transfer occurs when the chemical bonds in a material are exposed to infrared radiation, where the electric fields of photons at specific frequencies exactly match the frequencies of the various bonds in the material. Only molecules with a net dipole, that is, molecules whose dipoles do not cancel, can absorb infrared radiation and are thus termed, infrared active. The intensity of the absorption is also a function of the dipole moment. The greater the difference in atom electronegativities, the greater the change in the dipole moment and hence the greater the intensity of the absorption band.

1.4.1.3 Types of vibrational modes

While a diatomic molecule can only exhibit stretching vibrations, molecules with three or more atoms have many more types of vibrational modes. Stretching vibrations include in-phase, or symmetric stretching and out-of-phase, or asymmetric stretching. Types of bending vibrations include scissoring, twisting, wagging and rocking.

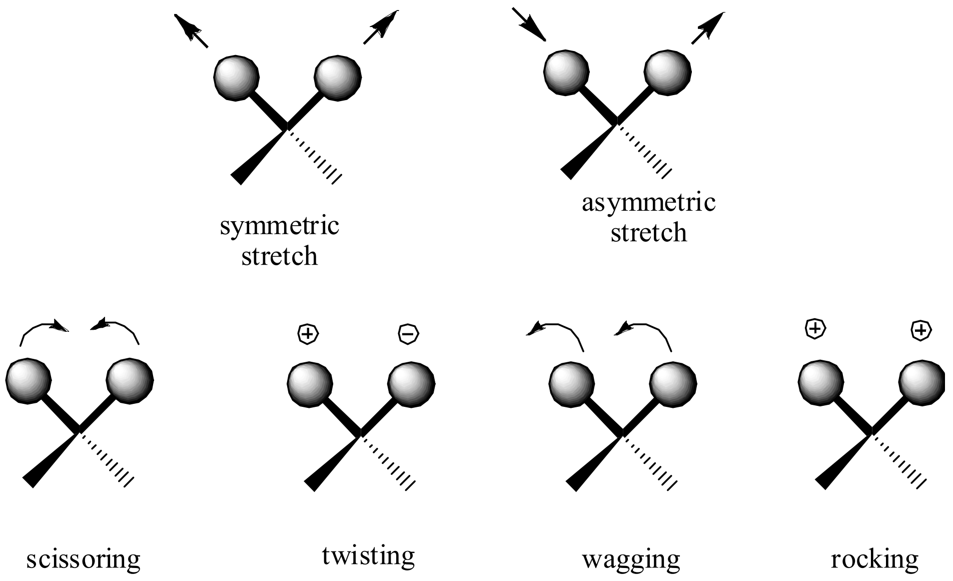

Figure 1.6. Vibrational modes of the CH_2 moiety.

1.4.1.4 Spectrometers

The infrared absorption spectrum is obtained through a spectrometer, which separates radiation by frequency. In earlier years, this process was performed by dispersive spectrometers, in which a dispersive element such as a prism or grating directly dispersed light by frequency. More recently, interferometers were developed which form an interference pattern between two light beams called an interferogram, that is subsequently transformed into a frequency spectrum mathematically using Fourier Transformation.

1.4.1.4.1 Comparison between dispersive spectrometers and interferometers

The grating spectrometer was commonly used before the interferometer was developed for practical use. In a grating spectrometer, the grating disperses the light into a continuum of wavelengths which is then scanned across a slit through which only a small frequency range can pass at a time to a detector. Hence, a resolution element is limited by slit width and contains only a fraction of all the frequencies in the spectrum at any given time.

In contrast, an interferometer collects light of all frequencies simultaneously. Light incident on a beam splitter is separated into two beams. One of these beams is reflected off of a moving mirror, which creates a continuum of path length differences from the first beam, creating a continuum of phase differences between the beams. When the beams recombine, they interfere. The interference pattern is then transformed into a complete frequency spectrum. Hence, even the smallest element scanned in the shortest time increment contains the entire frequency spectrum.

There are two main advantages that interferometers have over dispersive spectrometers that are based on the differences between the above spectrometer qualities. The Fellgett or multiplex advantage is based on the fact that during each time element of a scan, an interferometer receives information about the entire spectrum, while a grating spectrometer only receives that of the spectral range that passes through the slit. If a grating spectrometer can collect the entire spectrum over time T, then its resolution will be proportional to time T/M, the time it takes to scan each of M elements at instrument resolution. The signal to noise ratio is then proportional to $(T/M)^{1/2}$.

In contrast, for an interferometer, the information in the entire spectrum is present in each element of a scan. Then, each spectral element is proportional to T and the signal to noise ratio is proportional to $T^{1/2}$.

On comparison of spectrometers, the signal to noise ratio of the interferometer will be $M^{1/2}$ times better than that of the grating spectrometer. Since resolving power for a grating spectrometer is proportional to M, for comparable spectrometers with a resolving power of 10^4-10^6, the interferometer will have a better signal to noise ratio than the grating spectrometer by a factor of 10^2-10^3 [47].

The second advantage is called the Jacquinot or throughput advantage. An instrument's throughput is a function of the amount of energy that can be collected by the instrument. Interferometers have the ability of to collect large amounts of energy at high resolution. In a lossless system, the brightness of an image projected by a source is equal to the brightness of the source itself, and brightness is proportional to radiant flux or power. Then, the area of the aperture that radiation is transmitted through determines the power or energy throughput of the instrument.

For interferometers, resolution is independent of aperture size and shape, but not so for grating spectrometers, since frequency resolution depends on slit width. Therefore, an interferometer can have a large circular aperture as an effective source without compromising resolution. A grating spectrometer on the other hand, must have very small slit width through which the light passes in order to have high resolution. Hence the area of its effective source is small and its power throughput is small compared to that of the interferometer.

Some additional advantages of the interferometer follow from the Fellgett and Jacquinot advantages. These include large resolving power, high wavenumber accuracy, faster scanning time, reduced stray flux, ability to scan broad wavenumber ranges, and smaller image size in the sample compartment [47].

1.4.1.4.2 Interferometers

Figure 1.7 is a diagram of a Michelson interferometer (named after its inventor). Basically, a source (S) emits infrared radiation to a collimating mirror (C), making the beams parallel and reflecting them to a beamsplitter (B). The beamsplitter reflects half of the radiation at a right angle to incidence to a stationary mirror (M_1) and transmits the other half to a moveable mirror (M_2). After reflecting off their respective mirrors, the beams recombine at the beamsplitter. The combined beam is then sent to the focusing mirror and into the path of the sample. Then beam, now carrying the information of the sample goes into the detector (D).

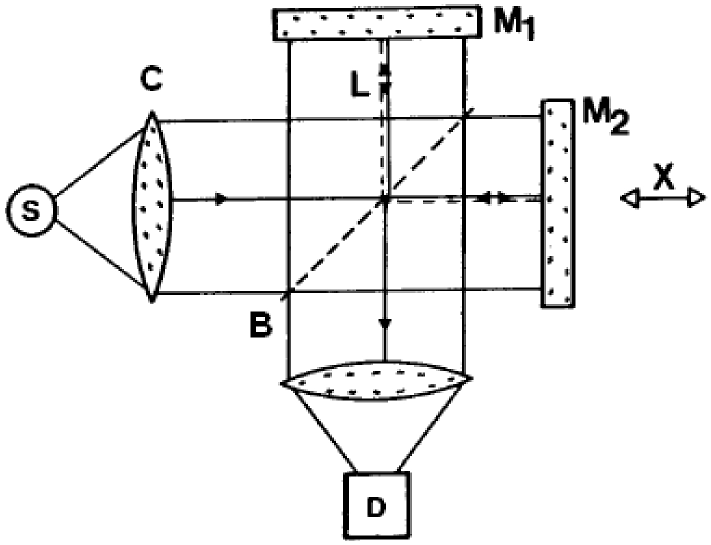

Figure 1.7. Schematic of a Michelson interferometer.
Taken from [51].

The moveable mirror adds an optical path difference to the beam it reflects that is twice the distance of the mirror displacement from its starting position. As the mirror moves, it creates a range of optical path differences that cause the beams to recombine and interfere with each other at a continuum of phase shifts. The interferogram is a plot of the radiation intensity values at each optical path difference from the mirror starting position.

1.4.1.4.3 Interferogram

The interferogram is the interference pattern created as the two beams separated by the beam splitter recombine at a continuum of phase shifts. For a single frequency emitted from a monochromatic source, the interferogram is a cosine (Figure 1.8A). This waveform occurs due to periodic constructive and destructive interference between two sine waves of the same frequency. For a continuum of frequencies emitted from a polychromatic source, a Fourier transform is required to convert the interferogram into its frequency spectrum. The Fourier Transform is given by the equation,

$$B(\bar{\nu}) = \int_{-\infty}^{+\infty} I(\delta) \cos 2\pi\bar{\nu}\delta \ d\delta \qquad \text{(eqn. 1.8)}$$

where I is the interferogram intensity as a function of mirror displacement, δ, integrated across the full range of optical path differences. B is the power spectral density, the intensity at each frequency as a function of $\tilde{\nu}$. Figure 1.8 shows various types of spectra and the interferograms they are transformed from. The broader the spectrum, the greater the damping in the interferogram.

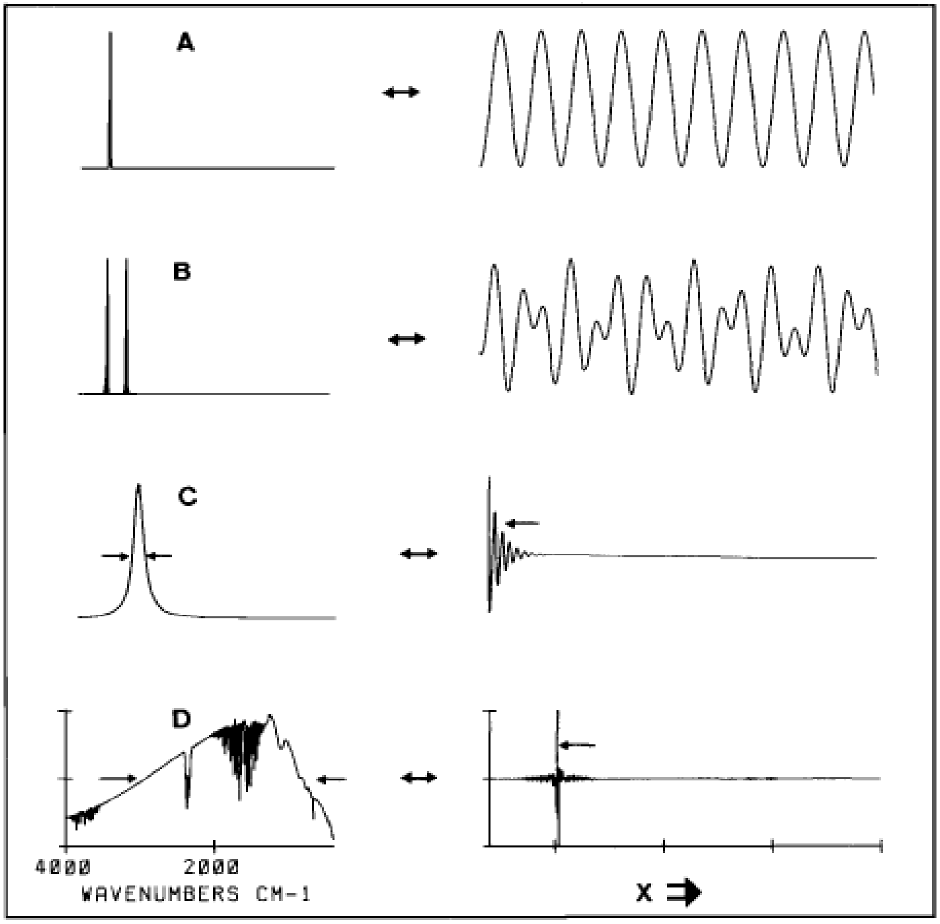

Figure 1.8. Examples of spectra and their corresponding interferograms.
A) One monochromatic line. B) Two monochromatic lines very near each other. C) Lorentzian line. D) Broadband spectrum from polychromatic source. Taken from [51].

1.4.1.4.4 Limitations of FTIR

The resolution of the interferogram is limited by the maximum displacement of the moving mirror. This can be intuitively understood by recognizing that for two superposed sine waves, the closer in frequency two sine waves are, the longer the distance required for them to move out of phase and back in phase [48].

Furthermore, since the moveable mirror cannot be moved to infinite distance, there is a truncation effect on the interferogram that translates to the addition of side lobes in the transformed frequency spectrum. To eliminate these side lobes or "pods", an apodization function is applied to the interferogram. The function used for spectra here is the Happ-Genzel function.

Because the interferogram is not perfectly symmetrical on either side of the point of zero mirror displacement, phase correction is also necessary. This operation ensures that the sampling intervals are the same on either side of this zero displacement position.

1.4.1.4.5 Fourier Transformed Spectrum: The Single Beam

A typical frequency spectrum from the broad infrared source used in an interferometer is called a single beam (Figures 1.8D and 1.9). The single beam has a sharp fall off at low frequency near 400 or 650 cm^{-1} due to the frequency cutoff of the specific detector and beamsplitter used and a high frequency cutoff of 7400 cm^{-1} (typically observed to 4000 cm^{-1}) [52]. The single beam essentially shows the transmission of radiation in the mid-IR region to the detector. Absorptions that occur along the path of the infrared beam appear as negative bands and are due to water vapor (sharp features of O-H stretch near 3600 – 3900 cm^{-1} and H-O-H bend near 1400 – 1800 cm^{-1}) and carbon dioxide (C=O stretch doublet near 2340 and 2360 cm^{-1}).

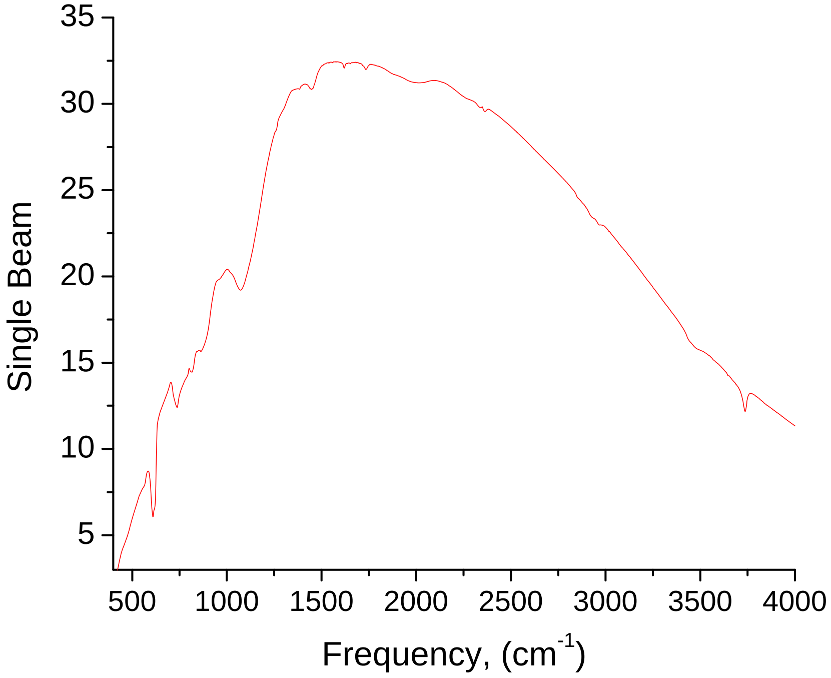

Figure 1.9. Single beam spectrum.

1.4.1.4.6 Sample analysis

The FTIR study of biofilms on silicon oxide surfaces was typically performed on silicon wafers, transparent to infrared radiation in the mid-IR region. To observe the chemical and biochemical modification of the surface, an initially clean, unmodified sample (0.5 mm thick) is placed in the path of the IR beam in the sample compartment of the interferometer. The spectrum collected is called the reference spectrum. Subsequently, the silicon wafer is removed from the sample compartment and chemically modified. The sample is then returned to the exact position in the sample compartment on a sample holder and another spectrum is taken, the experiment spectrum. Two point by point calculations can then be performed:

$$transmittance = \frac{experiment}{reference}$$ (eqn. 1.9)

$$absorbance = -ln\left[\frac{experiment}{reference}\right]$$ (eqn. 1.10)

The transmittance shows the absorptions in the spectrum as negative bands, similar to the single beam spectrum. In an absorbance spectrum, positive bands are observed for vibrational modes of bonds formed, while negative bands are observed for modes of molecular bonds lost or broken. It is worth noting that the infrared absorption features of thin films adsorbed at the wafer surface (typically on the order of 0.001) are much smaller than features such as those due to bulk silicon (on the order of 1.0) visible in the single beam (Figure 1.10). Such small features are present in the absorbance

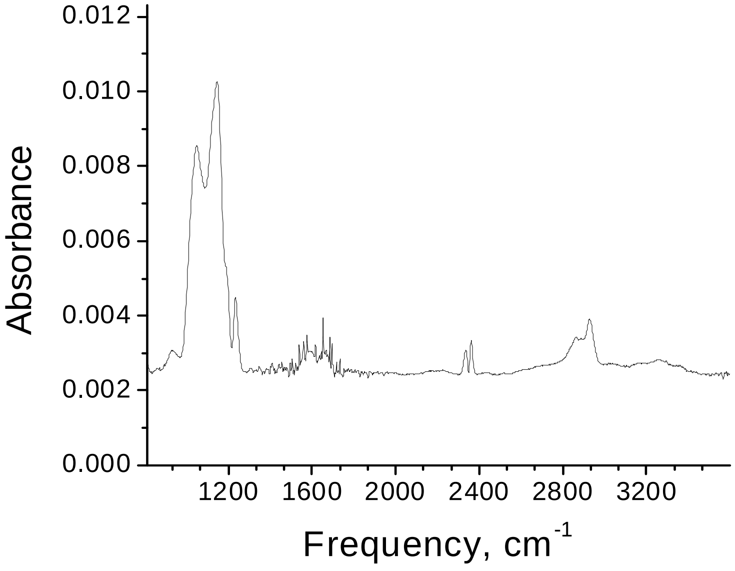

Figure 1.10. Absorbance spectrum.

spectrum because all large features present in both the experiment and reference samples cancel out. Furthermore, for the absorbance, the natural logarithm operation magnifies the absorption of small bands, which are positive in this spectrum. The amount of water vapor present, however, changes from moment to moment and therefore does not cancel out fully. To compensate, a separate absorbance spectrum of water vapor can be collected and scaled to subtract water vapor features from other spectra.

Two common geometries for the silicon wafer in the sample compartment are transmission and attenuated total reflection (ATR). In transmission geometry, the sample is positioned vertically and at an angle of 74° relative to the IR beam, the Brewster angle (for silicon), which optimizes transmission of radiation through the sample (Figure 1.11). This geometry is typically used with thin films and enhances the sensitivity of the film to the IR. ATR geometry is useful when the silicon wafer is in contact with a great deal of material, particularly liquids (Figure 1.12). Here, the silicon wafer is placed horizontally and often supports a cell containing a liquid or gel in contact with one side of the wafer. Gold mirrors are used to reflect the IR into the edge of the wafer which must be beveled for the light to enter. The light is then trapped inside the wafer and reflects internally multiple times until it exits through a beveled edge on the opposite side and is reflected by a mirror into the detector.

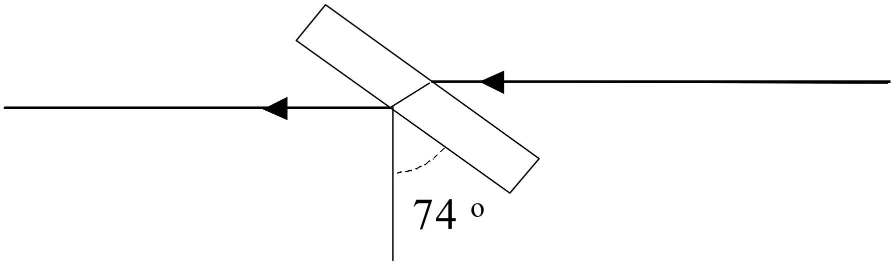

Figure 1.11. Transmission geometry.
The Brewster angle (74° for silicon) transmits a maximum amount of light through the sample.

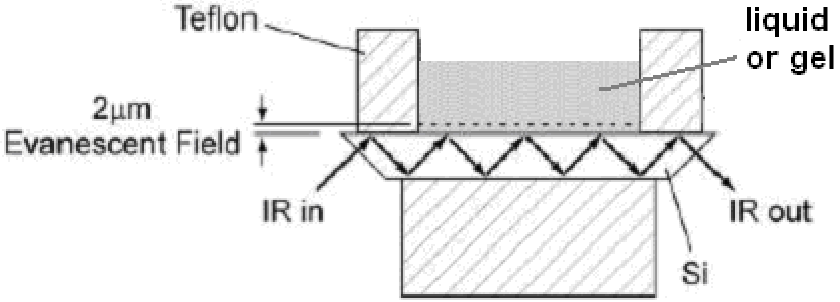

Figure 1.12. ATR geometry.
When IR is totally reflected within the silicon wafer, an evanescent field is created within 2 μm of the surface that can probe the surface and bulk material in this region. This geometry is useful for probing liquids and gels that can be contained with Teflon above the wafer surface.

1.4.2 Fluorescence Measurements (for Chapter 5) [53-56]

Fluorescence microscopy is employed in Chapter 5 to monitor the amount of protein adsorbed to protein microarray surfaces and the amount removed from those surfaces by Surface Acoustic Wave Streaming (SAWS). The basics of fluorescence spectroscopy and microscopy are explained here.

Fluorophores (fluorescent reporter molecules) can be attached to proteins to visually track and quantify them. The amount of protein present is directly proportional to the intensity of the light emitted by the fluorophores labeling the protein. Calculations for protein concentration and degree of fluorescent labeling are explained below.

Similar to the absorption of infrared light by molecules in IR spectroscopy, fluorophores absorb light at visible and ultraviolet frequencies. This absorption raises the energy of the electrons in the fluorophore, bringing them to an excited state, a process called electronic transition. Only photons of specific frequency ν, corresponding to the energy difference between ground and excited states of the electrons of the fluorophore (E_e - E_g) are absorbed:

$$\Delta E = E_e - E_g = h\nu \qquad \text{(eqn. 1.11)}$$

For fluorophores in solution at low concentration, fluorescence intensity is uniformly distributed and increases linearly with fluorophore concentration. The absorption of light by the fluorophore obeys the Lambert-Beer Law:

$$A = -\log(I/I_0) = \varepsilon C l \qquad \text{(eqn. 1.12)}$$

where A is called the absorbance, relating the intensity of the light transmitted through the absorbing molecules, I, to the light incident on the molecules, I_0. ε is the molar absorptivity or extinction coefficient (a characteristic of the electronic transition specific to the absorbing molecule), C is the concentration of absorbing molecules in solution and l is the path length of the light through the sample in solution.

Absorptions can occur from the lowest vibrational level of the ground state, S_0 to a number of excited states S_1, S_2, etc. called singlet states (Figure 1.13, A). The term "singlet" refers to electronic states with an angular momentum of one. Upon reaching one of these states, the molecule enters one of a number of vibrational levels ($\nu = 1,2,3$). After several molecular vibrations, the state of the molecule is brought to the lowest vibration level of the singlet state ($\nu = 0$), a process called vibrational relaxation (VR), that occurs over the lifetime of the fluorophore in the excited state. From this lowest vibrational level, fluorescence (F) can occur: the emission of photons bringing the molecule from the lowest excited singlet state back to the ground state.

This emission usually occurs at a frequency lower than that of the excitation, due to the loss of energy in the excited state by vibrational relaxation. The difference in excitation and emission frequencies is known as the Stokes shift and can be observed on a plot of excitation and emission spectra (absorbance vs. frequency) (Figure 1.14). The emission spectrum is usually a mirror image of the excitation spectrum.

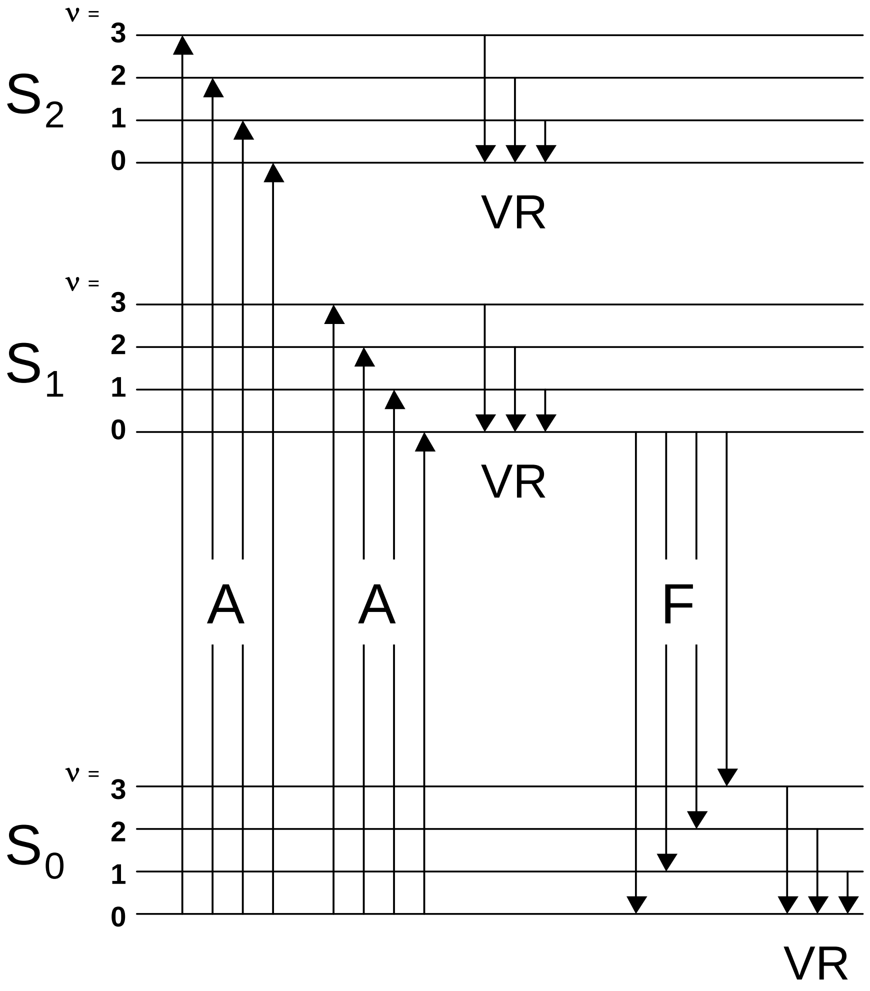

Figure 1.13. Electronic transitions diagram demonstrating fluorescence. (based on [55] p.14). Fluorophores in the lowest vibrational level (ν = 0) of the ground state, S_0, can absorb photons (A) to enter excited singlet states, S_1, S_2, etc. From the S_1 state, after vibrational relaxation (VR) to the lowest level (ν = 0) of this state occurs, fluorescence (F) can occur to any level of the ground state, after which VR occurs again, returning the fluorophore to the lowest vibrational level (ν = 0) of the ground state.

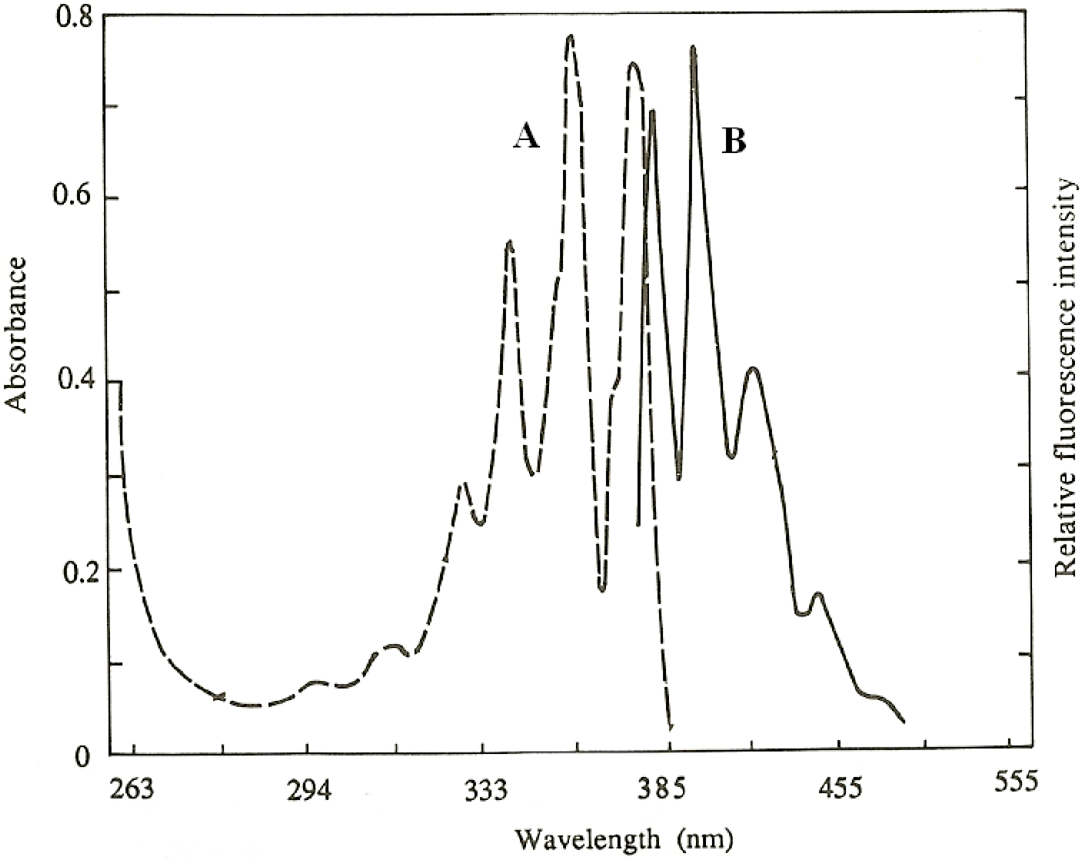

Figure 1.14. Absorption and fluorescence spectra of anthracene in ethanol. Anthracene absorption (A) and anthracene fluorescence at longer wavelength (B). Taken from [54] p.12 and modified.

Upon labeling protein with fluorophores, both protein concentration in solution and degree of labeling of the protein can be determined [53]. The concentration of fluorophore-conjugated protein is determined by measuring the absorbance of the sample at frequencies of fluorophore and protein absorbance maxima, measured with a spectrophotometer. While fluorophores absorb light at a variety of frequencies in the visible and ultraviolet region from about 300 – 800 nm, proteins absorb at 280 nm. Taking the example of immunoglobulin-G (IgG) labeled with AlexaFluor-488 (green emission), protein concentration is determined by a variation of the Lambert-Beer Law:

$$protein\ \ concentration\,(M) = \frac{[A_{280} - (0.11 \times A_{494})] \times dilution\,factor}{203,000}$$ (eqn. 1.13)

where A_{280} and A_{494} are absorbances of IgG and AlexaFluor-488 respectively and an 11% correction factor is applied to account for the tail of the fluorophore (dye) absorption at 280 nm and the molar extinction coefficient of IgG is 203,000 cm^{-1} M^{-1}, for a 1 cm path length, *l*.

To calculate the degree of labeling in moles of fluorophore per mole of protein, the ratio of fluorophore and protein concentrations is applied:

$$\frac{moles\ \ of\ dye}{mole\ of\ protein} = \frac{A_{494} \times dilution factor}{71,000 \times protein\ \ concentration\ (M)}$$ (eqn. 1.14)

where 71,000 cm^{-1} M^{-1} is the approximate molar extinction coefficient of the fluorophore at 494 nm.

To quantify fluorescently-labeled protein adsorbed to inorganic planar surfaces, an epi-fluorescence microscope coupled to a charge coupled device (CCD) camera is used (Figure 1.15). An epi-fluorescence microscope aims excitation frequency light at a sample and sends emitted light from the sample to a CCD camera. An inverted microscope is used here, where a spectrum of light emitted by a mercury or xenon arc lamp (A) enters a cube containing an excitation filter that selects excitation frequency light (in green) and a dichroic mirror (B) that reflects the light into an objective, focusing the light onto a sample (C). Fluorescent light emitted by the sample (in red) returns through the objective and is transmitted through the dichroic mirror and through an optical train to the CCD camera and/or eyepiece. Alternatively, excitation light (in yellow) can be transmitted to the sample from a tungsten or halogen lamp above.

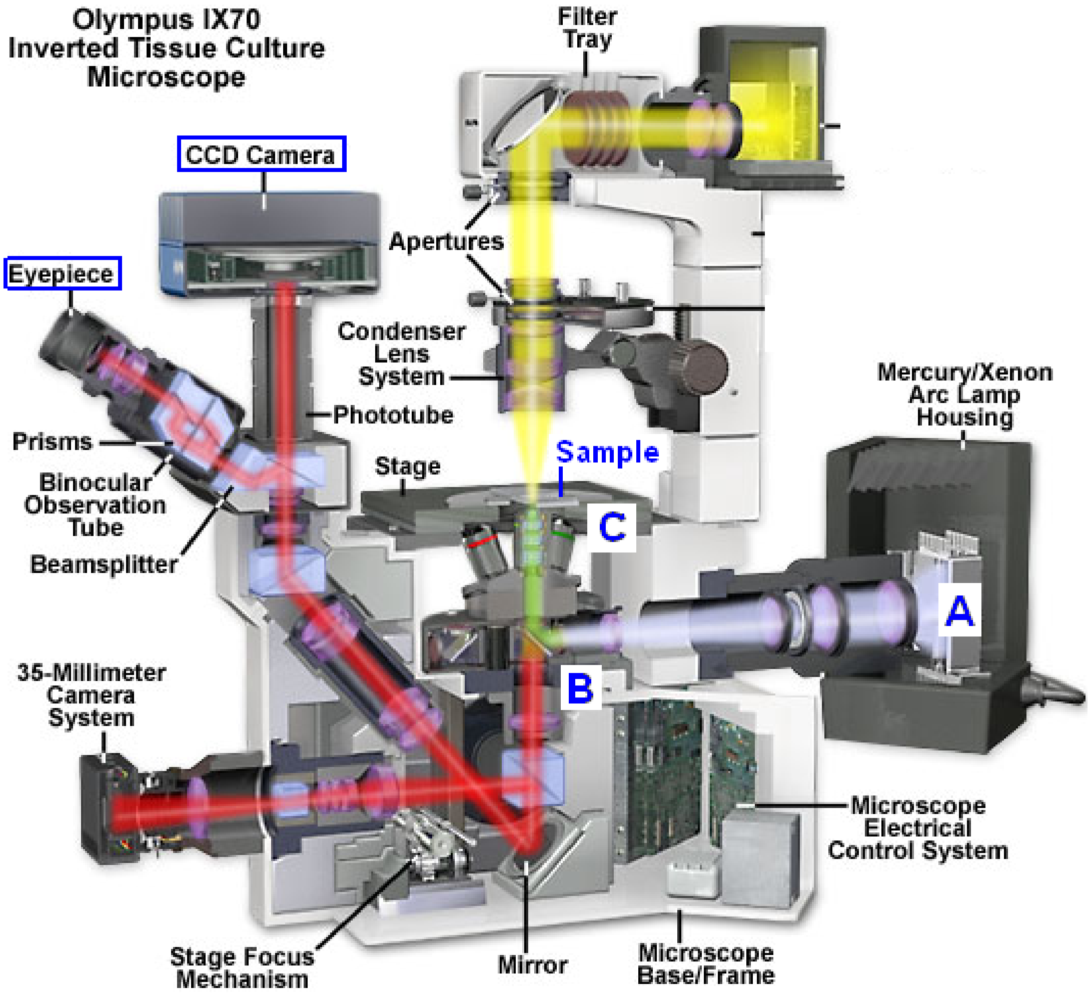
Olympus IX70
Inverted Tissue Culture
Microscope
Filter Tray
CCD Camera
Apertures
Eyepiece
Condenser Lens System
Phototube
Mercury/Xenon Arc Lamp Housing
Prisms
Binocular Observation Tube
Stage
Sample
C
Beamsplitter
A
35-Millimeter Camera System
B
Microscope Electrical Control System
Stage Focus Mechanism
Mirror
Microscope Base/Frame

Figure 1.15. Inverted epi-fluorescence (Olympus® IX-70) microscope. Broad spectrum emission from arc lamp (A) is filtered for excitation frequency and reflected by dichroic mirror (B) through objective to sample (C). Fluorescence from sample (green light) is transmitted through dichroic mirror (B) and distributed through the optical system to the CCD camera and eyepiece. Taken and modified from: http://www.olympusmicro.com/primer/techniqu es/fluorescence/ix70fluorescence.html

The CCD camera sensor is an array of semiconductor-based detectors that accumulate electrical charge over time as photons from the incident fluorescent light hit the detector surface. The charges, proportional to the intensity of the incident light, remain trapped in each pixel area and are later converted to a voltage signal. The intensity of fluorescence of the labeled protein relative to background fluorescent intensity can then be determined.

High intensity excitation light can result in photobleaching of the fluorophores in the sample. Photobleaching results in the dimming of the emission from the sample due to non-radiative processes such as photochemical changes in the fluorophore upon exposure of the fluorophore to intense light. Therefore, precautions must be taken, such as minimizing exposure time of the sample to the excitation light for image collection. Alexafluor dyes are less prone to photobleaching than other dyes such as fluorescein isothiocyanate (FITC).

1.4.3 Ellipsometry Measurements (Chapters 4 and 5) [57-59]

Ellipsometry is a convenient way to measure the thickness and refractive index of thin films on solid surfaces. When linearly polarized light reflects off a surface, its polarization state becomes elliptical. Combining the changes in the polarization of the light with the properties of the light and the surface, the properties of the thin film (thickness and refractive index) can be determined.

In the operation of the ellipsometer, laser light is initially polarized by a polarizer (Figure 1.16) prior to incidence at an oblique angle on a reflective surface. The electric field of the polarized light exists in a plane normal to the direction of propagation and can be broken down into two components, that parallel to the plane of incidence of the light with the surface, p, and that parallel to the surface (and perpendicular to the plane of incidence), s.

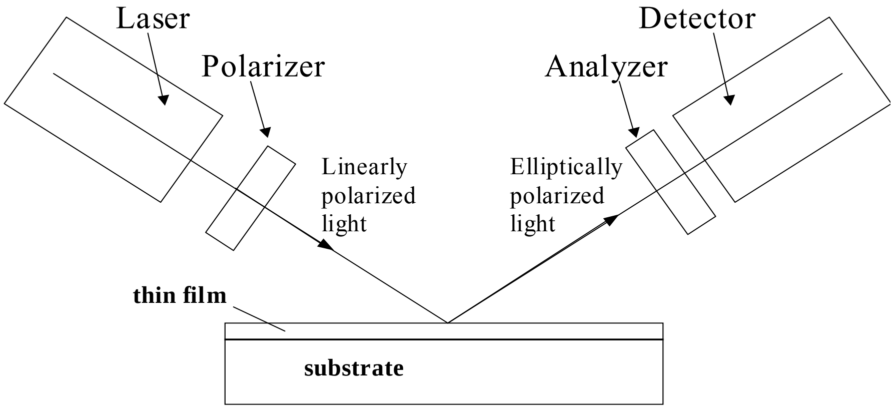

Figure 1.16. Ellipsometer.

Upon reflection from the surface, the polarization state of the light becomes elliptical. In this state, the locus of the electric field vector of the light traces out the shape of an ellipse. This ellipse (and the polarization state of the light) is described by ε (the ellipticity, equal to the arc tangent of the ratio of the major to minor axes, a:b, of the ellipse, related to ellipse shape) and θ (the azimuthal angle, the angle between the ellipse major axis and the s component of the electric field, related to ellipse orientation).

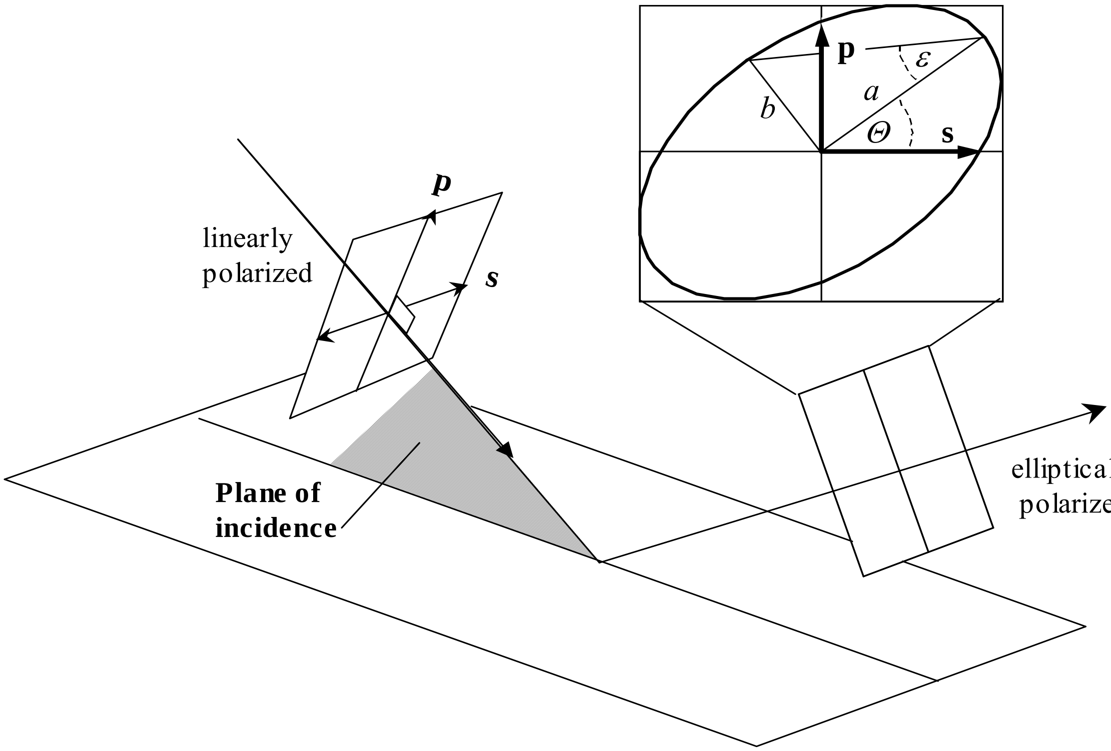

Figure 1.17. Orientation of linearly and elliptically polarized light relative to the surface. The ellipse of the elliptically polarized light can be expressed in terms of s and p components or major and minor axes (***a*** and ***b***) with the azimuthal angle, *θ*.

After reflecting off the surface, the light enters an analyzer and is transmitted to a detector (Figure 1.16). The analyzer is rotated until the transmission of light goes to zero. Based on its orientation at this position, the experimental values Δ and Ψ can be calculated. Δ is the phase difference between the electric field components s and p, and Ψ is their change in amplitude after reflection of the light from the surface. The intensity of the electric field components after reflection, R_s and R_p are related to Δ and Ψ by the equation

$$\rho = R_p/R_s = \tan\Psi\, e^{i\Delta} \qquad \text{(eqn. 1.15)}$$

Δ and Ψ are functions of the angle of incidence of the light, the wavelength of the light, the optical constants of the substrate and the properties of the film on the substrate. These functions are then combined to solve for the properties of the thin film, its refractive index, n and thickness, d.

1.5 References

1. Kambhampati, D., ed. *Protein Microarray Technology*. 2004, Wiley-VCH Verlag GmbH & Co. KGaA: Weinheim.
2. Kusnezow, W., A. Jacob, A. Walijew, F. Diehl, and J.D. Hoheisel, *Antibody microarrays: An evaluation of production parameters.* Proteomics, 2003. **3**: p. 254-264.
3. Vijayendran, R.A. and D.E. Leckband, *A quantitative assessment of heterogeneity for surface-immobilzed proteins.* Analytical Chemistry, 2001. **73**: p. 471-480.
4. Walter, G., K. Bussow, A. Lueking, and J. Glokler, *High-throughput protein arrays: prospects for molecular diagnostics.* TRENDS in Molecular Medicine, 2002. **8**(6): p. 250-253.
5. Spinke, J., M. Liley, H.-J. Guder, L. Angermaier, and W. Knoll, *Molecular recognition at self-assembled monolayers: The construction of multicomponent multilayers.* Langmuir, 1993. **9**: p. 1821-1825.
6. Lowe, C.R., *An introduction to the concepts and technology of biosensors. .* Biosensors, 1985. **1**: p. 3-16.
7. IUPAC, ed. *Compendium of Chemical Terminology*. 2nd ed. the "Gold Book", ed. A.D. McNaught and A. Wilkinson. 1997, Blackwell Scientific Publications: Oxford.
8. Glokler, J. and P. Angenendt, *Protein and antibody microarray technology.* Journal of Chromatography B, 2003. **797**: p. 229-240.
9. Branch, D.W. and S.M. Brozik, *Low-level detection of a Bacillus anthracis simulant using Love-wave biosensors on 36° YX LiTaO$_3$* Biosensors and Bioelectronics, 2004. **19**: p. 849-859.
10. Yacoub-George, E., L. Meixner, W. Scheithauer, A. Koppi, S. Drost, H. Wolf, C. Danapel, and K.A. Feller, *Chemiluminescence multichannel immunosensor for biodetection.* Analytica Chimica Acta, 2002. **457**(1): p. 3-12.
11. Mitchell, P., *A perspectie on protein microarrays.* Nature Biotechnology, 2002. **20**: p. 225-229.
12. Kardamakis, D., *Tumor serum markers: clinical and economical aspects.* Anticancer Research, 1996. **16**: p. 2285-2288.
13. Anthony, B.F., I.E. Concepcion, N.F. Concepcion, C.M. Vadheim, and J. Tiwari, *Relation between maternal age and serum concentration of IgG antibody to type III group B streptococci.* Journal of Infectious Diseases, 1994. **170**(3): p. 717-720.
14. Haab, B.B., M.J. Dunham, and P.O. Brown, *Protein microarrays for highly parallel detection and quantitation of specific proteins and antibodies in complex solutions.* Genome Biology, 2001. **2**(2): p. research0004.1–0004.13.
15. Sheiko, S.S., F.C. Sun, A. Randall, D. Shirvanyants, M. Rubinstein, H.I. Lee, and K. Matyjaszewski, *Adsorption-induced scission of carbon-carbon bonds.* Nature, 2006. **440**(7081): p. 191-194.
16. Baldrich, E., O. Laczka, F.J.D. Campo, and F.X. Muñoz, *Gold immuno-functionalisation via self-assembled monolayers:Study of critical parameters and comparative performance for protein and bacteria detection.* Journal of Immunological Methods, 2008. **336**: p. 203–212.

17. Huang, S.-C., K.D. Caldwell, J.-N. Lin, H.-K. Wang, and J.N. Herron, *Site-Specific Immobilization of Monoclonal Antibodies Using Spacer Mediated Antibody Attachment.* Langmuir, 1996. **12**: p. 4292-4298.
18. Turkova, J., *Review: Oriented immobilization of biologically active proteins as a tool for revealing protein interactions and function.* Journal of Chromatography B, 1999. **722**: p. 11-31.
19. Jin, L., A. Horgan, and R. Levicky, *Preparation of End-Tethered DNA Monolayers on Siliceous Surfaces Using Heterobifunctional Cross-Linkers.* Langmuir, 2003. **19**: p. 6968-6975.
20. Peluso, P. and OTHERS, *Optimizing antibody immobilization strategies for the construction of protein microarrays.* Analytical Biochemistry, 2003. **312**: p. 113-124.
21. Diamandis, E.P. and T.K. Christopoulos, *The Biotin-(Strept)Avidin System: Principles and Applications in Biotechnology.* Clinical Chemistry, 1991. **37**(5): p. 625-636.
22. Smith, C.L., J.S. Milea, and G.H. Nguyen, *Immobilization of Nucleic Acids Using Biotin-Strept(avidin) Systems.* Topics in Current Chemistry, 2006. **261**: p. 63-90.
23. Celej, M.S., G.G. Montich, and G.D. Fidelio, *Conformational flexibility of avidin: the influence of biotin binding.* Biochemical and Biophysical Research Communications, 2004. **325**: p. 922-927.
24. Gonzalez, M., L.A. Bagatolli, I. Echabe, J.L.R. Arrondo, C.E. Argarana, C.R. Cantor, and G.D. Fidelio, *Interaction of Biotin with Streptavidin - Thermostabilty and conformational changes upon binding.* The journal of biological chemistry, 1997. **272**(17): p. 11288-11294.
25. Ismoyo, F., Y. Wang, and A.A. Ismail, *Examination of the Effect of Heating on the Secondary Structure of Avidin and Avidin-Biotin Complex by Resolution-Enhanced Two-Dimensional Infrared Correlation Spectroscopy.* Applied Spectroscopy, 2000. **54**(7): p. 939-947.
26. MacBeath, G., A.N. Koehler, and S.L. Schreiber, *Printing Small Molecules as Microarrays and Detecting Protein−Ligand Interactions en Masse.* Journal of the American Chemical Society, 1999. **121**: p. 7967-7968.
27. Su, X., Y.-J. Wu, R. Robelek, and W. Knoll, *Surface plasmon resonance spectroscopy & quartz crystal microbalance study of streptavidin film struct effects on biotinylated DNA assy and target DNA hybridization.* Langmuir, 2005. **21**: p. 348-353.
28. Peluso, P., D.S. Wilson, D. Do, H. Tran, M. Venkatasubbaiah, D. Quincy, B. Heidecker, K. Poindexter, N. Tolani, M. Phelan, K. Witte, L.S. Jung, P. Wagner, and S. Nock, *Optimizing antibody immobilization strategies for the construction of protein microarrays.* Analytical Biochemistry, 2003. **312**: p. 113-124.
29. Qian, W., B. Xu, L. Wu, C. Wang, D. Yao, F. Yu, C. Yuan, and Y. Wei, *Controlled Site-Directed Assembly of Antibodies by Their Oligosaccharide Moieties onto APTES Derivatized Surfaces.* Journal of Colloid and Interface Science, 1999. **214**: p. 16-19.
30. Nisnevitch, M., M. Kolog-Gulco, D. Trombka, B.S. Green, and M.A. Firer, *Immobilization of antibodies onto glass wool.* Journal of Chromatography B: Biomedical Sciences and Applications, 2000. **738**(2): p. 217-223.

31. Routh, V.H. and C.J. Helke, *A novel technique for producing antibody-coated microprobes using a thiol-terminal silane and a heterobifunctional crosslinker.* Journal of Neuroscience Methods, 1997. **71**(2): p. 163-168.
32. Shriver-Lake, L.C., B. Donner, R. Edelstein, K. Breslin, S.K. Bhatia, and F.S. Ligler, *Antibody immobilization using heterobifunctional crosslinkers.* Biosensors & Bioelectronics, 1997 **12**(11): p. 1101-1106.
33. Dordi, B., H. Schonherr, and G.J. Vancso, *Reactivity in the Confinement of Self-Assembled Monolayers: Chain Length Effects on the Hydrolysis of N-Hydroxysuccinimide Ester Disulfides on Gold.* Langmuir, 2003. **19**: p. 5780-5786.
34. Grubor, N.M., R. Shinar, R. Jankowiak, M.D. Porter, and G.J. Small, *Novel biosensor chip for simultaneous detection of DNA-carcinogen adducts with low-temperature fluorescence.* Biosensors and Bioelectronics, 2004. **19**(6): p. 547-556.
35. Soultani-Vigneron, S., V. Dugas, M.H. Rouillat, J. Fedolliere, M.C. Duclos, E. Vnuk, M. Phaner-Goutorbe, V. Bulone, J.R. Martin, J. Wallach, and J.P. Cloarec, *Immobilisation of oligo-peptidic probes for microarray implementation: Characterisation by FTIR, Atomic Force Microscopy and 2D fluorescence.* Journal of Chromatography B, 2005. **822**: p. 304-310.
36. Tyan, Y.-C., S.-B. Jong, J.-D. Liao, P.-C. Liao, M.-H. Yang, C.-Y. Liu, R. Klauser, M. Himmelhaus, and M. Grunze, *Proteomic Profiling of Erythrocyte Proteins by Proteolytic Digestion Chip and identification Using Two-Dimensional Electrospray Ionization Tandem Mass Spectrometry.* Journal of Proteome Research, 2005. **4**: p. 748-757.
37. Warner, W.S., B.J. Tenge, J.M. Hungerford, and D.E. Honigs, *Diffuse reflectance infrared Fourier Transform spectroscopic characterization of a silica-immobilized N-hydroxysuccinimide active ester crosslinking agent and its precursors.* Analytical Biochemistry, 1989. **176**(1): p. 137-149.
38. Shen, G., M.F.G. Anand, and R. Levicky, *X-ray photoelectron spectroscopy and infrared spectroscopy study of maleimide-activated supports for immobilization of oligodeoxyribonucleotides.* Nucleic Acids Research, 2004. **32**(20): p. 5973-5980.
39. Shen, G., A. Horgan, and R. Levicky, *Reaction of N-phenyl maleimide with aminosilane monolayers.* Colloids and Surfaces B: Biointerfaces, 2004. **35**: p. 59-65.
40. Xiao, S.-J., M. Textor, and N.D. Spencer, *Covalent attachment of cell-adhesive, (Arg-Gly-Asp)-containing peptides to titanium surfaces.* Langmuir, 1998. **14**: p. 5507-5516.
41. Xue, C.-Y. and K.-L. Yang, *Chemical Modifications of Inert Organic Monolayers with Oxygen Plasma for Biosensor Applications.* Langmuir, 2007. **23**: p. 5831-5835.
42. Simonian, A.L., A. Revzin, J.R. Wild, J. Elkind, and M.V. Pishko, *Characterization of oxidoreductase–redox polymer electrostatic film assembly on gold by surface plasmon resonance spectroscopy and Fourier transform infrared–external reflection spectroscopy.* Analytica Chimica Acta, 2002. **466**: p. 201-212.
43. Liu, Z. and M.D. Amiridis, *FT-IRRAS spectroscopic studies of the interaction of avidin with biotinylated dendrimer surfaces.* Colloids and Surfaces B: Biointerfaces, 2004. **35**: p. 197-203.

44. Liu, Z. and M.D. Amiridis, *Quantitative FT-IRRAS spectroscopic studies of the interaction of avidin with biotin on functionalized quartz surfaces.* Journal of Physical Chemistry B, 2005. **109**: p. 16866-16872.
45. Pradier, C.-M., M. Salmain, Z. Liu, and G. Jaouen, *Specific binding of avidin to biotin immobilised on modified gold surfaces - Fourier transform infrared reflection absorption spectroscopy analysis.* Surface Science, 2002. **502-503**: p. 193-202.
46. Yam, C.-M., C. Pradier, M. Salmain, P. Marcus, and G. Jaouen, *Binding of Biotin to Gold Surfaces Functionalized by Self-Assembled Monolayers of Cystamine and Cysteamine: Combined FT-IRRAS and XPS Characterization.* Journal of Colloid and Interface Science, 2001. **235**: p. 183-189.
47. Bell, R.J., *Introductory Fourier Transform Spectroscopy*. 1972, New York: Academic Press, Inc.
48. Griffiths, P.R., *Chemical Infrared Fourier Transform Spectroscopy*. Chemical Analysis: A series of monographs on analytical chemistry and its applications, ed. P.J. Elving and J.D. Winefordner. 1975, New York: John Wiley & Sons.
49. Harris, D.C. and M.D. Bertolucci, *Symmetry and spectroscopy: An introduction to vibrational and electronic spectroscopy*. 1978, New York: Oxford University Press, Inc.
50. Stuart, B., W.O. George, and P.S. McIntyre, *Modern Infrared Spectroscopy*. Analytical Chemistry by Open Learning, ed. D.J. Ando. 1998, New York: John Wiley & Sons Ltd.
51. Herres, W. and J. Gronholz, *Understanding FT-IR Data Processing.* Comp. Appl. Lab., 1984. **2**: p. 216.
52. *Nicolet FTIR User's Guide*, Thermo Electron Corporation. p. 63.
53. *Alexa Fluor® 488 Protein Labeling Kit*. 2006, Molecular Probes, Inc. (Invitrogen): http://probes.invitrogen.com/media/pis/mp10235.pdf.
54. Guilbault, G.G., *Practical Fluorescence*. 2nd ed. Modern Monographs in Analytical Chemistry, ed. G.G. Guilbault. 1990, New York: Marcel Dekker, Inc.
55. Sharma, A. and S.G. Schulman, *Introduction to Fluorescence Spectroscopy*. Techniques in Analytical Chemistry. 1999, New York: John Wiley and Sons, Inc.
56. Wang, X.F. and B. Herman, *Fluorescence Imaging Spectroscopy and Microscopy*. Chemical Analysis: A Series of Monographs on Analytical Chemistry and its Applications, ed. J.D. Winefordner. 1996, New York: John Wiley and Sons, Inc.
57. McCrackin, F.L., E. Passaglia, R.R. Stromberg, and H.L. Steinberg, *Measurement of the Thickness and Refractive Index of Very Thin Films and the Optical Properties of Surfaces by Ellipsometry.* Journal of Research of the National Bureau of Standards - A. Physics and Chemistry, 1963. **67A**(4): p. 363-377.
58. *Ellipsometry Basic Principles*. [cited; Available from: http://www.horiba.com/scientific/products/ellipsometers/core-technologies/basic-principles/?L=0tx_horibafeuserregister_pi1[cmd]=create.
59. *What is Ellipsometry?* [cited; Available from: http://ice.prohosting.com/~jwah /ellipsometry.html.

CHAPTER 2: INFRARED CHARACTERIZATION OF BIOTINYLATED SILICON OXIDE SURFACES, SURFACE STABILITY AND SPECIFIC ATTACHMENT OF STREPTAVIDIN

Accepted for publication: Norman A. Lapin and Yves J. Chabal, Infrared Characterization of Biotinylated Silicon Oxide Surfaces, Surface Stability, and Specific Attachment of Streptavidin, J. Phys. Chem. B, Accepted, 2009.

2.1 Abstract

Biotinylation of silicon oxide surfaces, surface stability and evolution of these functionalized surfaces under bio-specific attachment of streptavidin were studied using Fourier Transform Infrared Spectroscopy. Adsorption and stability of species or changes in the resulting surfaces were monitored after each step of the attachment processes. The silicon oxide surface was initially derivatized by 3-aminopropyltriethoxysilane (APTES) and the quality of the 3-aminopropylsiloxane (APS) surface was monitored using the Si–O–Si and Si–O–C region of its vibrational spectrum. A strong correlation between surface quality and pre-silanization atmospheric moisture content was established. The vibrational fingerprint of biotinylation was determined, both for physisorption and chemisorption to the surface. A new band (i.e. not previous associated with biotin) at ~1250 cm^{-1} was identified as a vibrational mode of the biotin ureido group, making it possible to track changes in the biotinylated surface in the presence of streptavidin. Some of the biotin ureido at the surface was found to be affected by the protein adsorption and rinse steps while remaining chemisorbed to the surface. The stability of the APS was found to impact the behavior of the biotinylated surface (measured using the Si–O–Si/Si–O–C and ~1250 cm^{-1} absorption bands respectively).

2.2 Introduction

The biotin-(strept)avidin system (parentheses denote either of two analogues) is a widely used intermediate between the surface and the active biolayer. It is also employed as a model system to study biorecognition events between proteins and other biomolecules [1]. Biomolecules such as proteins and DNA can be easily biotinylated and bound to (strept)avidin coated surfaces (Scheme 2.1). The biotin-avidin system is the most stable non-covalent biological binding couple known, with a binding affinity of 10^{15} M^{-1} for free complexes. This binding couple is highly stable under a wide range of conditions, including extreme pH, salt concentration and temperature. In a study of multiple attachment methods the biotin-streptavidin system mediated the greatest degree of homogenous binding and surface coverage of antibodies compared with other attachment methods, although antibody specific activity was not improved significantly [2].

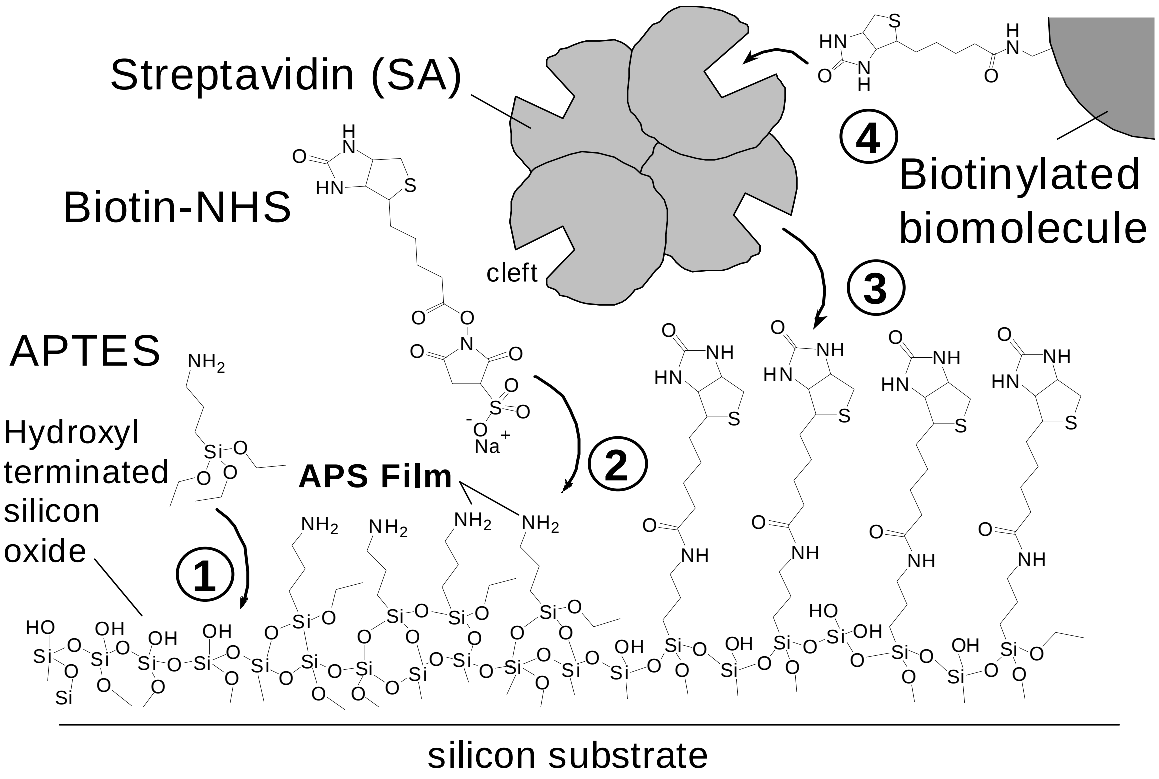
Streptavidin (SA)
Biotin-NHS
APTES
Hydroxyl terminated silicon oxide
APS Film
cleft
①
②
③
④
Biotinylated biomolecule
silicon substrate

Scheme 2.1. Steps to attach biomolecules to silicon oxide surfaces.
The APTES molecules are covalently bound to silicon oxide forming a 3-aminopropyl-siloxane (APS) film with Si-O-Si bonds to the surface (1), biotin-NHS is covalently bound to the amine-terminated surface forming amide bonds (2), SA is biospecifically attached to biotin via the SA cleft (3), then biotinylated biomolecules can be bio-specifically attached to SA (4).

Streptavidin (SA) can be bound to a surface via biotin or covalent linkage, but attachment to biotinylated surfaces provides both increased stability and organization of the SA film at the surface [3]. A study employing both surface plasmon resonance (SPR) and quartz crystal microbalance with energy dissipation monitoring (QCM-D) demonstrated that a streptavidin layer bound to a surface via biotin contained fewer trapped water molecules and was hence more compact than a SA layer attached covalently to a surface, suggesting greater organization of the streptavidin surface bound via biotin [4].

IR spectroscopy is a highly sensitive technique that yields direct information about the chemical bonds formed and broken in surface reactions. A better understanding of the underlying surface chemistry of biological assays is essential to controlling the quality and properties of assay surfaces. IR spectroscopy has been employed previously to characterize the chemical attachment of biotin to inorganic surfaces modified with a variety of chemical functionalities as well as to quantify the amount of SA specifically bound to such surfaces. Attempts have also been made to identify and/or quantify unreacted biotin derivatives physisorbed at these surface as well as SA non-specifically bound to such surfaces [5-9]. Quantification of SA at the surface was achieved through use of an alkyne dicobalt hexacarbonyl probe that labeled SA outside of the region of absorption by organic compounds (1400-1700 cm^{-1}), avoiding interference [5-8].

This is the only published study that employs Fourier Transform Infrared Spectroscopy (FTIR) in transmission geometry on a planar surface to study surface biotinylation and subsequent attachment of SA. Transmission FTIR is highly sensitive at planar surfaces and is further enhanced when IR is incident on the surface at the Brewster angle, increasing transmission of the p-polarized component of infrared light. Nitrogen purging of the spectrometer sample compartment and mathematical water subtraction further enhance the clarity of vibrational modes of interest above interference and noise in this study.

Furthermore, in previous IR studies, biotinylation of surfaces has not been controlled for atmospheric moisture (critical for silane-based attachment [10, 11]), nor has physisorbed biotin derivative been completely removed from the surface in the rinse step [5-8, 12]. These factors may affect bioassay surface quality. In this study, surface aminosilanization was performed under anhydrous conditions and biotinylated surfaces were sonicated after biotin attachment to aminosilane to remove all physisorbed biotin derivative. It is hypothesized that IR features associated with these and similar factors can be tracked at each stage of surface attachment and indicate surface quality. Various features identified at each surface modification step are correlated with each other or with initial atmospheric conditions suggesting that conditions at prior steps affect those at subsequent steps. For example, pre-silanization atmospheric moisture is taken into account as a continuous variable, not done previously for the characterization of silane adsorption to surfaces.

The scope of this study is limited to the characterization of biotinylated surfaces and the effect that streptavidin attachment and subsequent rinsing procedures have on these surfaces. Hence, this study aims to characterize Steps 1-3 of Scheme 1, and in accordance with the premise that molecular underlayers affect the organization and/or function of overlayers, show a relationship between changes in the biotinylated and APS layers. Not noted in previous studies is the observation that surface-attached biotin may undergo changes as a result of the protein adsorption and/or rinse steps. This finding is explored quantitatively through the identification of a low frequency biotin feature to avoid interference between biotin and protein bands present in the same region of IR absorption.

2.3 Experimental Methods

The following procedures were also used for sample preparation and data collection for Chapter 3, unless otherwise stated.

Reagents. All purchases are from Sigma-Aldrich unless otherwise noted. 3-aminopropyltriethoxysilane (APTES), Biotin 3-sulfo-N-hydroxysuccinimide ester sodium salt (biotin-NHS), biotin, toluene (anhydrous, 99.8%), Streptavidin (SA) from *Streptomyces avidinii*, Dulbecco's Phosphate Buffered Saline (PBS), Tween20®. All reagents were used as received unless otherwise noted.

Substrate. Float Zone Si(100) silicon wafers initially passivated by a layer of native oxide (~65 Angstroms) were cut to dimensions 1.5×3.8 cm.

Preparation of amine-terminated surfaces. Attachment of SA to a biotinylated silicon oxide surface begins with silanization of the silicon oxide surface to prepare it for chemical modification with biotin. To prepare the oxide surface for silanization, the wafer was cleaned in a solution of water:hydrogen peroxide:ammonium hydroxide (4:1:1) at 80° C for 10 minutes to remove organic contaminants (SC1). In the process, 10-15 Angstroms of silicon oxide was removed from the surface and reformed. After copious rinsing with deionized (DI) water (18 MΩ-cm), this clean was followed by a second similar clean, where the base was replaced by hydrochloric acid for the removal of metal particles from the surface, with no additional oxide formation (SC2). The wafer was then rinsed in DI water as above, and dried under a stream of nitrogen gas. All glassware was cleaned in SC1, rinsed copiously with DI water and dried under a nitrogen stream. Glassware prepared for use in the dry box was subsequently heated to 200 ^{o}C for 5-10 minutes to decrease surface water layers.

After collecting reference spectra of the oxide surface, the silicon wafers were transferred to a dry box. To silanize the oxide surface (i.e., form an APS surface), the wafer was submerged in 0.1 % APTES in anhydrous toluene. Anhydrous toluene was pre-heated to 110°–120°C and APTES pipetted into the test tube, followed immediately by the wafer. After 20 or more hours (times at which the surface has reached saturation [13]), the wafer was removed from the solution, rinsed copiously with anhydrous toluene and dried under a stream of nitrogen gas.

Biotinylation of amine-terminated surfaces. After silanization, biotin-NHS was chemically attached to the APS-terminated surface. Fresh solutions of biotin-NHS in DI water with a concentration ranging from 2.5 to 4.0 mg/ml were transferred to one side of the wafer situated on a minimally-contacting Teflon® stand, via pipette. The wafer on the stand was sealed in a humidity chamber to prevent evaporation of the biotin-NHS solution for 60 minutes. The wafer was then rinsed copiously with DI water and subsequently sonicated in DI water for ~10 to 15 minutes.

Bio-specific attachment of streptavidin to biotinylated surfaces. Bio-specific attachment of streptavidin to the biotinylated surface was performed by exposing one side of the wafer to 100 μg/ml streptavidin in phosphate buffered saline (PBS, pH 7.4) for adsorption times ranging from one to 60 minutes for various experiments. The setup to attach streptavidin to the biotinylated surface, is analogous to that for biotinylation. The wafer was subsequently rinsed about four times in a 0.05% solution of Tween20® (Polyethylene glycol sorbitan monolaurate) in PBS (PBST), one minute per rinse under constant agitation at 150-200 shakes per minute to remove non-specifically bound streptavidin from the surface, followed by an additional four rinses in PBS under the same agitation. The total rinse time was about 15 to 20 minutes. Samples were then rinsed briefly in DI water and dried under a nitrogen stream.

Data Collection. Immediately following drying by a stream of nitrogen after each adsorption step, FTIR spectra were collected on a Thermo® 760 FTIR spectrometer at a 4 cm^{-1} resolution for a minimum of 1000 scans (~20 min data collection).

Additional procedure for pre-heated samples. After samples were dried under a stream of nitrogen, they were placed into a clean, dried glass test tube and heated to about 200 ^{o}C for 10 to 15 minutes to reduce the amount of physisorbed water on the surfaces. The moment heating of the wafer was stopped, the wafer was cooled by blowing a stream of nitrogen gas into the test tube for one minute before immediately sealing the test tube with a screw-type cap. The wafers in the test tubes were then stored in the dry box prior to APTES adsorption.

Non-specific binding experiments. To observe non-specific binding of SA to a biotinylated surface, the active sites of SA were blocked with biotin. SA was incubated with an excess of biotin for three hours to block its active sites or “clefts”. The solution was then filtered to remove free biotin using gel chromatography, by pouring the solution into an Econo-Pac10DG desalting column (Biorad Laboratories, Hercules, California) packed with Bio-Gel® P-6DG gel, excluding solutes greater than 6000 daltons, which come out first. The first 3 ml fraction was collected at the bottom of the column containing only biotin-blocked SA. This solution was then adsorbed to the biotinylated side of a silicon wafer for 60 minutes, followed by the same rinsing protocol as for active SA (PBST/PBS/DI water) and dried under a stream of nitrogen gas.

Physisorption of biotin-NHS. To obtain a complete spectrum of unreacted biotin-NHS, biotin-NHS was dissolved in water and adsorbed onto the surface of an SC1/SC2-cleaned oxide surface of a silicon wafer. After 30-60 minutes, the liquid was removed by tilting the wafer on its side and drying it under nitrogen, leaving a film of biotin-NHS.

2.4 Results

2.4.1 Step 1: Aminosilanization: Characterization of amine-derivatized silicon oxide surfaces; observation and control of silane growth and stability.

Following Scheme 1, the silicon oxide surfaces are first modified with APTES. Representative FTIR spectra of silicon oxide surfaces exposed to APTES and referenced to the respective pre-treated surfaces show bands peaking near 1040 cm^{-1} and 1140 cm^{-1} (Figure 2.1). These bands correspond to a combination of Si-O-Si vibrational modes including those of bonds formed between the silane and oxide surface, crosslinking between silane molecules at the surface, polymerization of silane and unreacted Si-O-C (ethoxy) groups [13]. Bands in the region of 2800-2990 cm^{-1} (centered at 2930 cm^{-1}) and ~1500-1700 (centered near 1580 cm^{-1}) are assigned to CH_2 stretching and NH_2 bending, respectively [13, 14]. Surprisingly, the Si-O-Si band area in APS spectra (Figure 2.1) increases significantly from winter to summer indicating that more APS is adsorbed at the surface during the summer. The intensity of most components of the Si-O-Si band region is dependent on humidity.

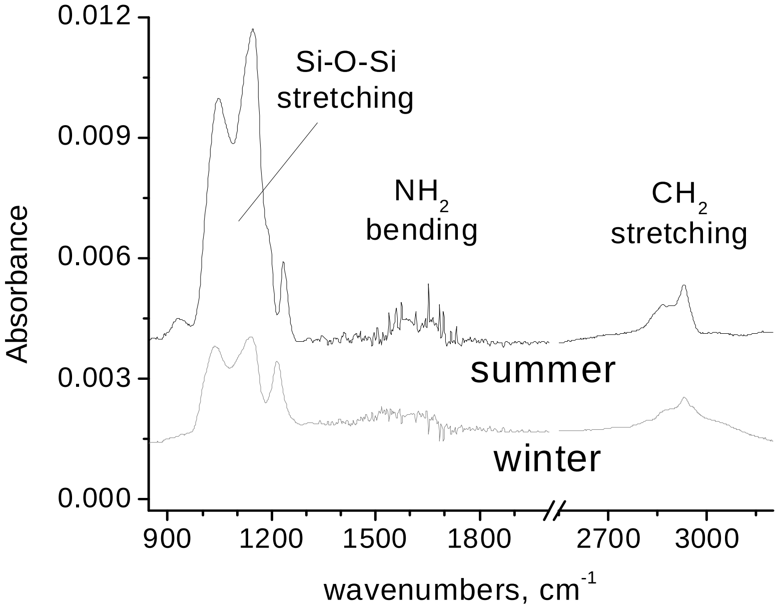

Figure 2.1. Representative FTIR spectra of APTES chemically attached and referenced to silicon dioxide surfaces in winter and summer. The Si-O-Si band area increase from winter to summer indicates that more APS is adsorbed at the surface in summer due to greater humidity.

Using the area under the Si-O-Si absorbance bands (integrated over the 900-1280 cm^{-1} region) as a measure of the amount of APTES adsorbed at the surface, the growth of the APS is first investigated. APS growth was monitored as a function of outdoor atmospheric moisture content prior to exposure of the silicon oxide surface to APTES in anhydrous solvent in a dry box. Outdoor humidity and temperature values are obtained from a website that collects data from a local weather center (http://weathersource.com) unless otherwise stated. These data are processed to obtain values of air moisture content using an online psychrometric calculator (WebPsycH Calculator®, Linric Company, Bedford, NH) at http://www.envirochex.com/psychro.htm. At low moisture content (< 3 g H_2O/m^3 air), Si-O-Si area is constant over a range of moisture values (Figure 2.2). In contrast, at high moisture content (> 7 g H_2O/m^3 air) both Si-O-Si area and the fluctuation in this area increase with increasing moisture content.

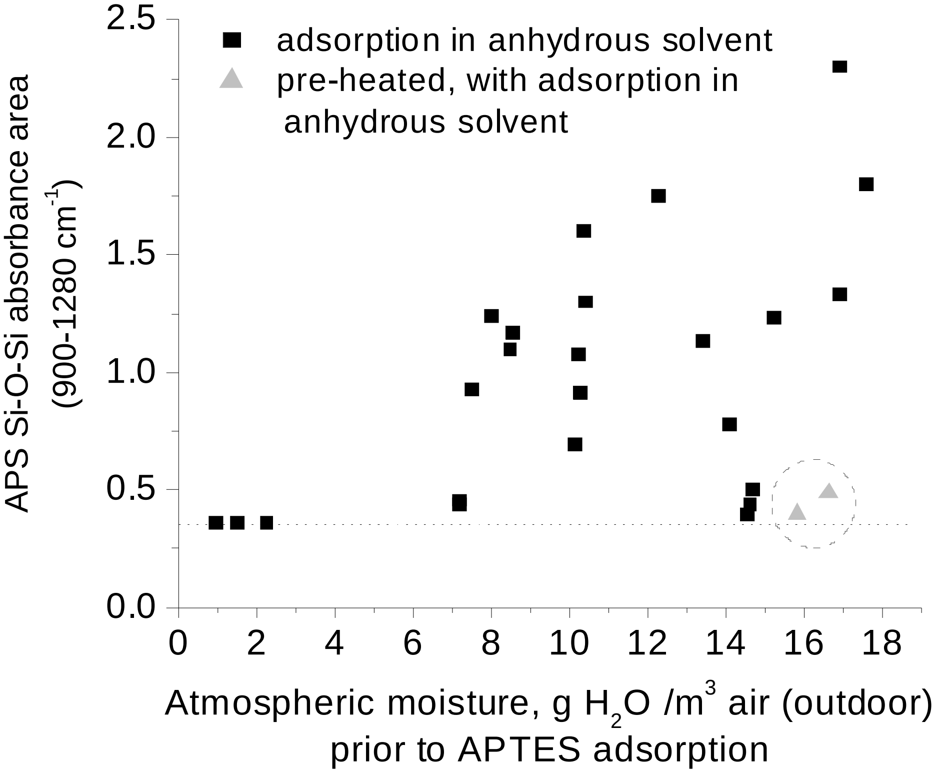

Figure 2.2. Amount of APS adsorbed to silicon oxide surface (Si-O-Si region, ~900-1280 cm^{-1} band area) versus pre-silanization atmospheric moisture content (outdoor humidity reading with indoor experiment). Black squares indicate APTES adsorption in anhydrous solvent. Additional samples were pre-heated to 100-200 °C, flushed with dry nitrogen gas, then sealed from atmospheric moisture prior to exposure to APTES in anhydrous solvent (circled triangles).

To explore the ability to limit APS film growth under humid pre-silanization conditions, samples were heated prior to entry into the dry box to lessen the effects of atmospheric moisture. Two of the data points in Figure 2.2 (triangles) are for samples heated for 5 to 10 minutes between 100 and 200 °C and kept under nitrogen continuously through sample entry into the dry box and subsequent APTES adsorption. Although these adsorptions took place under humid outdoor conditions, the Si-O-Si absorption areas are near those at low outdoor moisture values, demonstrating that it is possible to limit the amount of silane molecules attached to the surface.

The stability of the APS layer is the second measure of surface quality at this stage of attachment. It is determined by measuring the change in Si-O-Si band area after exposure of the APS surface to biotin-NHS in deionized (DI) water for one hour, followed by 10-15 minutes of sonication in DI water. A more stable surface shows less percent change in intensity (i.e., lower percent loss in APS Si–O–Si band intensity after rinsing and sonication). Figure 2.3 shows that the intensity of the Si-O-Si band is more stable when the moisture content (exposure of the sample to atmosphere prior to silanization in the dry box) is lower.

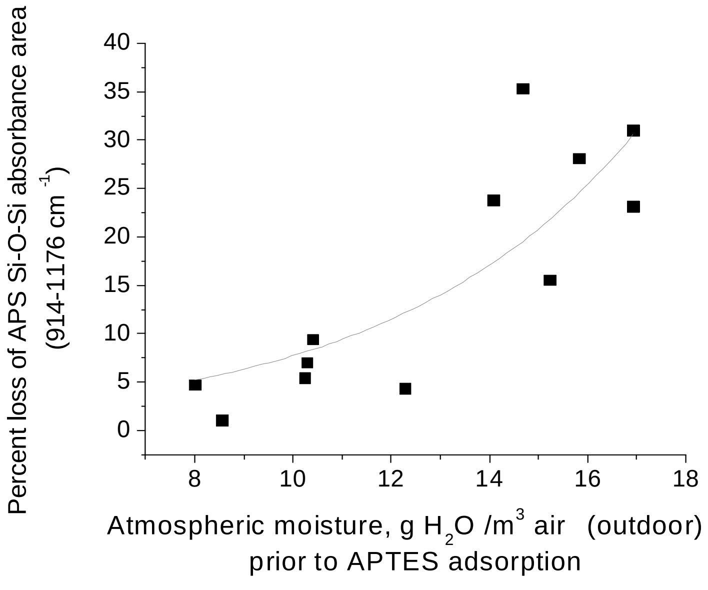

Figure 2.3. APS Si-O-Si band area percentage loss (taken as a measure of surface instability) after the APS surface was exposed to biotin-NHS in deionized water for 60 min and subsequently sonicated in deionized water for 10-15 min versus pre-silanization atmospheric moisture content (outdoor humidity reading with indoor experiment). Least squares fit; R^2 =0.69.

2.4.2 Step 2: Biotinylation: Surface Characterization and the Effects of Sonication

A representative spectrum of the amine-terminated surface exposed to biotin-NHS and referenced to the pre-exposed surface is shown in Figure 2.4, spectrum A. Here biotin-NHS is chemically attached to the amine-terminated surface. Bands unique to reacted biotin-NHS are present at 1540 cm^{-1} and ~1660 cm^{-1} , assigned to the amide II (N-H bend + C-N stretch) and amide I (C=O stretch) vibrational modes respectively and indicate the amide bond formed between biotin and the surface [5-8, 12, 14].

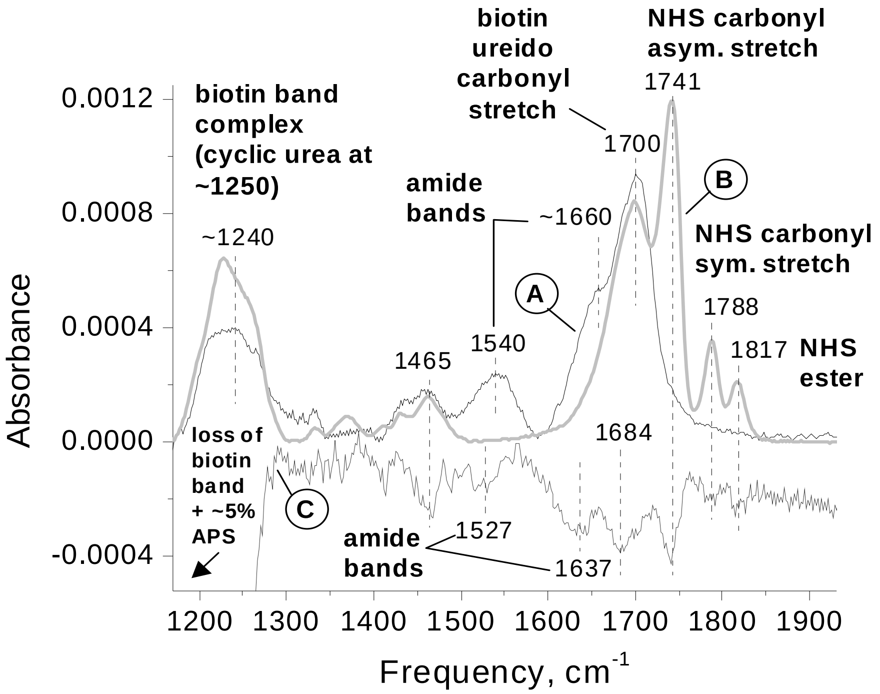

Figure 2.4. Representative FTIR spectra of biotin-NHS chemisorption and sonication. An APS surface exposed to biotin-NHS (for covalent attachment) and referenced to the pre-exposed APS surface (A), a silicon oxide surface exposed to biotin-NHS (for physisorption) and referenced to the pre-exposed silicon oxide surface (B), and a sonicated biotin-NHS treated APS surface referenced to the same biotinylated surface before sonication (amplified 5x) (C). Bands in spectrum C are negative due to decrease in amount of molecules after sonication.

To separate the vibrational modes of biotin-NHS moieties reacting with the surface from those not reacting with the surface, a representative spectrum of unreacted biotin-NHS physisorbed to a silicon oxide surface is obtained (Figure 2.4, spectrum B, reduced 2.7x) for comparison to spectrum A. Bands unique to unreacted biotin-NHS (not present in spectrum A) are at 1741, 1788 and 1818 cm^{-1} assigned to the asymmetric and symmetric stretch of the succinimide carbonyls and the ester of the NHS moiety respectively [15, 16]. The NHS bands present in this spectrum are not present in the chemisorbed biotin spectrum A, indicating loss of the NHS moiety in the reaction of biotin-NHS with the surface.

The features that are common to spectra A and B are the band complex centered near 1240 cm^{-1}, the band at 1465 cm^{-1} and the band at 1700 cm^{-1}. These bands are present in both chemisorbed and physisorbed biotin-NHS, suggesting that they correspond to modes of the nonchemically reactive part of biotin-NHS: the alkyl chain and the biotin fused rings. The band at 1465 cm^{-1} is assigned to the CH_2 scissor mode of the alkyl chain linking the biotin fused rings to the NHS moiety [14], while the band at 1700 cm^{-1} is assigned to the ureido carbonyl stretch mode [12, 14, 17] of biotin-NHS. The low frequency band complex at 1240 cm^{-1} has not been noted in the literature previously for biotin and will be discussed in greater detail in the following results and discussion sections.

The effects of sonication after biotinylation are examined in spectrum C showing bands removed by sonication (amplified 5x for clarity). Spectrum C was generated by referencing a spectrum of the biotinylated surface before sonication (spectrum A before sonication, not shown) to the same surface after sonication (spectrum A). Spectrum C shows that bands of both chemisorbed biotin (amide bonds to surface at 1527 and 1637 cm^{-1}) and physisorbed biotin (at 1741, 1787 and 1815 cm^{-1}) have been removed from the surface after sonication. Since sonication cannot break chemical bonds at a surface, the origins of these bands will be examined further in the discussion section.

Bands removed by sonication that are present in both chemisorbed and physisorbed spectra (at ~1240, 1465 and 1684 cm^{-1} in spectrum C) are due to chemically unreactive parts of the biotin-NHS. Due to amplification of spectrum C the negative band at ~1240 cm^{-1} extends beyond the region shown. This negative band includes both a decrease in the biotin complex at 1240 cm^{-1} as well as an ~5% decrease in APS after sonication of the biotinylated surface. The percent decrease in APS is calculated from the decrease in the area of the IR region of APS (~950-1320 cm^{-1}) after sonication compared to the total area of the APS region prior to sonication.

It is interesting to note that the positions of the negative bands in spectrum C corresponding to amide and ureido bands are ~10-20 cm^{-1} lower in frequency than similar bands in spectrum A (covalently attached), whereas bands associated only with physisorbed biotin-NHS are at the same position in both spectra B and C. Estimating the amount of material removed by sonication, the absorption area under the bands in spectrum C from ~1500-1800 cm^{-1} is calculated to be about 10% of the area under the bands in the same region for covalently bound biotin in spectrum A.

2.4.3 Step 3: SA Adsorption: Effect of SA attachment and rinse steps on the biotinylated surface

Upon adsorption of SA to the biotinylated surface and subsequent rinsing with PBST/PBS/DI water, bands were observed at 1530 and ~1630-1690 cm^{-1}, indicative of protein adsorption (Figure 2.5**a**). The major band at 1640 cm^{-1} is due to beta-sheets, the major secondary structural component of SA [18]. In certain trials of protein adsorption and/or rinsing, negative IR bands at ~1250 and ~1685 cm^{-1} were observed in these spectra (Figure 2.5). To resolve the origin of these negative bands, biotinylated surfaces were exposed to biotin-blocked SA followed by rinsing (part **b** of Figure 2.5) or to a PBST/PBS/DI water rinse only (part **c** of Figure 5). The same occurrence of negative bands was observed in these trials to varying degrees and was most pronounced in rinse-only trials with no protein present.

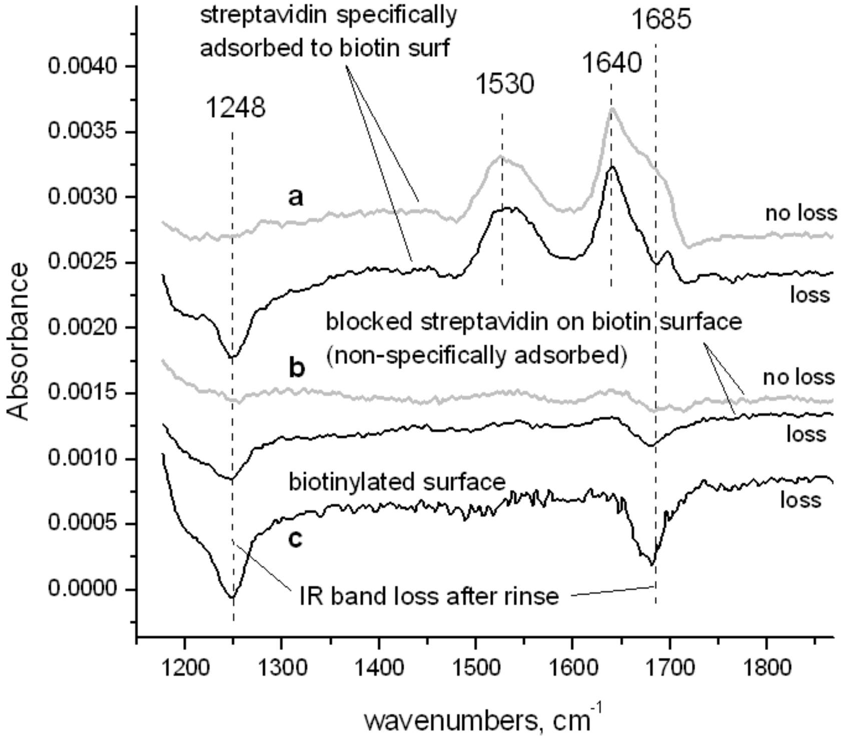

Figure 2.5. Representative FTIR spectra of biotinylated surfaces exposed to SA or rinse. Spectra of biotinylated surfaces exposed to SA and rinse step and referenced to pre-exposed biotinylated surfaces (a), biotinylated surfaces exposed to biotin-blocked SA and referenced to pre-exposed biotinylated surfaces (b), and a biotinylated surface rinsed with PBST/PBS/DI water referenced to same surface prior to rinse (c). "Loss" and "no loss" indicate presence or absence of band loss in these spectra. All samples were rinsed per Methods section protocol. All biotinylated reference surfaces were sonicated prior to spectra collection.

Figure 2.6 shows the spectrum of the same biotinylated surface as in Figure 2.5**c** before and after exposure to the rinse step. A part of the biotin band at 1685 cm^{-1} is observed to disappear after rinsing along with part of the complex at 1240 cm^{-1} (decreasing in intensity at 1254 cm^{-1}), while the aliphatic C-H scissor mode at 1459 cm^{-1} , the amide II band at 1542 cm^{-1} and amide I shoulder at ~1640 cm^{-1} do not noticeably decrease in intensity (Figure 2.6). The band at ~1250 cm^{-1} has been cited as a vibrational mode of a cyclic urea, the ring of which the ureido carbonyl is a part [14]. Hence, these data suggest that a change in the biotin fused rings has taken place due to the rinse and/or protein adsorption steps while the biotin remains attached to the surface.

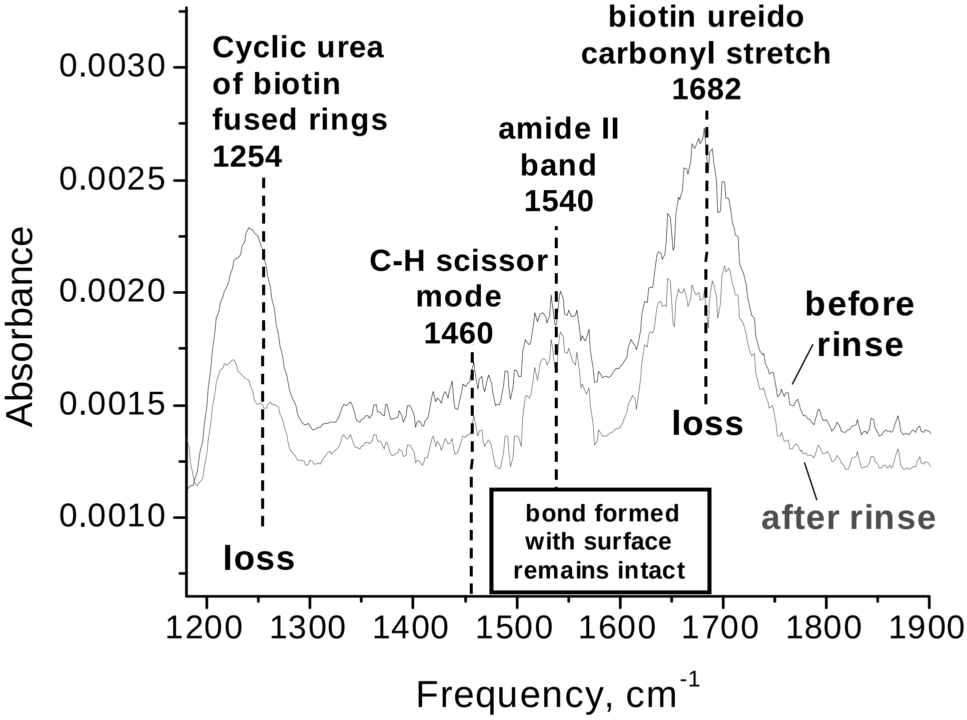

Figure 2.6. FTIR spectra of an APS surface exposed to biotin-NHS and rinse step. FTIR spectra of an APS surface exposed to biotin-NHS, referenced to the APS surface (top) and the same surface after rinsing with PBST/PBS/DI water, referenced to the APS surface (bottom). While spectral decrease in the biotin ureido is observed at 1254 and 1682 cm^{-1}, amide and aliphatic scissor mode band areas did not decrease.

The study of biotinylated surface exposure to SA is made difficult by the fact that protein IR bands of SA in the 1400-1700 cm^{-1} range interfere with bands of chemisorbed biotin in the same region. This overlap prevents quantification of the change in intensity of biotin IR modes after SA adsorption and rinse steps. Only the high frequency shoulder at ~1250 cm^{-1} (Figure 2.4, spectrum A) is outside of this region and is therefore selected to track changes in the biotinylated surface upon protein attachment and rinse.

Figure 2.7 shows a correlation between the change in intensity in the APS Si-O-Si modes (after the biotinylation step) and the change in intensity of the band at ~1250 cm^{-1} (after SA adsorption to and rinsing of the biotinylated surface). Data points for adsorption of biotin-blocked SA (open square with "X") and the surface subjected to the rinse step only (circle) also fit within this correlation.

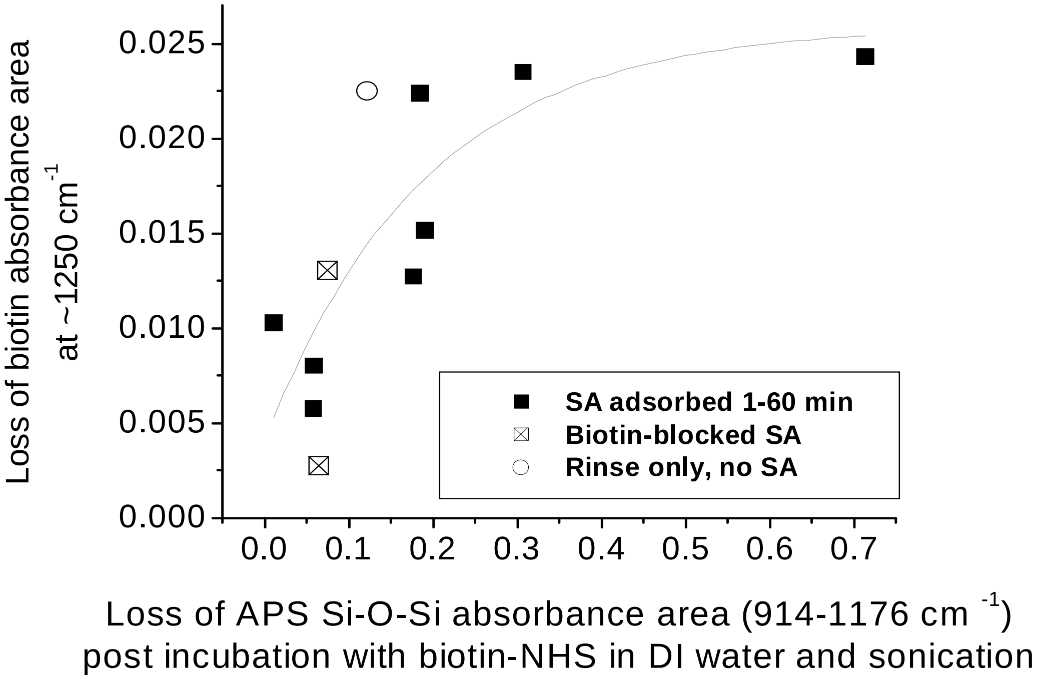

Figure 2.7. Loss of biotin band absorbance area with loss of APS absorbance area. Loss of biotin band absorbance area at ~1250 cm^{-1} after SA adsorption and PBST/PBS/DI water rinse (or rinse step without SA adsorption) versus APS Si-O-Si band area loss after exposure of the APS surface to biotin-NHS in DI water and subsequent sonication (black squares, open squares and open circle indicate SA specific adsorption, biotin-blocked SA adsorption and PBST/PBS/DI water rinse only, respectively). Least squares fit; $R^2 = 0.61$, all points included.

Table 2.1. IR band assignments for molecules present at each surface modification step.

APTES and APS			
frequency (cm^{-1})	assignments	References	
900-1280	Si-O-Si and Si-O-C stretching	[14, 19]	
1570-1590 vb	NH_2 deformation	[14]	
2930	CH_2 asymmetric stretch	[14]	
Biotin-NHS and biotinylated surface			
frequency	assignments	adsorption type	references
1043‡	unassigned	both	n/a
1074‡	C-H deformations on NHS succinimide ring	physical	[14]
1212‡	NHS C-N-C stretching mode	physical	[20, 21]
1240-1260*	Biotin ureido ring	both	[14]
~1660	Amide I (C=O stretch)	chemical	[5-8, 12, 14]
~1540	Amide II (NH deformation with C-N stretch)	chemical	[5-8, 12, 14]
1637	Amide I (attached to physisorbed APTES)	chemical	[5-8, 12, 14]
1527	Amide II (attached to physisorbed APTES)	chemical	[5-8, 12, 14]
1685-1700†	Biotin ureido carbonyl stretch	both	[14]
1741	NHS C=O asymmetric	physical	[15, 16]
1788	NHS C=O symmetric	physical	[15, 16]
1818	NHS ester	physical	[15, 16]
Streptavidin (SA)			
frequency	Assignments	references	
~1640	Amide I band	[5-8, 12, 14]	
~1540	Amide II band	[5-8, 12, 14]	

Bands for chemisorption of biotin-NHS are distinguished from those of physisorption.

*Assignments not previously noted for biotin.

†Bands assignments clarified. vb = very broad bands.

‡Assignments of spectra in Figure S1 of Supporting Information (Appendix, Section 2.9).

2.5 Discussion

In this section, we consider each adsorption step sequentially and use the band assignments of all spectra shown in the results section, as displayed in Table 1.

2.5.1 Step 1: Aminosilanization: Dependence of APS film growth and degradation on pre-silanization atmospheric moisture content.

At the APTES attachment stage of surface modification, we examine the surface quality in terms of growth of the Si-O-Si band area, an indicator of the amount of APTES adsorbed at the surface (Figure 2.2), and its percent intensity loss in the subsequent biotin attachment step (Figure 2.3). This section addresses the behavior of these features under a continuum of atmospheric moisture values.

Atmospheric moisture content is an important factor for the quality of aminosilanization. Although aminosilanization is performed with anhydrous solvents in a dry box, silane growth varies with exposure of the silicon oxide surface to atmospheric moisture prior to sample introduction to the dry box for silanization.

Moisture content can be divided into low and high regimes, where the growth behavior of APS films differs. Below a critical moisture of about 3 g H_2O/m^3 air, the Si-O-Si band area was low and remained constant with change in atmospheric moisture. This behavior suggests that film growth was self-terminating under these conditions. Above a critical moisture content of ~7 g H_2O/m^3 air, not only did the amount of silane at the surface increase with increasing air moisture, but the fluctuation in this amount increased as well. APS Si-O-Si absorbance area values ranged widely from small to large, in some cases even close to absorbance areas as small as those under low moisture conditions.

First, we examine mechanisms for high moisture conditions. As the moisture content of air increases, an increasing amount of water molecules adsorbs to the oxide surface [22]. Water can adsorb to silicon oxide when free hydroxyls are available, the maximum density of which is estimated at 5 hydroxyls/nm^2 [11]. For a surface with 3 hydroxyls/nm^2, the maximum density of water molecules adsorbed as a monolayer is estimated to be 2.5 to 4 water molecules/nm^2. Beyond this degree of surface hydration, multilayers are believed to be present [23]. Hence, the thickness of the water layer that adsorbs to the surface is a function of both density of surface hydroxyls and moisture content of the air. Difficulty controlling these parameters in high humidity environments may explain the fluctuation in amount of APS at the surface.

In previous studies, silane film growth was shown to be dependent on atmospheric moisture, but only in terms of relative humidity and not across a continuous range of values. LeGrange et al. reported a doubling of octadecylsilane film thickness from a relative humidity of 10-30% in winter to 50-60% in summer on dehydrated silica [10]. Even though moisture was initially removed from the surface by heating, the amount that re-adsorbed to the surface from the atmosphere between the time of dehydration and the time of silane deposition affected silane growth.

In this study, the circled data points (triangles) in Figure 2.2 are for samples preheated for 5-10 minutes at ~200 ^{o}C then flushed with nitrogen and kept continuously in a nitrogen environment until APTES molecules are adsorbed to the surface. In contrast to the report by Legrange et al., the moisture content that the sample surface is exposed to is kept low even in the high humidity of summer. It was previously reported that pre-heating silicon oxide to a similar temperature resulted in complete removal of all surface water from silicon oxide surfaces [11]. Hence, it is probable that water at the surface of our pre-heated samples is minimized or eliminated as well. Since surface hydration is very difficult to control, dehydration below a critical value may be an effective method to limit the amount of aminosilanization of silicon oxide surfaces.

The amount of moisture in the air prior to APTES deposition appears to have a destabilizing effect on the APS surface. As pre-silanization moisture increases, more APS desorbs from the surface after the biotinylation and sonication steps (both in DI water) as indicated by percentage loss of Si-O-Si band intensity (Figure 2.3). An explanation for this behavior is based on both increased polymerization and detachment of APS when the water layer at the surface is thicker. A thicker water layer may cause increased APTES polymerization at the surface and hence covalent attachment to the surface of large polymerized silane clusters. Due to packing constraints, polymerized films are less dense than self-terminating thinner films and hence may be more prone to hydrolysis [13]. Each cluster contains many Si-O-Si bonds (not related to surface bonding) and hence the detachment of increasingly larger clusters would show increasing Si-O-Si intensity loss. Alternatively, a thicker water layer may prevent the silane from attaching covalently. Therefore, more silane and silane clusters may be physisorbed at the surface and subsequently removed in the sonication step.

In summary, these results show that APS film growth and desorption are highly sensitive to atmospheric moisture prior to silanization of the silicon oxide surface. However, this sensitivity may be dependent on the preparation of the starting oxide surface. In this study, native silicon oxide surfaces of thickness of ~65 Angstroms were used. Yet in a related study, pre-silanization humidity dependence was not observed on samples from which the native oxide was removed by hydrofluoric acid treatment and regrown by wet chemical oxidation (~10-15 Angstroms thick) [13]. Such chemically oxidized surfaces differ from the former in terms of surface roughness, oxide density and number of hydroxyls available for silane attachment, factors that may affect the thickness of the water layer at the surface during silane attachment as well as the ability of the silane to bind covalently to the substrate. Both studies have value in different applications: a native silicon oxide surface may behave more closely to glass (used in biotechnology), while the study of thinner oxides may be more applicable to modification of semiconductor surfaces (used in the microelectronics industry or in sensor applications).

2.5.2 Step 2: Biotinylation: Distinguishing chemisorbed from physisorbed biotin-NHS and the effects of sonication.

While the assignment of bands observed at ~1540 cm^{-1} and ~1660 cm^{-1} to amide vibrations indicating covalent attachment of biotin to amine-terminated surfaces is widely accepted [5-8, 12], identification of the biotin ureido carbonyl vibrational mode has been less clear in the literature [5-8, 12]. In a number of IR reflection studies, the biotin ureido band near 1700 cm^{-1} was not observed [5-8]. This study, however, confirms the presence and assignment of this band by comparing physisorbed to chemisorbed forms of biotin-NHS.

Furthermore, in some cases in the literature where the amide I and II bands are small or undetected, it is possible that much of the biotin-NHS is instead physisorbed to the surface. In the spectra of surfaces exposed to biotin-NHS in this study, the band at ~1740 cm^{-1} is due to the carbonyl stretch of the unreacted NHS moiety [15, 16] and thus indicates the presence of physisorbed biotin-NHS. However, in spectra exhibited in the literature, a number of references have assigned this or nearby higher frequency bands to the carboxylic acid moiety of unreacted biotin [5-8, 12]. In these studies, to produce biotin-NHS, biotin was reacted with a succinimide-based compound such as N,N-diisopropylethylamine (DIPEA) or O-(Nsuccinimidyl)-N,N,N,N',N"-tetraethyluronium (TSTU), replacing the carboxylic acid of biotin with an NHS ester. Depending on the degree to which the reaction to form biotin-NHS took place, bands observed from 1740-1770 cm^{-1} may instead be due to NHS carbonyl stretch vibrations or due to a combination of this vibrational mode with the carboxylic acid group.

Sonication plays an important role in removal of physisorbed biotin derivative. Figure 2.4, spectrum C shows negative bands corresponding to removal of both the NHS moiety and ureido carbonyl, indicating that physisorbed biotin-NHS is removed from the surface. Furthermore, the absence of NHS bands in the spectrum of the biotinylated surface (Figure 2.4, spectrum A) indicates that no detectable physisorbed biotin remains at that surface. In addition to these features, the intensity decrease in chemisorbed biotin features after sonication (negative amide bands in spectrum C) suggests that some of the biotin chemically bound to the surface could be removed. However, such removal is not possible with sonication. A more plausible explanation is that some of the biotin-NHS is attached covalently to physisorbed APTES or physisorbed APS film and is subsequently removed along with it. The 10-20 cm^{-1} red-shift of the negative amide and ureido bands in spectrum C suggests instead that the environments of these species are different from that of biotin covalently bound to a silicon oxide surface. In contrast, there is no frequency shift in the NHS bands of removed physisorbed biotin in spectrum C compared with physisorbed biotin-NHS bands in spectrum B. Hence, such shifts in vibrational modes may be a way to distinguish biotin that is chemically attached to the substrate from that chemically attached to physisorbed molecules.

2.5.3 Step 3: SA Adsorption: Change in the biotinylated surface upon SA adsorption.

Changes in the organization of the molecules of the biotinylated surface may affect the SA layer and hence the organization of the layer of functioning biomolecules that can attach to the SA layer. The presence of negative bands at ~1250 and ~1685 cm^{-1} in the spectra of specifically bound SA, blocked SA or biotinylated surfaces rinsed only (no SA adsorption) referenced to the pre-exposed biotinylated surface suggest that a change in the biotinylated surface results from this adsorption step (Figure 2.5). These negative bands occur in some but not all cases, suggesting variation in the quality of the biotinylated surface. Possible explanations for such intensity decreases include screening or chemical modification of the biotin ureido. Screening could be due to the proximity of SA to the surface and/or change in the organization or environment of the biotin molecules upon rinsing of the surface. Chemical modification may be less likely as it has only been observed previously under harsher conditions [24, 25]. Complete removal of biotin is unlikely since amide bands in the spectrum, indicative of chemical attachment of biotin to the surface, do not decrease in intensity (Figure 2.6).

Correlation between intensity decrease in the biotin ureido band at 1250 cm^{-1} during SA adsorption/rinse and decrease in intensity of APS in the preceding biotinylation step may suggest that the biotinylated surface is more susceptible to disorganization when attached to less stable APS surfaces (Figure 2.7). The degree to which APS is removed from the surface in the presence of water and hence the stability of its attachment to the surface is likely a reflection of the degree of organization of APS chains bound to the surface [13]. Furthermore, although APS film loss was directly dependent on air moisture prior to silanization, the lack of correlation between biotin ureido band decrease and air moisture further illustrates the complexity of the relationship between these layers.

2.6 Conclusions

In this study, we have shown how IR spectroscopy has made it possible to identify each step of a complex process, involving both covalent and physical attachment of molecules to the surface. We have shown that the attachment of APTES is sensitive to atmospheric moisture prior to anhydrous adsorption to the surface. We have further shown that changes in biotinylation of the surface are dependent on APS film stability. Stability of the APS film can be controlled to an extent by pre-heating of the silicon oxide surface and employing anhydrous adsorption conditions. Sonication is effective in removing physisorbed biotin prior to SA adsorption. We have shown that features associated with the moieties of physisorbed biotin can be used to distinguish covalent attachment of biotin derivative from derivative merely physisorbed to the surface. We have further identified a low frequency IR band of biotin that is not subject to interference from protein bands and can be effectively used to monitor the biotinylated surface during SA adsorption and rinsing. Although the mechanisms responsible for the observed molecular behavior at biotinylated surfaces are not well understood, there is a clear dependence of the properties of each layer on the chemical nature and quality of previously adsorbed layers.

As devices are scaled down and the need for improved assay sensitivity increases, finer control at the molecular level will likely be critical to device performance. This study describes a method for tracking and ultimately controlling the initial stages of bioassay surface modification.

2.7 Acknowledgements

This work was supported in part by the National Science Foundation (grant CHE-0415652) and in part by the National Institutes of Health (Kirschstein-NRSA Fellowship 5-T32-GM008339-18). The authors gratefully acknowledge Robert Pasternack and Sandrine Rivillon-Amy for their insightful input into discussion of the chemistry of APTES at the SiO_2 surface, Richard Ludescher for his insights into the behavior of biotin and SA at inorganic surfaces and Meng Li for discussion on APTES attachment under low moisture conditions.

2.8 References

1. Wilchek, M., E.A. Bayer, and O. Livnah, *Essentials of biorecognition: The (strept)avidin-biotin system as a model for protein-protein and protein-ligand interaction.* Immunology Letters, 2006. **103**: p. 27-32.
2. Vijayendran, R.A. and D.E. Leckband, *A quantitative assessment of heterogeneity for surface-immobilzed proteins.* Analytical Chemistry, 2001. **73**: p. 471-480.
3. Smith, C.L., J.S. Milea, and G.H. Nguyen, *Immobilization of nucleic acids using biotin-strept(avidin) systems.* Top Curr Chem, 2005. **261**: p. 63-90.
4. Su, X., Y.-J. Wu, R. Robelek, and W. Knoll, *Surface plasmon resonance spectroscopy & quartz crystal microbalance study of streptavidin film struct effects on biotinylated DNA assy and target DNA hybridization.* Langmuir, 2005. **21**: p. 348-353.
5. Liu, Z. and M.D. Amiridis, *FT-IRRAS spectroscopic studies of the interaction of avidin with biotinylated dendrimer surfaces.* Colloids and Surfaces B: Biointerfaces, 2004. **35**: p. 197-203.
6. Liu, Z. and M.D. Amiridis, *FT-IRRAS quantitative analysis of specific avidin adsorption on biotinylated Au surfaces.* Surface Science, 2005. **596**: p. 117-125.
7. Liu, Z. and M.D. Amiridis, *Quantitative FT-IRRAS spectroscopic studies of the interaction of avidin with biotin on functionalized quartz surfaces.* Journal of Physical Chemistry B, 2005. **109**: p. 16866-16872.
8. Pradier, C.-M., M. Salmain, Z. Liu, and G. Jaouen, *Specific binding of avidin to biotin immobilised on modified gold surfaces - Fourier transform infrared reflection absorption spectroscopy analysis.* Surface Science, 2002. **502-503**: p. 193-202.
9. Ye, L., R. Pelton, and M.A. Brook, *Biotinylation of TiO_2 nanoparticles and their conjugation with streptavidin.* Langmuir, 2007. **23**: p. 5630-5637.
10. LeGrange, J.D. and J.L. Markham, *Effects of Surface Hydration on the Deposition of Silane Monolayers on Silica.* Langmuir, 1993. **9**: p. 1749-1753.
11. Zhuravlev, L.T., *Concentration of Hydroxyl Groups on the Surface of Amorphous Silicas.* Langmuir, 1987. **3**: p. 316-318.
12. Yam, C.-M., C. Pradier, M. Salmain, P. Marcus, and G. Jaouen, *Binding of Biotin to Gold Surfaces Functionalized by Self-Assembled Monolayers of Cystamine and Cysteamine: Combined FT-IRRAS and XPS Characterization.* Journal of Colloid and Interface Science, 2001. **235**: p. 183-189.
13. Pasternack, R.M., S. Rivillon-Amy, and Y.J. Chabal, *Attachment of 3–(aminopropyl) triethoxysilane on silicon oxide surfaces: Dependence on solution temperature* Langmuir, 2008. **24**: p. 12963-12971.
14. Socrates, G., ed. *Infrared and Raman Characteristic Group Frequencies - Tables and Charts*. 3rd ed. 2001, John Wiley & Sons Ltd: West Sussex, England.
15. Frey, B.L. and R.M. Corn, *Covalent attachment and derivatization of poly(L-lysine) monolayers on gold surfaces as characterized by polarization-modulation FT-IR spectroscopy.* Analytical Chemistry, 1996. **68**: p. 3187-3193.
16. Voicu, R., R. Boukherroub, V. Bartzoka, T. Ward, J.T.C. Wojtyk, and D.D.M. Wayner, *Formation, Characterization, and Chemistry of Undecanoic Acid-*

Terminated Silicon Surfaces: Patterning and Immobilization of DNA. Langmuir, 2004. **20**: p. 11713-11720.

17. Hegde, S., S. Kapoor, S. Joshi, and T. Mukherjee, *Self-assembly of Ag nanoparticle–biotin composites into long fiberlike microstructures.* Journal of Colloid and Interface Science, 2006. **297**: p. 637-643.
18. Gonzalez, M., L.A. Bagatolli, I. Echabe, J.L.R. Arrondo, C.E. Argarana, C.R. Cantor, and G.D. Fidelio, *Interaction of Biotin with Streptavidin - Thermostabilty and conformational changes upon binding.* The journal of biological chemistry, 1997. **272**(17): p. 11288-11294.
19. Pasternack, R.M., S. Rivillon-Amy, and Y.J. Chabal, *Attachment of 3–(aminopropyl) triethoxysilane (APS) on silicon oxide surfaces: Dependence on solution temperature* Langmuir, 2007. **Accepted, in press**.
20. McKittrick, P.T. and J.E. Keaton, *Infrared and Raman Group Frequencies of Cyclic Imides.* Applied Spectroscopy, 1990. **44**: p. 812-817.
21. Parker, S.F., S.M. Mason, and K.P.J. Williams, *Fourier Transform Raman and infrared spectroscopy of N-phenylmaleimide and methylene.* 1990.
22. Tripp, C.P. and M.L. Hair, *An Infrared Study of the Reaction of Octadecyltrichlorosilane with Silica.* Langmuir, 1992. **8**: p. 1120-1126.
23. Tripp, C.P. and M.L. Hair, *Direct observation of the surface bonds between self-assembled monolayers of octadecyltrichlorosilane and silica surfaces: A low-frequency IR study at the solid/liquid interface.* Langmuir, 1995. **11**: p. 1215-1219.
24. Hofmann, K., D.B. Melville, and V.d. Vigneaud, *Characterization of the functional groups of biotin.* Journal of Biological Chemistry, 1941. **141**.
25. Ruis, H., D.B. McCormick, and L.D. Wright, *Equilibration and acid hydrolysis of biotin sulfoxides.* Journal of Organic Chemistry, 1967. **32**(6): p. 2010-2012.

2.9 Appendix

Supporting information accepted for publication: (free of charge via the Internet at http://pubs.acs.org.). *Norman A. Lapin and Yves J. Chabal, Infrared Characterization of Biotinylated Silicon Oxide Surfaces, Surface Stability, and Specific Attachment of Streptavidin, J. Phys. Chem. B, Accepted, 2009.*

2.9.1 Supplement to Experimental Methods

2.9.1.1 Reagents for NHS-terminated surface.

Undecylenic acid, N-Hydroxysuccinimide (NHS), and 1-ethyl-3-(3-dimethylaminopropyl) carbodiimide hydrochloride (EDC), methylene chloride and tetrahydrofuran (THF) were purchased from Sigma-Aldrich and used as received.

2.9.1.2 Preparation of oxide-free NHS-terminated surfaces.

These surfaces were prepared to help distinguish all moieties of biotin-NHS that are not components of the biotin fused rings. By comparison to a spectrum of physisorbed biotin-NHS, all bands due to the fused rings can be determined. Silicon wafers were cleaned using the SC2 protocol and rinsed copiously with DI water, followed by immersion in a solution of DI water:hydrofluoric acid (49%) (2:1) for 30 seconds, and copious rinse with DI water.

A bath of silicon oil was brought to 120°C, while neat undecylenic acid was heated separately to liquefy it. The neat undecylenic acid was then poured into a two-necked flask and degassed for 30 minutes at room temperature by bubbling nitrogen gas through a needle (submerged in the undecylenic acid) and sealing the test tube with a cap permitting small openings for nitrogen gas flow in and out only. Next, the hydrogen-terminated silicon wafer was submerged in the undecylenic acid, the flask was re-sealed and the system was purged again for 15 minutes. The flask was then transferred to the silicon oil bath and partially submerged in it for two hours, and the needle lifted out of the liquid, to blow nitrogen in the gas above the undecylenic acid. Finally, the wafer was removed from the flask, rinsed twice with tetrahydrofuran and twice with methylene chloride, then dried under a stream of nitrogen. The wafer was subsequently submerged in a bath of acetic acid and water (1:10) at 80°C for 10 min to decouple a second layer of carboxylic acid that formed with the first with the carboxylic acid of the layers in contact [1]. The wafer was then rinsed copiously with DI water and dried under a stream of nitrogen gas. To convert the carboxylic acid termination to that of NHS, EDC and NHS were next dissolved in DI water at a molar ratio of 5:1. The silicon wafer was added to the solution for one hour at room temperature, then rinsed copiously with DI water and dried under a stream of nitrogen.

2.9.2 Supplement to Results

2.9.2.1 Low frequency spectroscopic feature of biotin.

To identify IR features belonging solely to the biotin fused rings, the spectrum of biotin-NHS referenced to silicon oxide prior to biotin-NHS exposure (Figure 2.9.1, top) was compared to the spectrum of an NHS ester bound via alkyl chain directly to a silicon surface (Figure 2.9.1, bottom). The bottom spectrum contains all and only features present in the top spectrum, except for the vibrational modes of the biotin fused rings. In both spectra, the band at 1074 cm^{-1} is assigned to the four C-H deformations on the succinimide ring of NHS [2]. The band at 1212 cm^{-1} in the NHS spectrum and the low frequency shoulder in the band complex centered at 1226 cm^{-1} in the biotin-NHS spectrum are assigned to the succinimide C-N-C stretching mode [3, 4]. The band at

1465 cm^{-1} is assigned to the C-H scissor mode of the aliphatic chain linking NHS to the silicon surface and of the aliphatic chain in the biotin-NHS spectrum linking the biotin fused rings to the NHS moiety. Bands at 1747, 1788 and 1819 cm^{-1} are assigned to the NHS moiety of both spectra as described in Figure 2.4, spectrum B. These bands account for all significant vibrations of the NHS moiety and aliphatic chain present in the spectra of both molecules in Figure 2.9.1.

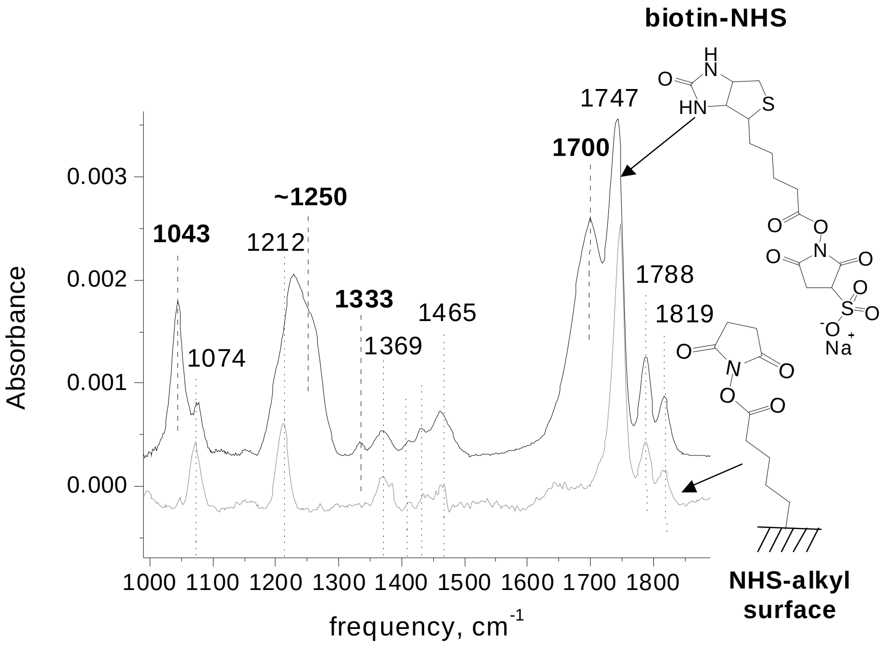

Figure 2.9.1. FTIR spectra of biotin-NHS and NHS-terminated surface.
Spectra of (top) silicon oxide surface exposed to biotin-NHS (physisorbed) and referenced to pre-exposed silicon oxide surface, and (bottom) NHS-terminated alkyl chain surface chemically attached to and referenced to hydrogen-terminated silicon surface. The bottom spectrum is expected to contain all moieties of biotin-NHS except for the biotin fused rings.

Bands unique to the biotin-NHS spectrum include the band at 1043 cm^{-1}, the high frequency shoulder at ~1250 cm^{-1} and the band at 1700 cm^{-1}. Of these unique biotin bands, protein bands in the spectra of the subsequent adsorption step interfere with the band at 1700 cm^{-1}, and APS Si-O-Si band area intensity decrease in the same spectrum interferes with the band at 1043 cm^{-1}. Only the high frequency shoulder at ~1250 cm^{-1} is outside of these regions and was therefore selected to track changes in the biotin fused rings upon protein attachment and rinse. To further confirm association of the band at ~1250 cm^{-1} with the biotin fused rings, its area was correlated with the band area at ~1700 cm^{-1} ($R^2 = 0.68$, Figure 2.9.2).

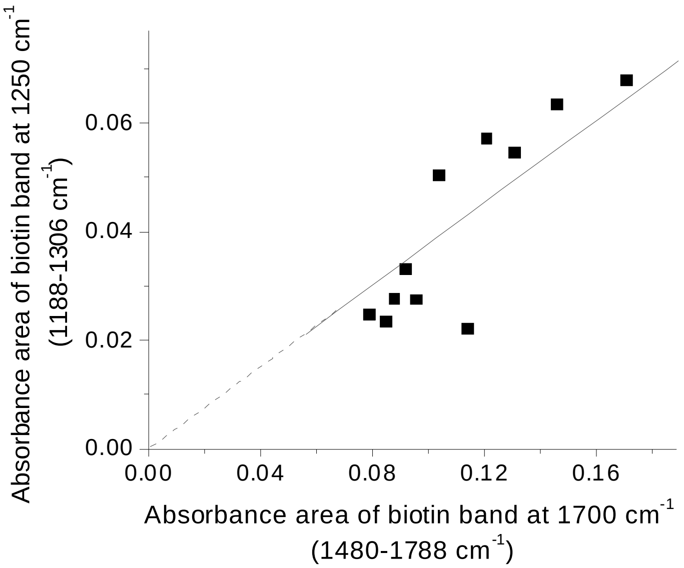

Figure 2.9.2. IR absorption band area correlation.
IR absorption band area at 1250 cm^{-1} in spectrum of biotinylated surface versus band area at 1700 cm^{-1} in spectrum of same surface. $R^2 = 0.68$.

2.9.2.2 Additional analysis of biotinylated surface behavior.

To expand on analysis of the behavior of the biotinylated surface as described in Figure 2.7, additional results are presented here (see also section 2.9.3.7). While Figure 2.7 relates the decrease in intensity in the biotin band at ~1250 cm^{-1} after SA adsorption and rinse to the decrease in APS Si–O–Si band intensity after biotinylation, additional relationships are also observed. We observe that loss of biotin ~1250 cm^{-1} band intensity

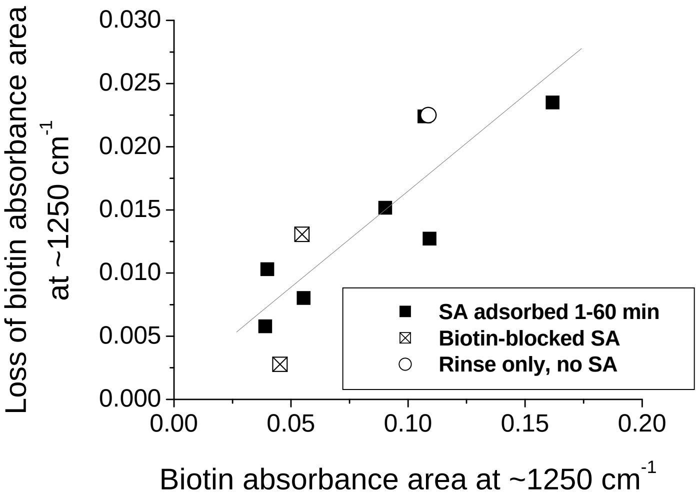

Figure 2.9.3. Loss of biotin band absorbance area vs initial band area.
Loss of biotin band absorbance area at ~1250 cm^{-1} after SA adsorption and PBST/PBS/DI water rinse (or rinse step without SA adsorption) vs initial biotin band absorbance area at ~1250 cm^{-1} after biotin-NHS adsorption to the APS surface, sonication and rinse (black squares, open squares and open circle indicate SA specific adsorption, biotin-blocked SA adsorption and PBST/PBS/DI water rinse only, respectively). Least squares fit; $R^2 = 0.72$, all points included.

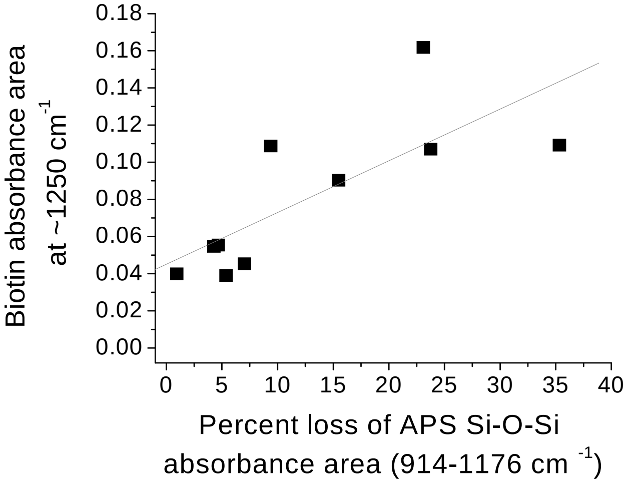

Figure 2.9.4. Biotin band absorbance area vs percent APS band area loss.
Biotin band absorbance area at ~1250 cm^{-1} after biotin-NHS adsorption to the APS surface, sonication and rinse vs APS Si–O–Si band area percentage loss after the APS surface was exposed to biotin-NHS in DI water for 60 min and subsequently sonicated in DI water for 10-15 min. Least squares fit; $R^2 = 0.58$.

is directly correlated with the ~1250 cm^{-1} band area of biotin upon adsorption of biotin-NHS to the APS surface (Figure 2.9.3). In addition to biotin ~1250 cm^{-1} band intensity loss, biotin ~1250 cm^{-1} band area is also correlated with APS Si–O–Si band intensity loss, presented in terms of percent loss of the APS band (Figure 2.9.4).

2.9.3 Supplement to Discussion

2.9.3.1 Explanation for fluctuation in APS growth (Figure 2.2).

A possible explanation for fluctuation in amount of APTES growth with increasing humidity is that at increasingly high atmospheric moisture, the thickening water layer may both hinder chemisorption to the oxide surface and increase APTES polymerization near the surface, depending on the total water content in the system. Even while using anhydrous solvent, a greater number of water molecules at the surface likely causes increased silane polymerization. However, the thicker the water layer, the less likely the silane will be able to reach the surface to attach to it. With such a high sensitivity to the thickness of the water layer, fluctuations in indoor moisture content (due to intermittent air conditioner operation) also become critical. While the moisture content of outdoor air in summer months is usually high, as the air conditioner cools the air indoors, the temperature may reach the dew point, causing moisture to condense on surfaces and thus lowering the moisture content of the indoor air. Therefore, the actual air moisture content corresponding to Si-O-Si absorbance area values at high outdoor humidity may be lower than recorded. Such a correction to (and lowering of) the recorded moisture content might decrease the observed fluctuation in the data of Figure 2.2, reinforcing the upward trend.

2.9.3.2 Biotin ureido orientation and assignments in the 1600-1700 cm^{-1} region.

In a number of IR grazing angle reflection studies, the biotin ureido band near 1700 cm^{-1} was not observed [5-8]. While vibrational modes perpendicular to the surface are sensitive to IR in reflection, modes parallel to the surface do not absorb IR in this geometry. Hence, the lack of observation of the ureido may suggest that this vibrational mode (and hence, the biotin fused rings) is parallel to the surface. Additionally, IR features may be shifted from expected positions due to differences in environment or organization of the molecules at a surface.

In other studies, certain assignments may not be correct. In one study, where a vibrational mode near 1700 cm^{-1} was observed, it was assigned to the amide I band and a band at 1641 cm^{-1} to an amino group [9], while we propose that these bands are due to the ureido carbonyl stretch and amide I band respectively. In another case, a region from 1680-1710 cm^{-1} was assigned to both ureido carbonyl and amide I bands [10] Indeed, in another sample in the same work, a stronger band at 1660 cm^{-1} was identified as amide I [10]. Clearly, there is some inconsistency in the literature in both the appearance of certain expected IR features and assignments of vibrational modes at biotinylated surfaces [2, 5-10].

2.9.3.3 Possible downstream effects of physisorbed biotin-NHS.

Sonication cannot be used in environments where protein is already present, since there is a risk of denaturing the protein in the process. Therefore, it is of value to learn more about the effects of biotin derivatives that can remain physisorbed at surfaces after biotinylation and rinsing. The amount of such molecules remaining at a surface could have downstream effects on bioassay quality. Non-covalently bound biotin derivatives at the surface may compete with covalently bound biotin for streptavidin binding sites and could thereby decrease the quantity of streptavidin bound to the surface. This possibility is based on the use of a solution of free biotin to regenerate biotinylated surfaces by competitively binding to and removing SA or anti-biotin IgG from the biotinylated surface [11]. Free biotin or its derivatives may also compete with biotinylated biomolecules for attachment to streptavidin-coated surfaces [12]. Such competitive binding, resulting in fewer active biomolecules at the surface may lead to decreased device or assay sensitivity. Additionally, surface robustness is important for regeneration of biotinylated surfaces as specific binding may be reduced by 15-20% after the first regeneration cycle [13].

2.9.3.4 Selection of the ~1250 cm^{-1} band to monitor changes in the biotinylated surface.

It is difficult to measure changes in the biotin ureido after protein adsorption and rinse steps by using the absorption band at ~1700 cm^{-1} because protein bands including amide I and II and CH_2 scissor modes interfere with the biotin band in the same region (1400-1700 cm^{-1}). Possible changes in APS Si-O-Si and substrate silicon oxide modes (1000-1250 cm^{-1}) also limit selection of a biotin band to monitor changes in the biotin ureido moiety. Although close to the APS Si-O-Si region, the biotin band near 1250 cm^{-1} (1240-1260 cm^{-1}) is selected and shown to be a reliable means of monitoring biotin ureido band intensity loss under protein attachment to the surface. Supporting this selection, it is observed that there is close correspondence between the loss of intensity of the biotin band at 1250 cm^{-1} and that at 1685 cm^{-1} after SA adsorption and rinsing. This observation, though, is qualitative due to protein interference in the region around 1685 cm^{-1} (Figure 2.5).

2.9.3.5 Ruling out other molecules as assignments for the ~1250 cm^{-1} band (APS film and underlying silicon dioxide).

To confirm that the band near 1250 cm^{-1} exists in the absence of APTES, biotin-NHS was physisorbed to a silicon oxide surface. In the spectrum of this surface, a band near 1250 cm^{-1} is present, confirming its independent existence (Figure 2.9.1, top). Subsequent removal of this band along with other biotin-NHS bands after a brief rinse of the surface further confirms that this band was due to biotin-NHS and not growth of silicon oxide upon contact of water (the solvent) with the surface. Additional check experiments show that there is no oxide growth or loss in the region of 1250 cm^{-1} upon exposure of the silicon oxide surface to the aqueous solvent, PBS, while small bands did appear near 1020 and 1110 cm^{-1} (data not shown). Furthermore, the APS film likely acts to insulate the oxide from interaction with the solution. Moieties of the APS film are again ruled out as possible assignments since loss of APS in the biotinylation step results in negative Si-O-Si bands ranging from ~950 to ~1200 cm^{-1}, while the intensity of the band near 1250 cm^{-1} is in the positive direction after this step.

The remote possibility that the 1250 cm^{-1} band may belong to the SO_3^- group that is used to make the biotin-NHS soluble in water is also ruled out. Since this SO_3^- is attached to the end of the NHS moiety, it is also removed with NHS and cannot therefore be associated with the band at ~1250 cm^{-1}.

2.9.3.6 Correlation between ~1250 and 1685 cm^{-1} band integrated areas.

With the band near 1250 cm^{-1} in the spectrum of the biotinylated surface clearly due to chemisorbed biotin, its association with the vibrational mode of the ureido moiety at 1685 cm^{-1} is studied more closely. There is reasonably good linear correlation between the areas under the bands of these moieties (Figure 2.9.2), considering possible error due to vibrational modes in the region near 1200-1250 cm^{-1} that may be due to oxide formation or changes in APS Si-O-Si bands after exposure of the surface to water. The linear relationship between these bands reflects the amount of biotin adsorbed to the surface. Surface exposure times to biotin-NHS were all within 60-75 minutes, well above the saturation time for reaction of biotin-NHS with the surface. Variation in quantity of biotin attached to the surface may be accounted for by fluctuations in the APS layer from trial to trial varying the number of amino groups available for reaction with the NHS moiety of biotin-NHS. This observation further corroborates the evidence that most of this band cannot be due to oxide growth, since if significant oxide growth did occur in the biotin attachment step, it should not be linearly correlated with the amount of biotin at the surface, as quantified by the integrated area of the biotin band at ~1685 cm^{-1}.

2.9.3.7 Clarification of biotinylated surface behavior.

A potential misinterpretation may exist in the understanding of Figure 2.7. Rather than a direct relationship between loss of the biotin band at ~1250 cm-1 and APS loss, the relationship is more complex. We found that the loss of this biotin band is directly correlated with initial biotin band intensity at ~1250 cm-1 (Figure 2.9.3). Hence, the more biotin that attaches to the surface, the more loss of biotin band intensity that takes place in subsequent adsorption and rinse steps. Combining this correlation with that in Figure 2.7, it follows that initial biotin band intensity is also correlated with loss in the APS Si–O–Si band, shown in terms of percent APS loss (Figure 2.9.4). Thus, there is more loss of the ~1250 cm-1 biotin band with greater loss of APS because more biotin attaches to the surface with greater APS loss. Such an increase in biotin at the surface may occur because with more loss of APS, surface roughness may increase, thereby increasing the APS surface area that biotin-NHS can attach to.

2.9.3.8 Possible chemical modification of biotin: Speculation on mechanism of biotin degradation.

Here, we explore the possibility that biotin degradation rather than dipole screening is the cause of the IR intensity decrease in biotin ureido vibrational modes after SA adsorption and rinse steps. As there is no known study of the degradation of biotin at inorganic surfaces, we can only speculate on a mechanism of degradation based on known chemical reactions of compounds with the biotin fused rings. One report mentions that biotin can be converted to a diaminocarboxylic acid (3,4 diaminothiophane-2-pentanoic acid, Scheme 2.9.1) through hydrolysis with $Ba(OH)_2$ [14]. It is also reported that the ureido ring opens up by initial conversion of biotin to biotin-sulfoxide through reaction with an equimolar amount of hydrogen peroxide. Subsequent acid hydrolysis using 1 M hydrochloric acid as a catalyst then forms the diaminocarboxylic acid of biotin with the ureido ring no longer present [15].

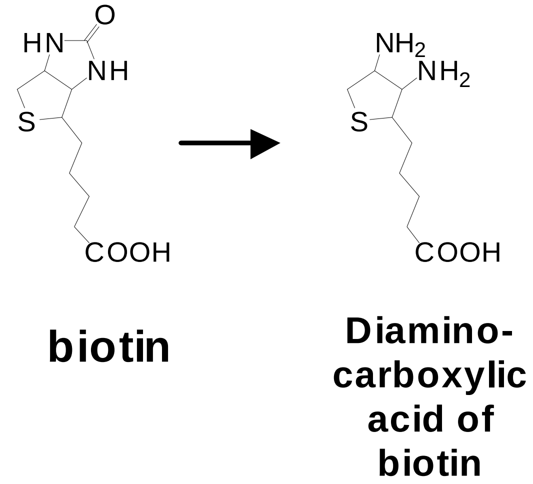

Scheme 2.9.1. Conversion of biotin to the diaminocarboxylic acid of biotin

Although the conditions in these previous studies are quite harsh and different from those of the present study, they represent possible pathways for the degradation of the biotin ureido ring. Chemistry taking place at surfaces can be quite different from seemingly similar chemistry in bulk solution and hence reactions that are not possible in solution may in fact occur at a surface. At surfaces, the geometry of the system is much more restrictive than that in bulk solution making certain reactions much more probable due to the restricted number of orientations of the molecules. In many cases, the surface itself may act as a catalyst.

The loss of part of the APS film during adsorption of biotin-NHS solvated in DI water and adsorption of SA solvated in PBS, then rinsed with PBST followed by PBS and DI water is due to exposure of the film to water present in these solutions [16]. Degradation of the APS film during these adsorption steps may result in exposure of areas of the silicon oxide surface beneath, revealing hydroxide moieties (Si-OH) at the surface. Cleavage of APS Si-O-Si bonds by water may also form Si-OH moieties. When the biotinylated surface is exposed to these moieties in the SA attachment and rinse steps, the possible reaction of biotin with its local environment at the surface may involve Si-OH and may suggest a mechanism similar to that of biotin hydrolysis by $Ba(OH)_2$. Since the chloride ion is also present (in PBS and PBST), it may also participate in a possible reaction with biotin, similar to biotin ureido ring opening by hydrochloric acid catalysis, although the solutions involved here are neutral (pH 7.4).

2.9.4 References

1. Faucheux, A., A.C. Gouget-Laemmel, C.H.d. Villeneuve, R. Boukherroub, F. Ozanam, P. Allongue, and J.-N. Chazalviel, *Well-Defined Carboxyl-Terminated Alkyl Monolayers Grafted onto H-Si(111): Packing Density from a Combined AFM and Quantitative IR Study.* Langmuir, 2006. **22**: p. 153-162.
2. Socrates, G., ed. *Infrared and Raman Characteristic Group Frequencies - Tables and Charts*. 3rd ed. 2001, John Wiley & Sons Ltd: West Sussex, England.
3. McKittrick, P.T. and J.E. Keaton, *Infrared and Raman Group Frequencies of Cyclic Imides.* Applied Spectroscopy, 1990. **44**: p. 812-817.
4. Parker, S.F., S.M. Mason, and K.P.J. Williams, *Fourier Transform Raman and infrared spectroscopy of N-phenylmaleimide and methylene.* 1990.
5. Liu, Z. and M.D. Amiridis, *FT-IRRAS spectroscopic studies of the interaction of avidin with biotinylated dendrimer surfaces.* Colloids and Surfaces B: Biointerfaces, 2004. **35**: p. 197-203.
6. Liu, Z. and M.D. Amiridis, *FT-IRRAS quantitative analysis of specific avidin adsorption on biotinylated Au surfaces.* Surface Science, 2005. **596**: p. 117-125.
7. Liu, Z. and M.D. Amiridis, *Quantitative FT-IRRAS spectroscopic studies of the interaction of avidin with biotin on functionalized quartz surfaces.* Journal of Physical Chemistry B, 2005. **109**: p. 16866-16872.
8. Pradier, C.-M., M. Salmain, Z. Liu, and G. Jaouen, *Specific binding of avidin to biotin immobilised on modified gold surfaces - Fourier transform infrared reflection absorption spectroscopy analysis.* Surface Science, 2002. **502-503**: p. 193-202.
9. Ye, L., R. Pelton, and M.A. Brook, *Biotinylation of TiO_2 nanoparticles and their conjugation with streptavidin.* Langmuir, 2007. **23**: p. 5630-5637.
10. Yam, C.-M., C. Pradier, M. Salmain, P. Marcus, and G. Jaouen, *Binding of Biotin to Gold Surfaces Functionalized by Self-Assembled Monolayers of Cystamine and Cysteamine: Combined FT-IRRAS and XPS Characterization.* Journal of Colloid and Interface Science, 2001. **235**: p. 183-189.
11. Yoon, H.C., D. Lee, and H.-S. Kim, *Reversible affinity interactions of antibody molecules at functionalized dendrimer monolayer: affinity-sensing surface with reusability.* Analytica Chimica Acta, 2002. **456**: p. 209-218.
12. Peluso, P., D.S. Wilson, D. Do, H. Tran, M. Venkatasubbaiah, D. Quincy, B. Heidecker, K. Poindexter, N. Tolani, M. Phelan, K. Witte, L.S. Jung, P. Wagner, and S. Nock, *Optimizing antibody immobilization strategies for the construction of protein microarrays.* Analytical Biochemistry, 2003. **312**: p. 113-124.
13. Dupont-Filliard, A., M. Billon, T. Livache, and S. Guillerez, *Biotin/avidin system for the generation of fully renewable DNA sensor based on biotinylated polypyrrole film.* Analytica Chimica Acta, 2004. **515**: p. 271–277.
14. Hofmann, K., D.B. Melville, and V.d. Vigneaud, *Characterization of the functional groups of biotin.* Journal of Biological Chemistry, 1941. **141**.
15. Ruis, H., D.B. McCormick, and L.D. Wright, *Equilibration and acid hydrolysis of biotin sulfoxides.* Journal of Organic Chemistry, 1967. **32**(6): p. 2010-2012.

16. Pasternack, R.M., S. Rivillon-Amy, and Y.J. Chabal, *Attachment of 3–(aminopropyl) triethoxysilane on silicon oxide surfaces: Dependence on solution temperature* Langmuir, 2008. **24**: p. 12963-12971.

CHAPTER 3: FURTHER INVESTIGATION OF IR FEATURES OF THE BIOTINYLATED SURFACE AND BIOTIN-SA SPECIFIC ATTACHMENT

3.1 Abstract

The biotin-streptavidin linkage is a widely used and highly stable system for attaching biomolecules to surfaces. An understanding of the behavior of this system is therefore important to optimizing the behavior of biomolecules bound to assay surfaces in this manner.

In this study, we report the behavior of infrared bands of the biotinylated surface under varying solvent conditions, and changes in these bands upon attachment of streptavidin to the surface. We observe that the biotin ureido carbonyl band is more prone to intensity loss as its frequency changes from 1710 to 1680 cm^{-1}, and that a biotin ureido band at 1250 cm^{-1} increases in intensity with such a decrease in frequency. These changes are associated with increasing film disorder, as they are found to occur when water (which attacks silane Si-O-Si bonds at the surface) is used as a solvent for biotin deposition in lieu of anhydrous solvent. Upon interaction of the biotinylated surface with streptavidin, an interesting and repeatable dip is observed. This dip may result from changes in the state of hydrogen bonding of the biotin carbonyl stretch mode due to interaction with protein and/or solvent. By manipulating biotin ureido carbonyl spectra, a frequency shift (in the differential form of a dip) can be fit to the dip observed in the data.

3.2 Introduction

The focus of Chapter 2 was on the effects of environmental conditions on biotinylated surfaces; both that of initial surface chemistry and post adsorption of streptavidin (SA). In this chapter, the relationship between IR features of the biotinylated surface is investigated further, as are changes in features of the biotinylated surface upon adsorption of SA and other proteins or rinsing in aqueous solution.

To recap, a major advantage of attaching biomolecules to inorganic surfaces through biotin-(strept)avidin linkage is that the connection is made through a highly stable binding couple. Since the (strept)avidin protein is further stabilized by binding to biotin [1, 2], a SA layer bound on both sides to biotinylated molecules maximizes the stability to be gained through biotin-(strept)avidin linkage. Furthermore, an intermediate (strept)avidin layer prevents or lessens direct interaction between the biolayer above it and the surface below, which may help to protect the biomolecules from denaturation at the surface.

In practical applications, it was found that biotinylated DNA bound in greater quantity and with more activity (hybridizing with complementary DNA) to SA attached to biotinylated surfaces than SA films covalently bound to the surface [3]. In another study it was found that antibodies bound via biotin-immobilized SA had four times the fractional coverage and twice the specific activity compared with antibodies bound to SA covalently attached to the surface [4]. These observations suggest that the organization of the SA layer has a significant effect on the quality and function of the biomolecular overlayer that it supports.

Further optimization of the (strept)avidin surface depends on the surface concentration of biotin to which it attaches. It has been shown that at about 30% biotin surface coverage, SA binds to the biotinylated surface through biotin-SA “bridges” in which two of four possible biotin-binding sites on SA are occupied [3, 5, 6]. At this coverage of biotin, the density and stability of SA binding to the biotinylated surface is maximized [5]. Beyond this percentage of biotin, the biotin molecules become disorganized, such that many no longer protrude from the surface and less SA binding results [5]. Hence, the organization of the biotinylated surface to which SA attaches is important to the optimal formation of the SA layer.

In this chapter, the biotin ureido carbonyl is examined in two respects. First, the relationship between the two biotin ureido IR bands (at ~1250 and ~1700 cm^{-1}) is observed. The ratio of the areas of these bands varies with adsorption conditions and may reveal information about the organization of the biotinylated surface. Second, an intensity decrease or “dip” is observed in the spectrum of protein adsorption to the biotinylated surface attributed to a change in the biotin ureido carbonyl. It may be possible to distinguish this dip from the biotin ureido carbonyl intensity loss discussed in Chapter 2. Several interpretations of this feature are explored, including the tentative interpretation that it is a shift in the biotin ureido vibrational mode due to specific binding of SA to the biotinylated surface. Based on this interpretation, a curve fitting method is applied to estimate the amount of shift in frequency (cm^{-1}) in the carbonyl stretch mode of the biotin ureido.

The interaction between biotin and SA occurs through hydrogen bonding in the SA clefts. The IR spectra of hydrogen bonded carbonyls in polymers have been studied previously and are typically red-shifted (to lower frequency) from the frequency of the same carbonyls free of hydrogen bonding [7]. Conversely, the stretch mode of the biotin ureido carbonyl bound to avidin was blue-shifted in frequency compared with biotin in aqueous solution [8]. This blue-shift could be interpreted as a reduction in hydrogen bonding, since there is a great deal of hydrogen bonding between biotin and water molecules in aqueous solution (including hydrogen-bonding cooperativity) [9] that could conceivably exceed the degree of hydrogen bonding of biotin to SA. In contrast, adsorbing SA to an initially dry biotinylated surface could increase hydrogen bonding to biotin and hence a red-shift would be expected.

3.3 Experimental Methods

3.3.1 Reagents (differing from those in Chapter 2)

N,N-Dimethylformamide (DMF), anhydrous, 99.8% purchased from Sigma-Aldrich.

3.3.2 Sample Preparation.

The preparation for biotinylation of silicon oxide surfaces and subsequent SA adsorption is the same as stated in the Experimental Methods section of Chapter 2, unless otherwise stated.

Samples where biotinylated surfaces were formed by adsorbing biotin-NHS dissolved in DI water to APS surfaces were prepared for use in Chapter 2 and corresponding data was reanalyzed for use in Chapter 3. Similar samples where biotin-NHS was instead dissolved in anhydrous DMF were prepared differently as follows:

Instead of adsorption to one side of a wafer (as in Chapter 2), biotin-NHS and SA were adsorbed to two sides. Biotin-NHS was dissolved in anhydrous DMF at ~2-4 mg/ml in a dry box. In the dry box, 200-300 μl of solution was then pipetted onto glass slides and the APS-terminated silicon wafer such that the wafer was sandwiched between the two glass slides and in contact with solution on both sides. After 60 min, the wafer was removed from the sandwich, rinsed 2-3 times in anhydrous DMF in a test tube and allowed to "air" dry in the nitrogen environment of the dry box.

For subsequent SA adsorption to the same wafer, SA was dissolved in PBS at 100 μg/ml. The sample was removed from the dry box and sonicated as stated previously. Subsequently the sample wafer was sandwiched between two glass slides wetted on both sides by SA in PBS for the desired length of time, using the same procedure as for biotin-NHS adsorption. The wafer was then removed from the sandwich setup and rinsed in PBST, PBS and DI water and dried under a stream of nitrogen as stated previously.

3.3.3 Data Analysis.

For samples on which biotin-NHS and SA solutions were adsorbed to two sides (all DMF exposed samples), IR absorbance is twice what it would be for samples modified on one-side. Therefore, for direct comparison between one-sided and two-sided samples, the absorbance values for two-sided samples must be divided by two. However, for Figure 3.1, it is the ratio of two bands from each spectrum that is compared. Hence for this figure, the factor of two cancels out. For Figure 3.2, spectra are shown as collected, but here again, it is the comparison of bands within each spectrum that matters.

Data analysis using Microcal Origin for band fitting: Peak fitting of the biotin complex (1600-1800 cm^{-1}) was done using a pseudo-Voigt (type 2) fitting function for each band component, based on equation 3.1. For simplification, either the gaussian or lorentzian term of the equation was zeroed out for each band component after determining whether a Lorentzian or Gaussian fit was best.

$$y = y_0 + A * mu * \frac{2}{\pi} * \frac{wL}{4 * (x - xc)^2 + wL^2} + (1 - mu) * \frac{\sqrt{4 * ln2}}{\sqrt{\pi} * wG} * e^{-\frac{4 * ln2}{wG^2} * (x - xc)^2}$$

Lorentzian term Gaussian term

(eqn. 3.1)

where,

y_o	is the baseline offset
A	is the band component amplitude
xc	is the band center point
wL	is the Lorentzian band full width at half maximum
wG	is the Gaussian band full width at half maximum
mu	determines the weight of the Gaussian and Lorentzian terms (taken as 0 or 1 in this analysis)

3.4 Results

3.4.1 Relationship between biotin ureido IR bands

In Chapter 2 evidence was presented suggesting that both the band at ~1700 cm^{-1} and the band at ~1250 cm^{-1} are due to vibrational modes of the biotin ureido and not due to other moieties or solvent. Here the relationship between these bands is examined and trends in their behavior noted.

It is first observed that the ratio of the band at ~1250 cm^{-1} to the band at ~1700 cm^{-1} decreases linearly with increase in frequency of the ureido carbonyl band from ~1680 to ~1710 cm^{-1} (Figure 3.1). It is interesting to note that the solvent used for biotin adsorption seems to influence the behavior of the bands of the surface bound molecules. For biotin-NHS dissolved in water, the ureido carbonyl stretch frequency of the surface bound biotin varies widely from 1680-1705 cm^{-1}, while the band at ~1250 cm^{-1} is relatively large. For biotin-NHS dissolved in anhydrous dimethylformamide (DMF), the band at ~1250 cm^{-1} is very small and the ureido carbonyl stretch is confined to a narrow frequency region from ~1705 to 1710 cm^{-1}. Data points from both solvent adsorptions conform to the same linear trend. Figure 3.2 shows selected spectra demonstrating the dependence of the two IR bands corresponding to the data points of Figure 3.1.

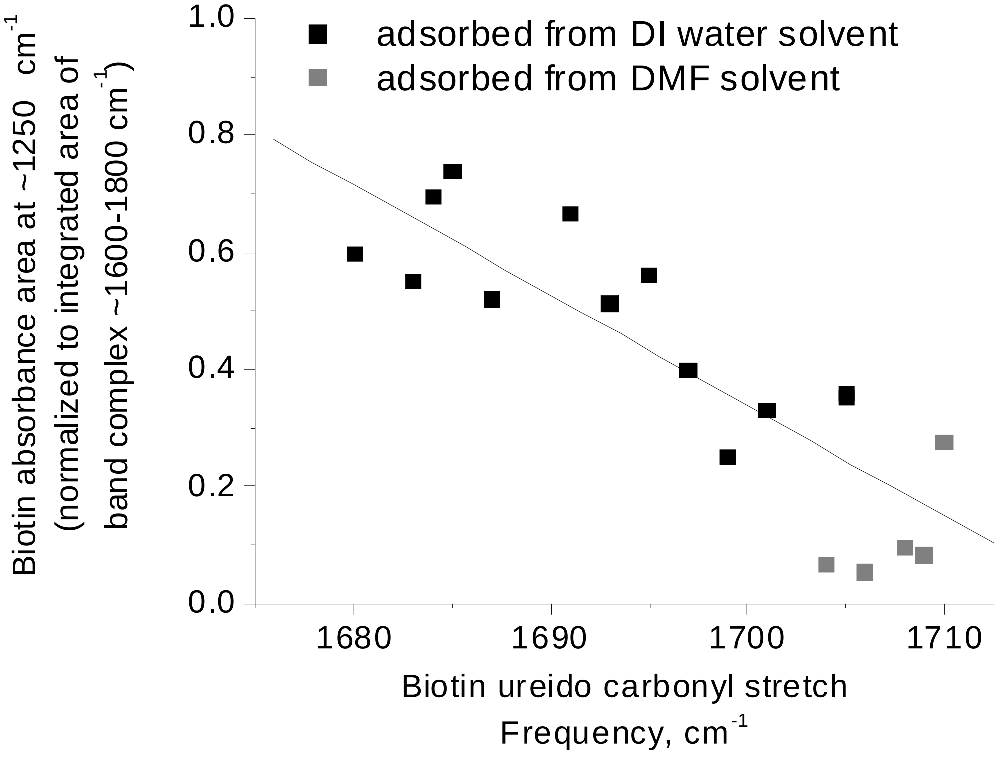

Figure 3.1. Change in biotin ~1250 cm^{-1} band area vs biotin ureido carbonyl frequency. Ratio of biotin ureido ~1250 cm^{-1} band area normalized to area of band complex at ~(1600–1800 cm^{-1}) vs biotin ureido carbonyl stretch frequency. Band area at ~1250 cm^{-1} decreases as ureido carbonyl stretch frequency increases. $R^2 = 0.71$.

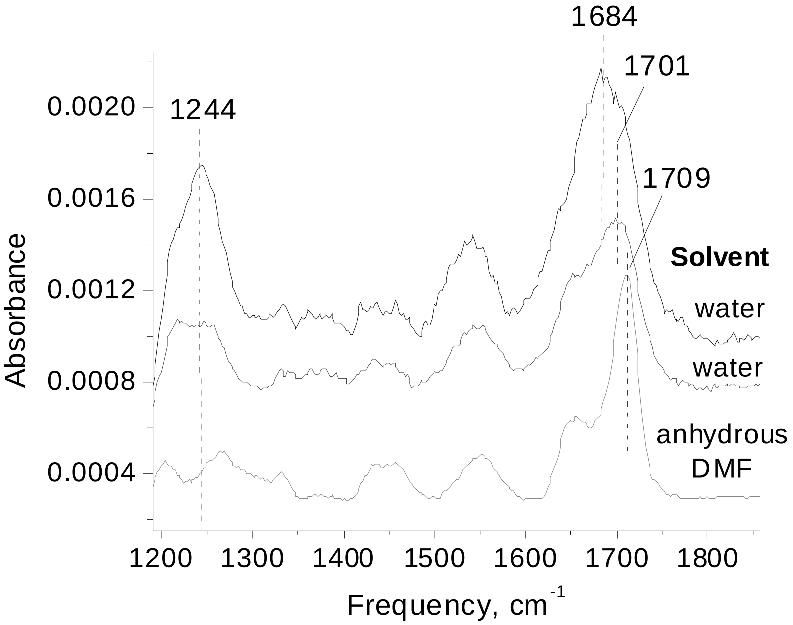

Figure 3.2. Selected spectra of biotinylated surfaces corresponding to data of Figure 3.1 demonstrating that the area of the biotin band at ~1250 cm^{-1} decreases with increase in the frequency of the ureido carbonyl stretch (1680-1700 cm^{-1}).

Rinsing of the biotinylated surface with PBST, PBS and DI water results in decrease in the ureido carbonyl stretch band intensity in the region from 1680-1700 cm^{-1}. Figure 3.3 shows two pairs of spectra corresponding to the spectrum of the biotinylated surface (top of each pair) and the ureido band decrease after rinsing the surface, referenced to the pre-rinsed biotinylated surface (bottom of each pair). In the top pair of spectra where the solvent for biotin attachment to the surface was water, the minimum position of band decrease is 1680 cm^{-1} (lower gray spectrum) exactly corresponding to the biotin ureido band maximum (higher black spectrum). In the bottom pair of spectra, the solvent used for biotin surface attachment was anhydrous DMF. In the lower gray spectrum, the overall band decrease is less than for the top pair of spectra. Furthermore, although the maximum of the ureido band is at 1710 cm^{-1}, there is more band decrease near 1680 cm^{-1}, suggesting that the bottom biotin spectrum also has a band component at 1680 cm^{-1}. It is also noted that the band decrease that does occur at 1710 cm^{-1} is directly in line with the biotin ureido peak at the same frequency.

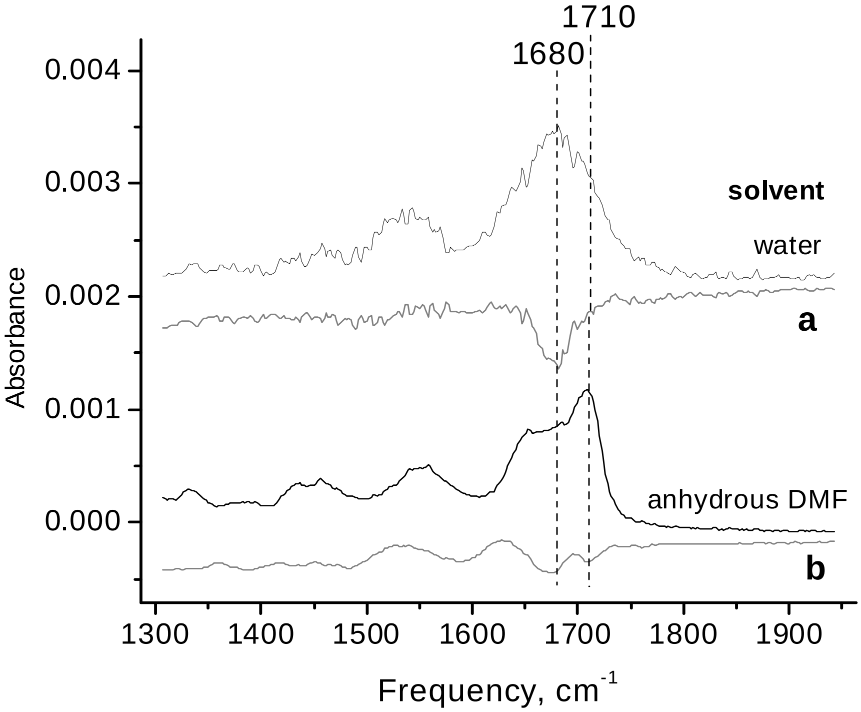

Figure 3.3. Spectra of biotinylated surfaces before and after rinse step.
Spectra of biotinylated surfaces referenced to respective APS-terminated surfaces (black spectra) and corresponding spectra of the rinsed biotinylated surface referenced to the biotinylated surface before rinsing (gray spectra). Biotin-NHS dissolved in DI water (a) and in anhydrous DMF (b) prior to adsorption to APS surface.

3.4.2 Streptavidin adsorption to biotinylated surface: Investigation of "dip" feature

Due to variation in results based on use of different solvents in the formation of the biotinylated surface, the results for protein adsorption to these surfaces are presented in two parts. The first spectra presented are for protein adsorbed to biotinylated surfaces formed from biotin-NHS dissolved in water (Figure 3.4). Amide I and II bands present in each spectrum at ~1530 and ~1640 cm^{-1} respectively are indicative of protein on the biotinylated surface. Additionally, the middle three spectra of SA specifically adsorbed to the biotinylated surface exhibit a negative band or "dip" at ~1716 cm^{-1}. The depth of the dip increases with SA adsorption time from 10 to 20 min. In contrast, no dip is present at 1716 cm^{-1} for immunoglobulin (IgG) and only a shallow dip (closer to 1700 cm^{-1}) for biotin-blocked SA, both non-specifically adsorbed to respective biotinylated surfaces.

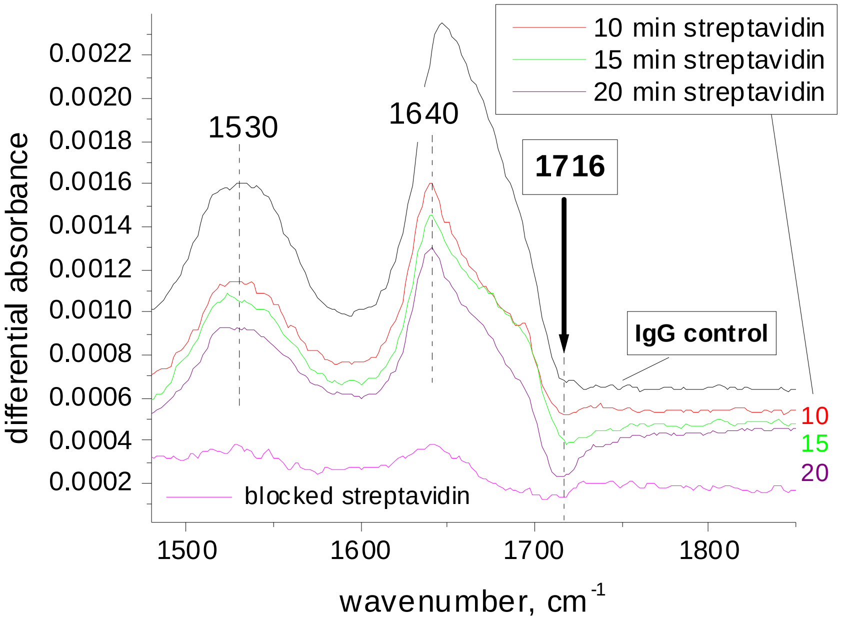

Figure 3.4. Spectra of protein adsorbed and referenced to biotinylated surfaces. IgG (top, black), SA for 10, 15 and 20 min (middle, red, green and purple respectively), and biotin-blocked SA (~60 min) (bottom, magenta). Biotinylated surfaces were formed from water as a solvent. Solvent for SA is PBS.

Figure 3.5 demonstrates that the dip at 1716 cm^{-1} does not occur significantly at SA surfaces where there is significant biotin ureido band loss at ~1250 and 1685 cm^{-1} (bottom spectrum). See also Figure 2.5 and related discussion. The slight dip that does occur at 1716 cm^{-1} is independent of SA adsorption time and is believed to have a different origin than the deeper 1716 cm^{-1} dip in the top spectrum. The top SA spectrum (redisplayed from Figure 3.4) does not exhibit significant biotin ureido band loss.

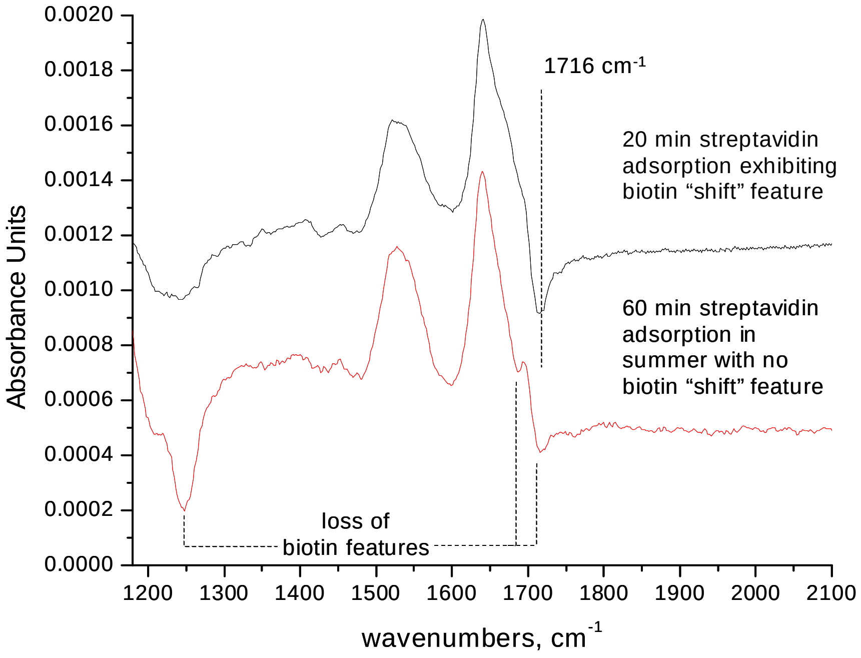

Figure 3.5. Comparison of spectra with and without "dip" at 1716 cm^{-1}. Spectra of SA adsorbed and referenced to a biotinylated surface exhibiting "dip" at 1716 cm^{-1} and no biotin "loss" features (top) and SA adsorbed and referenced to a biotinylated surface exhibiting "loss" features and no "dip" (bottom). Biotinylated surfaces are formed from water as a solvent. The solvent for SA is PBS.

Next, spectra are presented for protein adsorbed to biotinylated surfaces formed from biotin-NHS dissolved in DMF (Figure 3.6) These spectra also exhibit the 1716 cm^{-1} dip feature, but its time dependence on SA adsorption is fairly weak (Figure 3.7). As mentioned in section 3.3.1, biotinylated surfaces formed using DMF have little to no band at 1250 cm^{-1} in their spectra and hence, SA spectra show little to no loss of this band. Figure 3.8 shows that a dip at 1716 cm^{-1} is also caused by adsorption of IgG and BSA protein to biotinylated surfaces. The top spectrum in Figure 3.8 demonstrates that

BSA adsorbed to an APS (amine-terminated) surface that was pre-exposed to anhydrous DMF does not exhibit a dip at 1716 cm^{-1}.

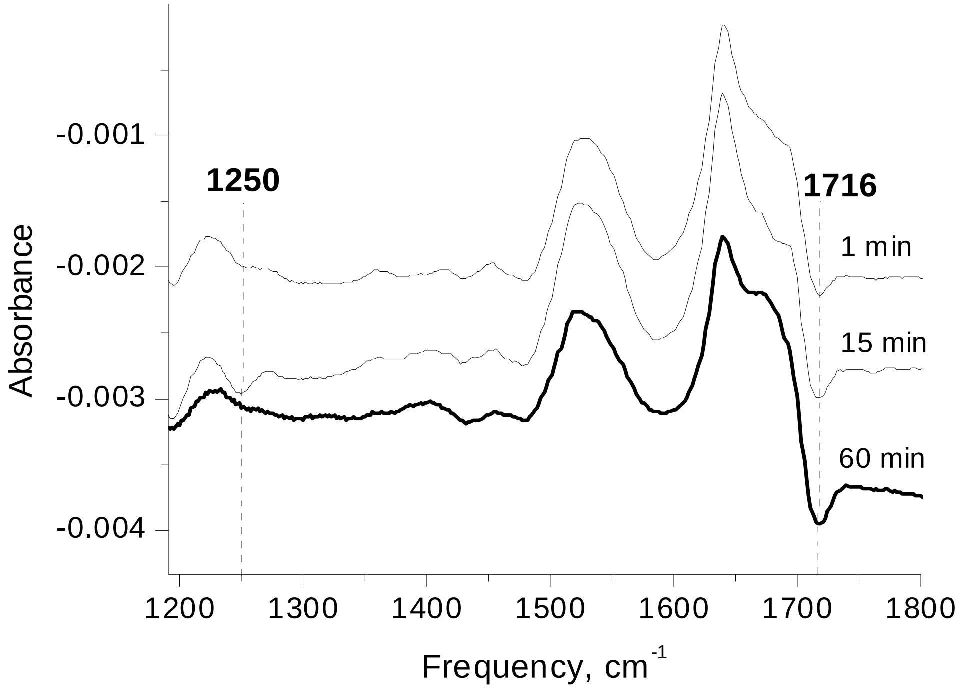

Figure 3.6. Spectra of SA adsorbed and referenced to biotinylated surfaces. Biotinylated surfaces are formed from anhydrous DMF as a solvent. The solvent for SA is PBS.

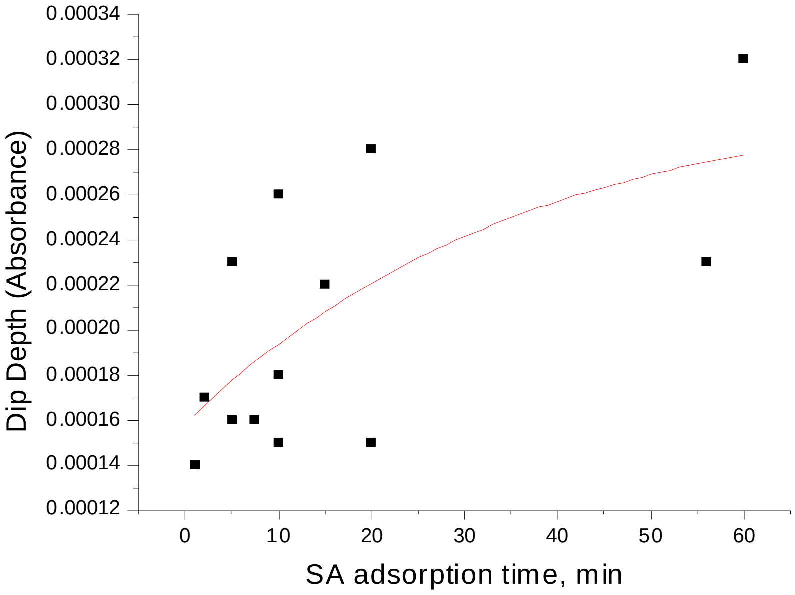

Figure 3.7. Depth of dip at 1716 cm^{-1} vs SA incubation time.
For SA adsorption to biotinylated surfaces. All biotinylated surfaces are formed from anhydrous DMF as a solvent. The solvent for SA is PBS. $R^2 = 0.41$.

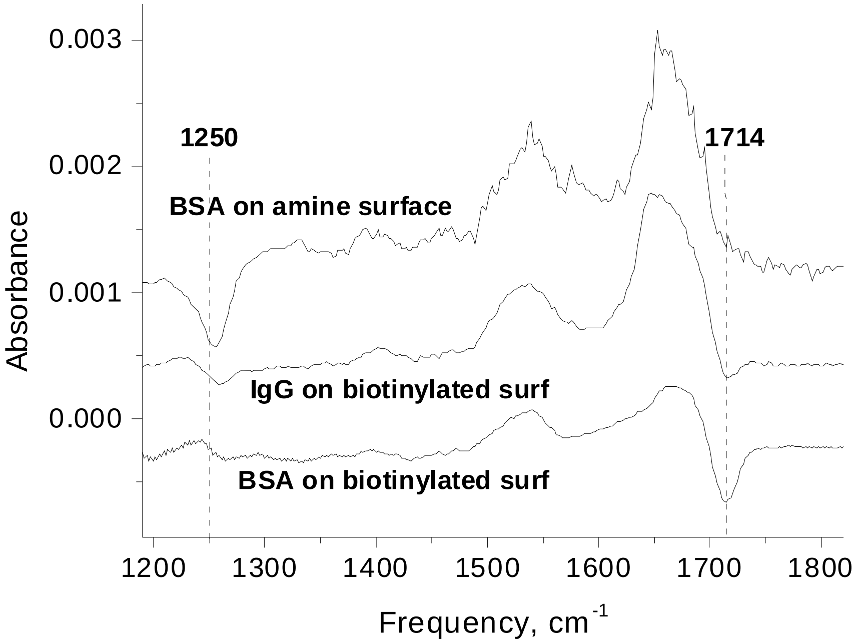

Figure 3.8. Spectra of protein adsorbed to biotinylated and APS surfaces.
Spectra of BSA adsorbed to APS surface pre-exposed to DMF (top), IgG adsorbed and referenced to biotinylated surface (middle), and BSA adsorbed and referenced to biotinylated surface. Biotinylated surfaces are formed from anhydrous DMF as a solvent. The solvent for IgG and BSA is PBS.

3.5 Discussion

3.5.1 Relationship between biotin ureido IR bands

First, the biotinylated surface is examined using the biotin ureido IR bands at ~1250 and ~1700 cm^{-1}. Significant variation is observed in the biotin ureido carbonyl stretch frequency (1680 – 1705 cm^{-1}) for biotinylated surfaces formed from biotin-NHS dissolved in water compared with that for surfaces formed from biotin-NHS dissolved in anhydrous DMF (1704-1710 cm^{-1}) (Figure 3.1). Such variation in frequency could suggest a wider range of variation in the environment of biotinylated surfaces formed in the presence of water compared with those formed with anhydrous solvent. As discussed in the previous chapter, water molecules can hydrolyze the APS surface, the substrate for biotin attachment. The attack on APS surfaces by water while biotin is simultaneously attached to the surface chemically, likely results greater disorder of the biotinylated surface and hence the creation of a wider range of biotinylated surface configurations. In contrast, APS surfaces exposed only to anhydrous solvent are likely more uniform in structure, allowing greater repeatability of biotinylated surfaces resulting in a narrower range of vibrational mode frequencies.

It is also observed that lower frequency biotin ureido carbonyl stretch mode components (~1680 cm^{-1}) experience greater loss than those of higher frequency after the biotinylated surface is exposed to an aqueous solution rinse (Figure 3.3). Greater decrease in this vibrational mode may suggest greater perturbation of the surface, possibly due to increased disorder of the biotin film. Hence, lower frequency ureido carbonyl stretch modes may suggest less stable and/or more disordered film structure. In accordance with this hypothesis, the range of ureido carbonyl frequencies of water-deposited biotin (1680 – 1705 cm^{-1}) is consistently lower than the range for anhydrous DMF-deposited biotin (1704-1710 cm^{-1}) (Figure 3.1), implying that surface exposure to water is the cause of greater film degradation and thus, disorder.

Furthermore, since Figures 3.1 and 3.2 show that the biotin ureido band at ~1250 cm^{-1} increases in area relative to the ureido carbonyl stretch band the lower the frequency of the carbonyl band, the 1250 cm^{-1} band could therefore be specific to biotin molecules in a disordered or "less stable" environment, possibly increasing with the degree of disorder. Consistent with this hypothesis is the observation that the 1250 cm^{-1} band is larger for the aqueous solvent data than the anhydrous solvent data, where in some spectra it is not present at all.

3.5.2 Streptavidin adsorption to biotinylated surface: Investigation of dip feature

For various spectra of protein adsorbed to biotinylated surfaces, in addition to amide bands indicative of protein adsorption, an interesting and reproducible dip is observed at ~1716 cm^{-1} suggesting a change in the biotinylated surface. Both intensity loss in the ureido band (due to screening or chemical modification as discussed in the previous chapter) and a shift in this band (as observed in the differential spectrum) would involve negative IR features of the same moiety, hence, it is difficult to separate these phenomena. Since it is not clear whether the dip is distinct from features of biotin band loss, two possible interpretations are presented.

The argument for a shift in the biotin ureido carbonyl stretch mode is supported by certain aspects of the dip. A red-shift would display a negative feature on the high frequency side of the original feature in the differential spectrum as opposed to a negative band at the precise frequency for band loss. Different from biotin band loss, the dip occurs at higher frequency than biotin band peak frequencies (Figure 3.5, top spectrum). In contrast, features of biotin band loss superimposed on protein spectra occur directly below biotin ureido features at ~1250 and 1685 cm^{-1} and may be accompanied by a shallower dip near 1716 cm^{-1} as part of the main negative band at ~1685 cm^{-1} (Figure 3.5, bottom spectrum). Furthermore, a shift can be fit to the shape of the dip, as demonstrated in Figure 3.10 (#3) and in fact is considerably deeper than shallow features at 1716 cm^{-1} in spectra attributed to ureido band loss.

If on the other hand the dip is due to biotin band loss, it may be caused by the loss of a tail part of a high frequency component of the ureido carbonyl band. It may be that the dip is not accompanied by much band loss at 1250 cm^{-1} since high frequency biotin ureido carbonyl bands are accompanied by little to no band at 1250 cm^{-1} in the first place (as discussed in section 3.3.1, see also Figure 3.6). This interpretation is then simply that biotin loss features are observed in the presence of protein adsorption. The following paragraphs expand on the former interpretation in order to investigate the details of this possibility further: that the dip is the result of a shift in the biotin ureido carbonyl band.

Examined first are spectra of protein adsorbed to biotinylated surfaces formed in the presence of water as the biotin-NHS solvent. These spectra suggest that the 1716 cm^{-1}

dip is due to specific binding of SA to the biotinylated surface, since the dip is only present for SA and not for IgG or biotin-blocked SA adsorbed to a biotinylated surface (Figure 3.4). For this set of spectra, dip depth appears to increase with SA adsorption time. The small broader dip near 1700 cm^{-1} for biotin-blocked SA (Figure 3.4, bottom spectrum) likely results from a small amount of biotin band loss due to rinsing.

It is noted that the dip at 1716 cm^{-1} is much smaller in spectra of SA specifically bound to the surface when biotin ureido band loss features are present at ~1250 and ~1685 cm^{-1} (Figure 3.5). It may be the case that at disordered surfaces (as suggested by biotin band loss) the dip due to SA specific binding is obscured. In other cases, for spectra of SA on biotinylated surfaces that have no negative bands at all, the dip is not observed.

For biotinylated surfaces formed with anhydrous DMF as the biotin-NHS solvent, spectra of protein adsorption suggest that the dip occurs due to the presence of protein, and is not specific to SA binding. Figure 3.6 and Figure 3.8 show that a dip at ~1716 cm^{-1} occurs in the presence of SA, IgG and BSA proteins and its depth is only weakly dependent on SA adsorption time (Figure 3.7). As discussed in section 3.4.1, the solvent used in formation of the biotinylated surface may well affect the organization of the surface. Hence, protein binding behavior on each biotinylated surface type may vary. Since the spectrum of DMF also exhibits a band near 1700 cm^{-1}, it might be the case that for DMF-formed surfaces, loss of residual DMF from the biotinylated surface upon protein adsorption in aqueous solution might contribute to the dip. This might explain why the dip occurs more often for DMF-formed biotinylated surfaces. However, the dip was not observed when bovine serum albumin (BSA) was adsorbed to an APS surface pre-exposed to DMF (Figure 3.8, top spectrum). Hence, in the absence of biotin, the dip was not present, suggesting that it is a feature of biotin rather than DMF.

Without resolution as to whether the dip is due to specific or non-specific binding of protein to biotinylated surfaces, the evidence suggests that the dip is likely a shift in the biotin ureido in response to protein adsorption. Since DMF is absent in certain experiments where the dip occurs, loss of DMF is ruled out as a factor in those cases.

3.5.3 Fitting the dip to the biotin ureido shift

For the interpretation of the dip as a shift in the biotin ureido carbonyl stretch mode upon protein adsorption, the amount of shift in frequency can be estimated by matching the dip to a fit of the shifted biotin ureido band, as demonstrated in Figure 3.11. To rule out DMF as a factor, the fit is demonstrated on spectra of surfaces deposited without DMF.

In this method, the biotin ureido carbonyl stretch band and the amide I and II bands (of the amide bond connecting biotin to the APS surface) are first estimated by Gaussian and Lorentzian peak fitting of the band complex (~1600-1800 cm^{-1}) and the band at ~1530 cm^{-1} (Figure 3.9). In most cases, the best fit is Lorentzian for the biotin ureido carbonyl stretch and Gaussian for the amide I and II bands. The Lorentzian fit is a narrower distribution of vibrational modes and may suggest that the biotin ureido moiety points away from the surface, free from environmental influences. The amide bonds to the surface are more embedded in the film and hence may interact more with their local environment creating a random distribution of vibrational modes as suggested by the broader Gaussian fit (See Scheme 2.1). In spectra where the ureido carbonyl band conforms better to a Gaussian fit, such a fit may suggest that many of the biotin ureido moieties are embedded in the film or turned downward in contact with other molecules [10].

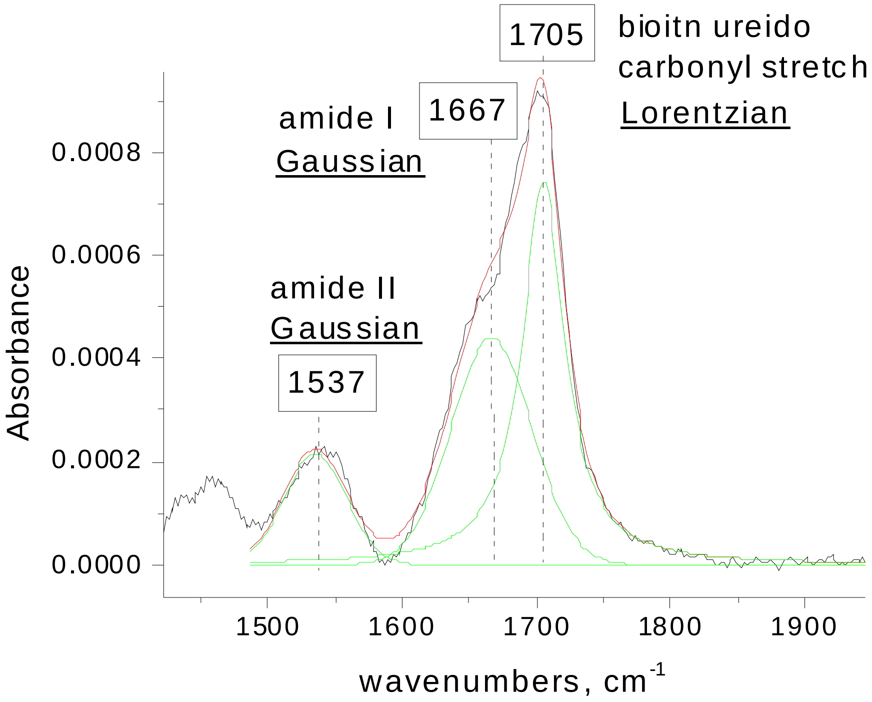

Figure 3.9. Deconvolution of biotinylated surface referenced to APS surface. Biotin ureido carbonyl stretch and amide bands are deconvolved using Gaussian and Lorentzian peak fitting.

Next (Figure 3.10), the biotin ureido carbonyl is manually shifted a number of incremental steps (2) and each shifted spectrum is referenced to the original biotin spectrum (1) creating a set of differentials (3). The differential spectra are similar to the dip spectra on their right side. The left rising part of the differential is not observed in SA spectra, since it is covered by the amide I band of the protein. These differentials are then lined up against the SA spectrum on their right side to identify the best match. Figure 3.11 shows a spectrum of streptavidin adsorbed to the biotinylated surface for 20 min at a concentration of 100 μg/ml with various biotin ureido differentials superimposed on the spectrum. The best fit to the data is an 8 cm^{-1} shift in the biotin ureido carbonyl stretch. The resolution of the fit is about 1 cm^{-1}.

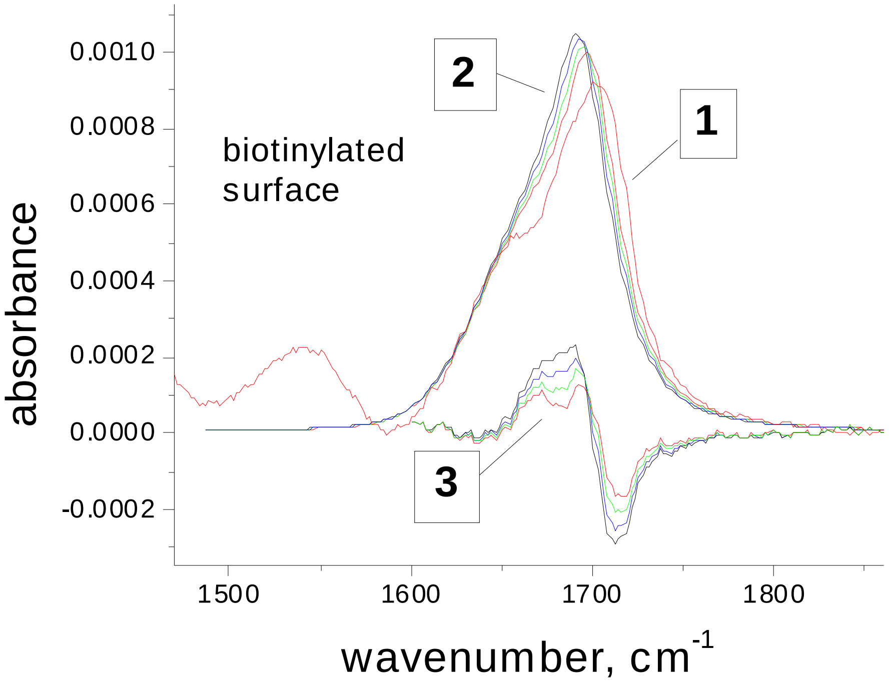

Figure 3.10. Manual generation of "dip" feature at ~1716 cm^{-1}.
Spectrum of a biotinylated surface referenced to the APS surface (prior to biotin attachment) (1), incremental shifts in biotin ureido carbonyl stretch mode (2) and differentials (3) resulting from spectra (2) referenced to spectrum (1).

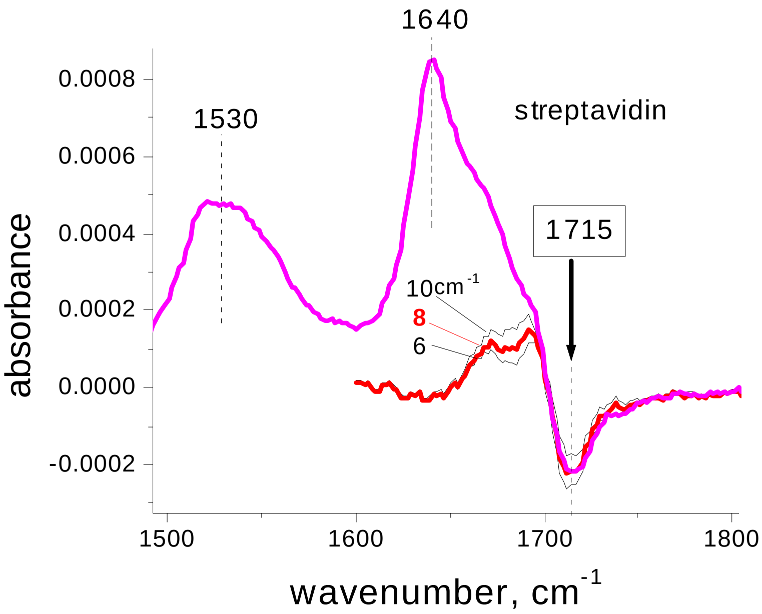

Figure 3.11. Demonstration of spectral fit to “dip” feature.
Spectrum of SA adsorbed to and referenced to a biotinylated surface, with various biotin ureido differentials superimposed on the spectrum. The best fit of the SA data is the 8 cm^{-1} shifted differential.

3.6 Conclusions

In this study, we found that IR features of the biotinylated surface varied with solvent type used in biotinylation and that the biotin ureido carbonyl stretch mode exhibited greater variation in frequency with water as a solvent. When the APS surface was exposed to water during biotinylation, the biotin ureido carbonyl stretch mode appeared at lower frequency (1680 – 1705 cm^{-1}) than upon exposure of the surface to anhydrous DMF as the solvent (1704 – 1710 cm^{-1}). When the biotinylated surface was subsequently exposed to aqueous solution, the lower wavenumber component (near 1680 cm^{-1}) of the biotin ureido band decreased in intensity. This loss of band intensity may be due to screening effects caused by perturbation of the surface and possibly disorganization of biotin molecules at the surface. Based on this putative association of the low frequency biotin ureido carbonyl mode with molecular disorder, observation of area increase in the biotin band at 1250 cm^{-1} with decreasing ureido carbonyl stretch frequency may suggest that the area under the 1250 cm^{-1} band can be used as a measure of disorder of the surface.

There are several possible interpretations of the dip appearing near 1716 cm^{-1} in spectra of the biotinylated surface exposed to protein adsorption and rinsing. 1) The dip is a shift in the biotin ureido carbonyl band due to specific binding of SA in certain environments, under certain conditions. 2) The dip is a shift in the ureido band due to non-specific interactions with protein (observed for biotin-NHS initially solvated in DMF but not when solvated in water). 3) The dip results from intensity loss in the biotin ureido stretching vibration due to changes in the environment of the surface resulting from rinsing with aqueous solution and/or proximity of adsorbed protein to biotin. In all interpretations, the dip is certainly a feature of change in the biotin ureido moiety and not an artifact due to solvent, since it was observed in a DMF-free system. Relevant to interpretations in which the dip results from a shift in the biotin ureido carbonyl band, we have shown that a manual shift in this band can be fit to the data (the observed dip), producing an estimate for the frequency shift within about 1 cm^{-1}.

3.7 References

1. Gonzalez, M., L.A. Bagatolli, I. Echabe, J.L.R. Arrondo, C.E. Argarana, C.R. Cantor, and G.D. Fidelio, *Interaction of Biotin with Streptavidin - Thermostabilty and conformational changes upon binding.* The journal of biological chemistry, 1997. **272**(17): p. 11288-11294.
2. Smith, C.L., J.S. Milea, and G.H. Nguyen, *Immobilization of Nucleic Acids Using Biotin-Strept(avidin) Systems.* Topics in Current Chemistry, 2006. **261**: p. 63-90.
3. Su, X., Y.-J. Wu, R. Robelek, and W. Knoll, *Surface plasmon resonance spectroscopy & quartz crystal microbalance study of streptavidin film struct effects on biotinylated DNA assy and target DNA hybridization.* Langmuir, 2005. **21**: p. 348-353.
4. Vijayendran, R.A. and D.E. Leckband, *A quantitative assessment of heterogeneity for surface-immobilzed proteins.* Analytical Chemistry, 2001. **73**: p. 471-480.
5. Jung, L.S., K.E. Nelson, P.S. Stayton, and C.T. Campbell, *Binding and Dissociation Kinetics of Wild-Type and Mutant Streptavidins on Mixed Biotin-Containing Alkylthiolate Monolayers.* Langmuir, 2000. **16**: p. 9421-9432.
6. Nelson, K.E., L. Gamble, L.S. Jung, M.S. Boeckl, E. Naeemi, S.L. Golledge, T. Sasaki, D.G. Castner, C.T. Campbell, and P.S. Stayton, *Surface Characterization of Mixed Self-Assembled Monolayers Designed for Streptavidin Immobilization.* Langmuir, 2001. **17**: p. 2807-2816.
7. Coleman, M.M., D.J. Skrovanek, J. Hu, and P.C. Painter, *Hydrogen Bonding in Polymer Blends. 1. FTIR Studies of Urethane-Ether Blends.* Macromolecules, 1988. **21**: p. 59-65.
8. Swamy, M.J., T. Heimburg, and D. Marsh, *Fourier-Transform Infrared Spectroscopic Studies on Avidin Secondary Structure and Complexation with Biotin and Biotin-Lipid Assemblies.* Biophysical Journal, 1996. **71**: p. 840-847.
9. Lei, Y., H. Li, R. Zhang, and S. Han, *Molecular Dynamics Simulations of Biotin in Aqueous Solution.* Journal of Physical Chemistry B, 2004. **108**: p. 10131-10137.
10. Rivillon-Amy, S., *Discussions on Lorentzian and Gaussian fits*. 2007.

CHAPTER 4: DIRECT ATTACHMENT OF PROTEIN TO SILICON SURFACES

4.1 Abstract

Covalent attachment of protein to biosensor surfaces is employed widely in biotechnology applications. With appropriate selection of sensor and protein surface chemistries, proteins can be bound to biosensor surfaces site-specifically, influencing molecular orientation and function.

We report the attachment and infrared characterization of both IgG peptide fragments and "test molecules" (small molecules that mimic protein attachment) to maleimide-terminated surfaces. Use of test molecules in lieu of protein to observe chemical reactions with the surface has several distinct advantages, including 1) lack of interference in the frequency region below 1700 cm^{-1} due to peptide vibrations, 2) small molecular footprint increasing number of binding sites (and hence signal) ~100 fold, and 3) attachment in anhydrous solvent, preventing degradation of the surface by aqueous solvent. Amine (aminopropyltriethoxysilane) and sulfhydryl-bearing (mercaptopropyltrimethoxysilane) small molecules were selected to mimic protein specific and non-specific attachment to maleimide surfaces, where amine attachment represents random attachment by primary amines on protein surfaces and sulfhydryl attachment represents free sulfhydryls created by cleavage of antibody Fab fragments.

We find that for both small molecules, chemical attachment is clearly indicated by infrared spectra, but that spectra of protein attachment to the same surface do not clearly indicate covalent binding. Polarization studies of mercaptopropyltrimethoxysilane attachment further suggest that molecular bond orientation is restricted upon chemical bonding to the maleimide surface. Ellipsometry measurements of the maleimide-

terminated surface elucidate aspects of the surface structure (such as polymerization) that the test molecules and protein bind to.

4.2 Introduction

In this chapter, covalent attachment of protein to the surface is investigated through maleimide crosslinking. Maleimides can be useful for both specific and non-specific covalent attachment of proteins to inorganic surfaces.

Heterobifunctional cross-linkers are often used to attach biomolecules to SAM-functionalized surfaces. These molecules are designed such that the moiety at one end of the molecule will react faster with the surface than the other end (suited to protein attachment), leaving a single moiety exclusively available for protein attachment. Maleimide-based crosslinkers have been selected for their high rate of reaction with sulfhydryl moieties [1, 2] that can be created in proteins in a variety of ways and are 1000× more reactive with maleimides than are random amines at neutral and acidic pH [3]. Xiao et al. used a variety of succinimidyl maleimides to attach peptide chains to titanium oxide surfaces pre-functionalized with aminosilanes [2]. Surfaces have also been functionalized with maleimides for the attachment of DNA in the development of DNA hybridization assays [1, 4, 5]. The maleimide cross-linker p-maleimidophenyl-isocyanate (PMPI) has been selected in recent studies because its isocyanate moiety reacts immediately with amine-terminated surfaces, saturating the surface before the maleimide moiety has a chance to react with it [1, 5].

For specific attachment to planar surfaces, proteins can be chemically modified to reveal sulfhydryls at specific locations on their surface that can react with maleimides at the planar surface. An important application of such specific attachment is the orientation of proteins such as antibodies at protein microarray surfaces. To orient antibodies at a surface, chemically active sites can be created in regions of the antibody away from the antigen-binding sites and the antibody fragments subsequently attached to the surface. One method is to chemically reduce disulfide bonds that connect antibody Fab fragments to each other, freeing sulfhydryls at the end of the Fab fragment opposite the antigen-binding site. The Fab fragment can then react with the maleimide-terminated surface through its sulfhydryl moieties, orienting the antigen binding sites away from the surface [1, 6, 7].

Maleimides also react with primary amines through Michael addition [1]. Since primary amines may be present at multiple locations on the surface of proteins, non-specific covalent attachment of proteins to maleimide surfaces can also occur.

4.2.1 Surface Characterization

FTIR has been used to characterize and quantify the attachment of DNA and peptides to maleimide terminated inorganic oxide surfaces [1, 2, 4, 5, 8]. The maleimide crosslinkers covalently bound to the surface were characterized primarily via amide region vibrations of urea bonds from 1500-1700 cm^{-1} [1] and via C-H stretching vibrations of the maleimide olefin bond from 3000-3150 cm^{-1} [5]. The conversion of maleimide to succinimide upon sulfhydryl attachement to the olefin bond was characterized by intensity increase in the C-N-C vibration based on the appearance of an IR band "shoulder" in the region of 1200 cm^{-1} [2]. Although researchers have observed direct evidence of chemical bonding between biomolecules and surfaces, their data have been limited in several ways. The IR regions from 1500-1700 cm^{-1} and 3000-3300 cm^{-1} can have interference by bending and stretching modes of gaseous water. Protein amide I and II bands also in the 1500-1700 cm^{-1} region can obscure the detection of other moieties that occur in the same region. Certain vibrational modes may also exhibit low signal intensity and may be out of range of the instrument, such as modes in the far region of the infrared spectrum from 600 - 1100 cm^{-1} [1, 2, 4, 5, 8]. In this investigation, with the sensitivity of IR transmission through planar surfaces, it is possible to probe the low frequency region from 800-1200 cm^{-1}.

In this study, FTIR is employed to characterize molecular layers and the formation and breaking of chemical bonds after each adsorption step as described in Scheme 4.1. The study begins with FTIR characterization of maleimide attachment to APS-terminated surfaces (characterized in Chapter 2). Additional analyses are performed as well, including FTIR polarization, yielding information about orientation of bonds relative to the surface, negative correlation, identifying moieties removed in chemical reactions, analysis of the far IR (low frequency) region and subtraction of water interference from spectra, not done in previous studies [1, 2, 4, 5, 8].

To characterize the covalent attachment of protein to maleimide-terminated surfaces, both proteins and "test molecules" are used. Test molecules are small molecules with the same surface attachment chemistry as their protein counterparts. An advantage of using such molecules is that they lack amide bands and thus do not interfere in the IR region where proteins do. Additionally, due to a size far smaller than proteins, such molecules can react with far more maleimide moieties at the surface, increasing the intensity of the signal of covalent attachment a great deal. To investigate covalent attachment of sulfhydryls to the maleimide surface for protein specific binding, the small molecule 3-mercaptopropyltrimethoxysilane (MPS) is attached to the maleimide-terminated surface in place of actual sulfhydryl-bearing protein. To investigate non-specific covalent binding of protein to maleimide surfaces through attachment of random amines, both the small molecule APTES and antibody fragments are attached to the surface via amine-maleimide addition and spectra of the surface attached test molecule and protein are compared.

4.3 Experimental Methods

Reagents. All purchases are from Sigma-Aldrich unless otherwise noted. 3-aminopropyltriethoxysilane (APTES), 3-mercapto-propyltrimethoxysilane (MPS), toluene, (anhydrous, 99.8%), acetonitrile (anhydrous 99.8%), Dulbecco's Phosphate Buffered Saline (PBS). All reagents were used as received unless otherwise noted. N-(p-maleimidophenyl)isocyanate (PMPI) was purchased from Pierce Biotechnology. Antibody scFv fragment kindly provided by Andreas Plückthun and Martin Yarmush.

Substrate. Float Zone Si(100) silicon wafers initially passivated by a layer of native oxide (~65 Angstroms) were cut to dimensions 1.5×3.8 cm.

Preparation of amine-terminated surfaces. Surface modification began with silanization of the silicon oxide surface to prepare it for chemical modification with

APTES. To prepare the oxide surface for silanization, the wafer was cleaned in a solution of water:hydrogen peroxide:ammonium hydroxide (4:1:1) at 80° C for 10 min to remove organic contaminants (SC1). Copious rinsing with DI water (18 MΩ-cm) followed this and every cleaning step. Next, this clean was followed by a second similar clean, where the base was replaced by hydrochloric acid for the removal of metal particles from the surface, with no additional oxide formation (SC2). After DI water rinse, the wafer was subsequently submerged in a solution of water:hydrofluoric acid (2:1) for 30 s at room temperature removing the oxide and leaving an hydrogen-terminated surface. Finally, the wafer was submerged in piranha solution (sulfuric acid:hydrogen peroxide, 7:3) at 90° C for about 10 min, increasing the number of hydroxyl groups on the silicon oxide surface. *Please note: Extreme caution must be taken when preparing piranha solution as this mixture can be explosive. An explosion-proof hood should be used.* The wafer was then rinsed in DI water as above, and dried under a stream of nitrogen gas. This clean is henceforth referred to as SC1/SC2/HF/Piranha clean. All glassware was cleaned in SC1, rinsed copiously with DI water and dried with nitrogen gas.

After collecting reference spectra of the silicon oxide surface, the silicon wafers were transferred to a dry box. To silanize the oxide surface (i.e. form a 3-aminopropylsiloxane (APS) surface), the wafer was submerged in 0.1 % APTES in anhydrous toluene. After about 24 h the wafer was removed from the solution, rinsed copiously with toluene, sonicated in toluene, rinsed with methanol (in some cases) and dried under a stream of nitrogen gas.

Attachment of PMPI to amine-terminated surfaces. After silanization, PMPI was chemically attached to the APS-terminated surface. Fresh solutions of PMPI in anhydrous acetonitrile were prepared at a concentration of ~0.1 mg/ml (a "pinch" of PMPI in 25 ml of acetonitrile) in a dry box. The silicon wafer was transferred to the dry box and submerged in the solution of PMPI in acetonitrile for ~12 h. The wafer was then removed from the solution, rinsed copiously with acetonitrile and dried under a stream of nitrogen gas.

Attachment of test molecule (MPS or APTES) to maleimide-terminated surface. After attachment of PMPI, the "test molecule" was adsorbed to the maleimide surface. To attach this small molecule, the wafer was submerged in 0.1 % APTES or 0.1 % MPS in anhydrous toluene for ~12 h. The wafer was then rinsed with and sonicated in toluene and subsequently dried under a stream of nitrogen gas.

Attachment of protein fragment to maleimide-terminated surface. Attachment of Fv antibody fragment to the maleimide-terminated surface was performed by exposing the maleimide-terminated silicon wafer to ~100 μg/ml Fv antibody fragment in PBS (pH 7.4) for adsorption times ranging from 30 min to overnight for various experiments. After protein adsorption, the wafer was rinsed copiously with PBS and DI water and dried under a stream of nitrogen gas.

Physisorption of small molecules (PMPI, MPS) To obtain a complete spectrum of unreacted PMPI and MPS, a SC1/SC2/HF/Piranha-cleaned silicon wafer was submerged in either 0.1% MPS in toluene or ~0.1 mg/ml PMPI in acetonitrile for ~15 min. Subsequently, the wafer was removed from the solution and dried under a stream of nitrogen gas, leaving a film of either PMPI or MPS physisorbed to the silicon oxide surface. While PMPI does not react with the silicon oxide surface, MPS may react with the silicon oxide to a small degree (in such a short time), but since the surface is not rinsed, far more physisorbed than chemisorbed molecules remain at the surface.

Polarization studies. To determine whether MPS molecules have a preferential orientation when adsorbed to the maleimide-terminated surface of a silicon wafer, polarization studies were performed. For the maleimide-terminated silicon wafer both before and after MPS adsorption to the surface, spectra were collected at both 20° and 74° angles of the IR beam from normal incidence to the surface. When the IR beam is near normal incidence to the surface (at a ~20° angle), its electric field is nearly parallel to the surface (Scheme 4.2). At this orientation, components of chemical bonds perpendicular to the surface do not line up with the IR electric field and cannot absorb IR photons, while components of bonds parallel to the surface can absorb IR. When the silicon surface is at a 74° angle from normal incidence with the IR beam (the Brewster angle for silicon), components of bonds both parallel and perpendicular to the surface may line up with components of the IR beam electric field and can therefore absorb IR photons.

Ellipsometry. To determine the thickness of the maleimide-terminated films, select samples were measured by ellipsometry after exposure of the surface to APTES and PMPI adsorption steps. A Rudolph AutoEL Ellipsometer was used with light incident on samples (silicon wafers) at 632.8 nm from a He-Ne laser. Prior to measurement, initial estimates were set for upper (thin film) and lower (silicon oxide) layer thickness and indices of refraction. APS and PMPI surface-attached molecules were treated as a single layer, due to uncertainty (and likely proximity) in their indices of refraction and lack of segregation of these molecules. Index of refraction of the

APS/PMPI layer was typically estimated from 1.45-1.46, similar to silicon oxide for which index of refraction was approximated at 1.455 or 1.462 [9]. Silicon oxide thickness was estimated from 0.5 – 1.5 nm with initial APS/PMPI film thickness estimates ranging from 2.0 – 5.0 nm.

Data Collection. Immediately following drying by a stream of nitrogen after each adsorption step, FTIR spectra were collected on a Thermo® 760 FTIR spectrometer at a 4 cm^{-1} resolution for a minimum of 1000 scans (~20 min data collection).

4.4 Results

Scheme 4.1 shows antibody chemical attachment to a silicon oxide surface. A wafer of silicon(100) is initially cleaned with SC1, SC2, HF and piranha cleans to obtain a layer of hydroxyl-terminated silicon oxide about 1.0-1.5 nm thick [10] (Scheme 4.1.A). This surface is subsequently derivitized with APTES in anhydrous toluene in a dry box free of oxygen and water (Scheme 4.1.B). Next, the crosslinker PMPI is attached to this surface via its isocyanate moiety (Scheme 4.1.C). Once this surface is prepared, antibody fragment (in aqueous solution) or test molecule in (anhydrous solvent) is attached via primary amine or sulfhydryl groups to the PMPI-terminated surface (Scheme 4.1.D).

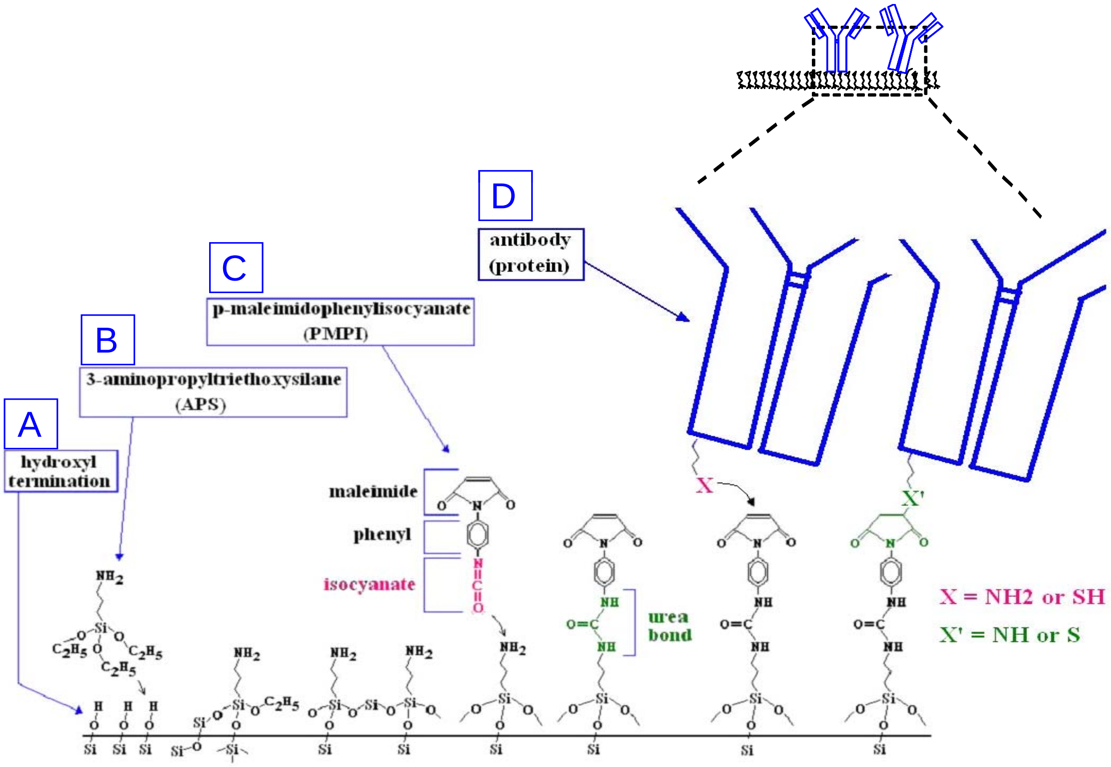
D
antibody (protein)
C
p-maleimidophenylisocyanate (PMPI)
B
3-aminopropyltriethoxysilane (APS)
A
hydroxyl termination
maleimide
phenyl
isocyanate
urea bond
X
X'
X = NH2 or SH
X' = NH or S
NH
NH2
Si
O
H
C2H5
O=C
N

Scheme 4.1. Antibody attachment to the silicon oxide surface. SC1/SC2/HF/piranha clean of a silicon wafer leaves 0.5-1.0 nm of silicon oxide at the surface (A). APTES is adsorbed to the silicon oxide surface forming a layer of APS (B). Maleimide cross-linker (PMPI) is covalently attached to the APS surface (C). Antibody or antibody fragment can then be attached via random amines ($X=NH_2$) of lysine residues on the antibody surface or free sulfhydryl moieties (X=SH) created in the antibody fragment (D).

4.4.1 PMPI attachment to the amine-terminated surface

4.4.1.1 IR Spectroscopy

Aminosilanization of the silicon oxide surface was described in Chapter 2. Figure 4.1 shows the covalent attachment of the maleimide crosslinker (PMPI) to an aminosilanized (APS-terminated) surface. The bottom spectrum shows PMPI physisorbed and referenced to the silicon oxide surface and exhibits features of the unreacted molecule. The top spectrum shows the chemical attachment between PMPI and the APS-terminated surface (referenced to the APS surface).

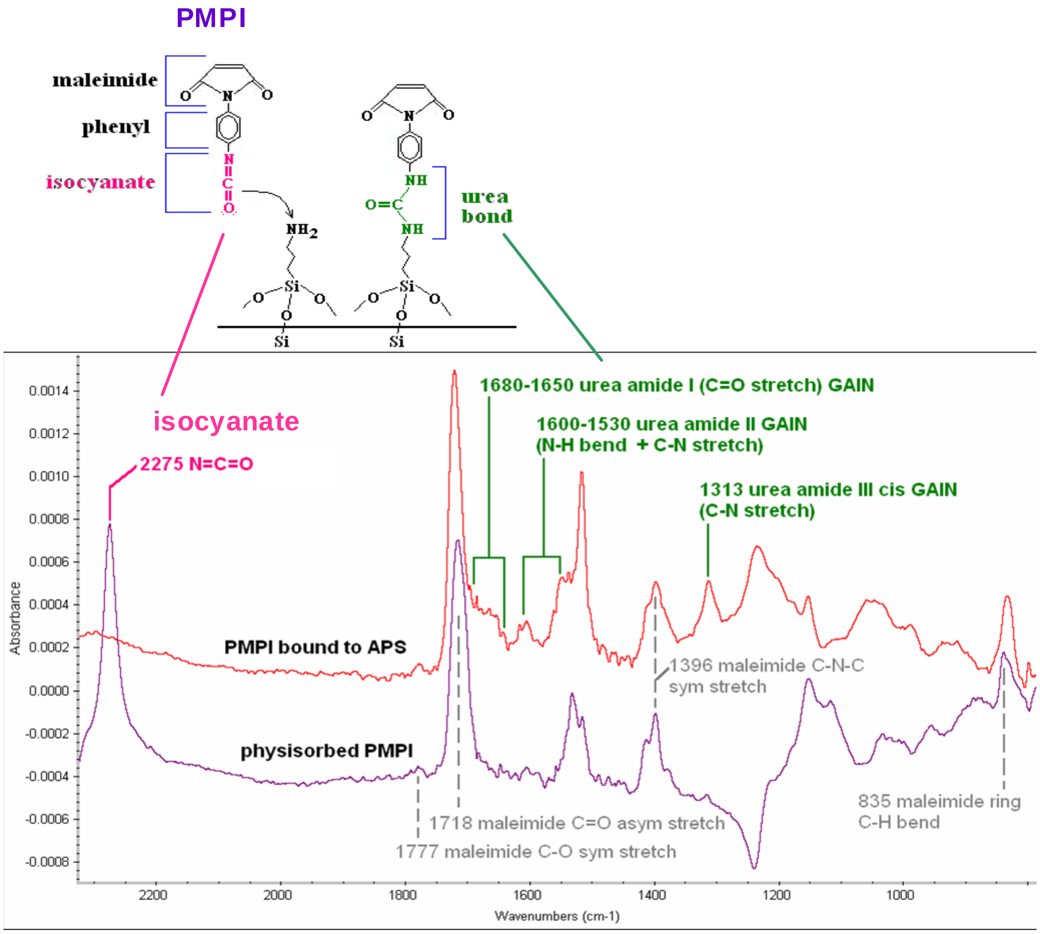

Figure 4.1. FTIR spectra of maleimide attachment to the APS surface.
Spectra of PMPI physisorbed and referenced to a silicon oxide surface (bottom), and PMPI chemisorbed and referenced to an APS-terminated surface (top). The isocyanate band present in the bottom spectrum at 2275 cm^{-1} is absent in the top spectrum, while amide bands due to the urea bond appear only in the top spectrum including the C=O stretch, NH bend and C-N stretch of the amide I, II and III bands, respectively. The other features of PMPI are preserved between both spectra.

In the top spectrum of Figure 4.1, the isocyanate (N=C=O) stretching mode is absent at 2275 cm^{-1} and three characteristic amide bands (features of urea bond formation between PMPI and APS) appear. These features include the maleimide urea carbonyl amide I band from 1650-1680 cm^{-1}, the N-H bend with C-N stretch of the amide II visible between 1515 and 1604 cm^{-1} and the C-N stretch of the amide III band at 1313 cm^{-1}. Other features of PMPI are preserved between the top and bottom spectra, including the maleimide ring carbonyl asymmetric stretch at 1718 cm^{-1}, the maleimide ring C-N-C symmetric stretch at 1396 cm^{-1} and the maleimide C-H out of plane bend at 835 cm^{-1} [11].

4.4.1.2 Ellipsometry of maleimide-terminated films

Ellipsometry is used to measure the thickness of the maleimide-terminated films. Film thicknesses given are for the total thickness for adsorption of APTES followed by PMPI molecules (Table 4.1, samples 1-5). The surface of Sample 6 contains an APS layer only.

In Figure 4.2, film growth is observed with adsorption time. Here, we observe significant variation in total film thickness and its dependence on both APTES and PMPI adsorption times (Figure 4.2). Additionally, we observe that IR absorption area for both APS and PMPI adsorption to the surface increases with total film thickness increase (Figure 4.3). Therefore, both components contribute to film thickness, but it is not clear to what extent.

Table 4.1. Values for APS and PMPI absorbance areas, total film thickness and estimated number of monolayers.

Sample no.	APS Si-O-Si absorbance area (940-1280 cm^{-1})	PMPI C=O absorbance area (1630-1750 cm^{-1})	Film thickness, nm (ellipsometry)	Estimated no. of monolayers
1	0.356	0.0281	2.07 ± 0.33	0.9
2	0.220	0.0402	3.00 ± 0.28	1.4
3	0.282	0.0410	3.38 ± 0.40	1.5
4	1.070	0.0785	9.45 ± 0.62	4.3
5	0.995	0.0892	8.41 ± 0.31	3.8
6	0.346	–	1.89 ± 0.55	2.1*

Monolayer height estimated at 2.2 nm = 0.9 nm for APS [12] + 1.3 nm for PMPI, based on [13] and [14]. Error shown is standard deviation. *Monolayer estimate for Sample 6, APS alone is 0.9 nm.

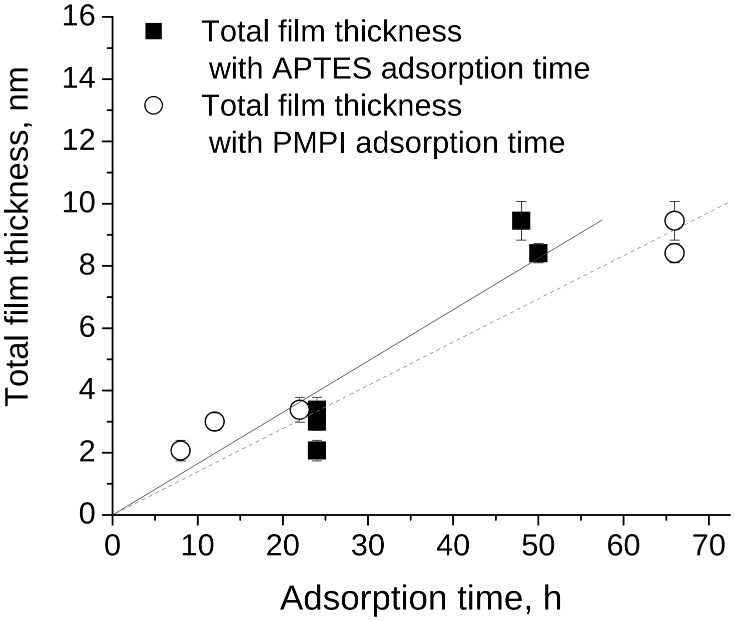

Figure 4.2. Total film thickness in nm vs APS ($R^2 = 0.85$) and PMPI ($R^2 = 0.92$) adsorption times.

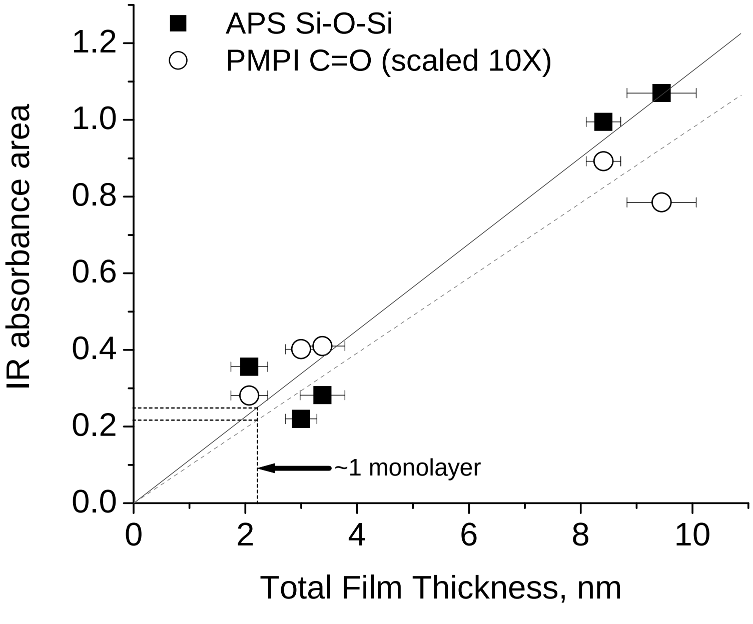

Figure 4.3. IR absorbance areas of APS and PMPI bands vs total film thickness.
IR absorbance areas of APS Si-O-Si band ($R^2 = 0.94$) and PMPI carbonyl stretch mode (scaled 10×, $R^2 = 0.83$) vs total film thickness in nm. Absorbance values for a monolayer are extrapolated based on estimated monolayer thickness of 2.2 nm.

To get a better sense of how film composition changes with increasing film thickness, APS and PMPI IR absorbance areas are observed on the basis of fold increase over minimum absorbance with fold increase over minimum total film thickness (Figure 4.4). We find that APS absorbance area increases nearly 4.5 – 5 fold with a 4 – 4.5 fold increase in total film thickness, whereas PMPI absorbance area only increases about 3 fold with the same increase in total film thickness.

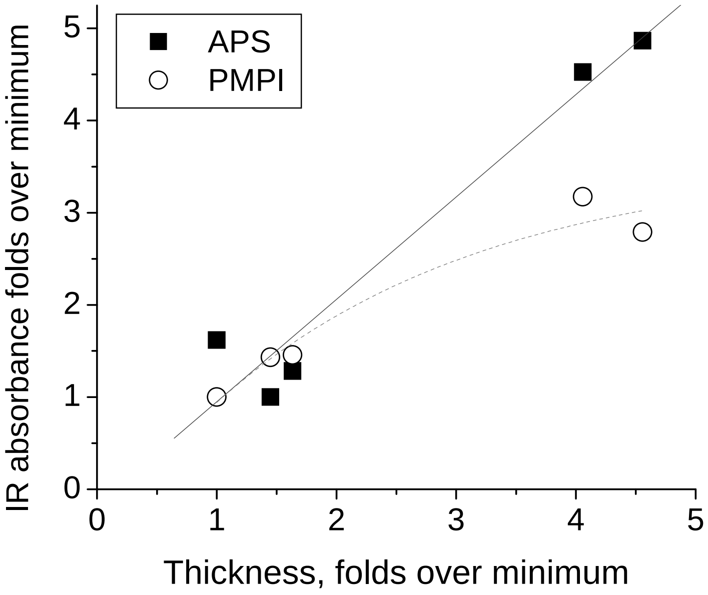

Figure 4.4. Fold increase over minimum (IR absorbance areas vs total film thickness). Fold increase over minimum IR absorbance area of APS ($R^2 = 0.94$) and PMPI ($R^2 = 0.96$, exponential decay) vs fold increase over minimum total film thickness. All values are normalized to respective minimum value in the series.

The height of an APS-PMPI monolayer is estimated at 2.2 nm by adding the length of APTES (0.9 nm) [12] to the length of the unreacted PMPI molecule: phenyl spacer (0.87 nm) [13] + maleimide (0.43 nm, estimated as half the spacer length based on [14]). Dividing observed film thickness by estimated monolayer height, equivalent number of APS-PMPI monolayers is estimated for each sample (Table 4.1).

Using the linear relationship between IR absorbance area and film thickness, APS Si-O-Si and PMPI carbonyl stretch mode IR absorbance values are extrapolated for one monolayer (Figure 4.3). Using estimated monolayer height in nm, absorbance areas for a monolayer are estimated at 0.25 for the APS Si-O-Si band and 0.022 for the PMPI carbonyl stretch mode.

4.4.2 Test molecule (MPS) chemical attachment to the maleimide-terminated surface

To identify the bonds formed between the protein and the surface without interference from protein IR bands, “test molecules” bearing the same reactive moieties as those on the protein are adsorbed to the surface in lieu of protein. Figures 4.5 – 4.8 show the similarities and differences between spectra of different test molecules and protein fragment adsorbed to maleimide-terminated surfaces. The spectra in these figures aid in the identification of antibody-surface chemical bond IR assignments as well as evaluation of the small molecule model as a tool for characterization of antibody attachment to silicon oxide surfaces.

Figure 4.5 shows a spectrum of the PMPI-terminated surface (bottom spectrum), physisorbed and unreacted MPS (top spectrum) and MPS chemisorbed to the PMPI surface (middle spectrum). The middle spectrum contains both features of MPS from the top spectrum and the PMPI surface from the bottom spectrum that are preserved in the surface reaction. Features missing from the middle spectrum that are present in either the top or bottom spectrum may be due to chemical bonds broken in the reaction of MPS with the surface. Likewise, new features present in the middle spectrum may be due to chemical bonds formed in the reaction. Such features include the loss of the maleimide

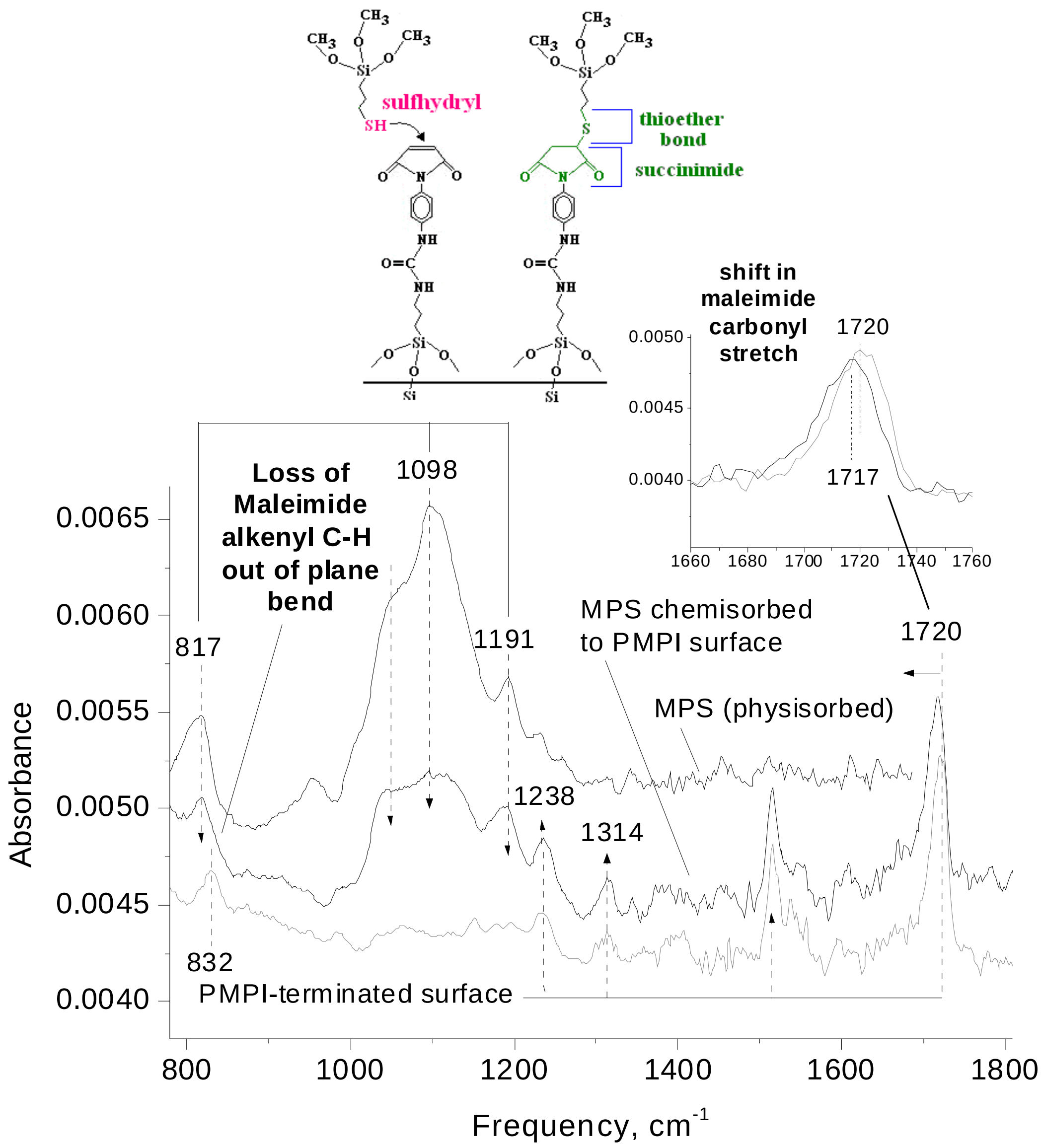

Figure 4.5. Spectra of sulfhydryl-linkage test molecule (MPS) to maleimide surface. FTIR spectra of sulfhydryl-linkage test molecule chemical attachment to a maleimide-terminated surface. Spectra of PMPI chemisorbed and referenced to an APS-terminated surface (bottom), MPS chemisorbed to the maleimide-terminated surface and referenced to the APS-terminated surface (middle), and MPS physisorbed and referenced to a silicon oxide surface (top). Dotted lines with arrows indicate spectral features of the PMPI-terminated surface and physisorbed MPS that remain intact after chemisorption of MPS to the surface. Red-shift in the carbonyl from 1720 to 1717 cm^{-1} and loss of the band at 835 cm^{-1} (middle spectrum) indicate changes due to chemisorption of MPS to the maleimide-terminated surface. Inset: PMPI-surface (gray) shifts to MPS chemisorbed to PMPI-surface (black).

alkenyl C-H out of plane bend at 832 cm^{-1} and a red-shift in the maleimide carbonyl asymmetric stretch from 1720 cm^{-1} to 1717 cm^{-1} in the spectrum of MPS chemically attached to the PMPI surface.

4.4.3 Polarization dependence of MPS chemical attachment

To further provide evidence of chemical attachment of MPS to the maleimide surface as well as information about the orientation of MPS relative to the surface, a polarization study is conducted. Figure 4.6 shows the results of the polarization study of the MPS-terminated surface (see also Scheme 4.2). In the top spectrum of MPS chemisorbed to the PMPI-surface, with IR at a 74° angle of incidence to the surface, the Si–O–C band is present from 900–1288 cm^{-1}. In the top spectrum with IR at a 20° angle of incidence, the Si–O–C band decreases to 24% of its intensity with IR at a 74° angle. In the bottom spectra of MPS physisorbed to a silicon oxide surface (control experiment), the Si–O–C band with IR at a 20° angle to the surface is 50% of its intensity with IR at a 74° angle to the surface.

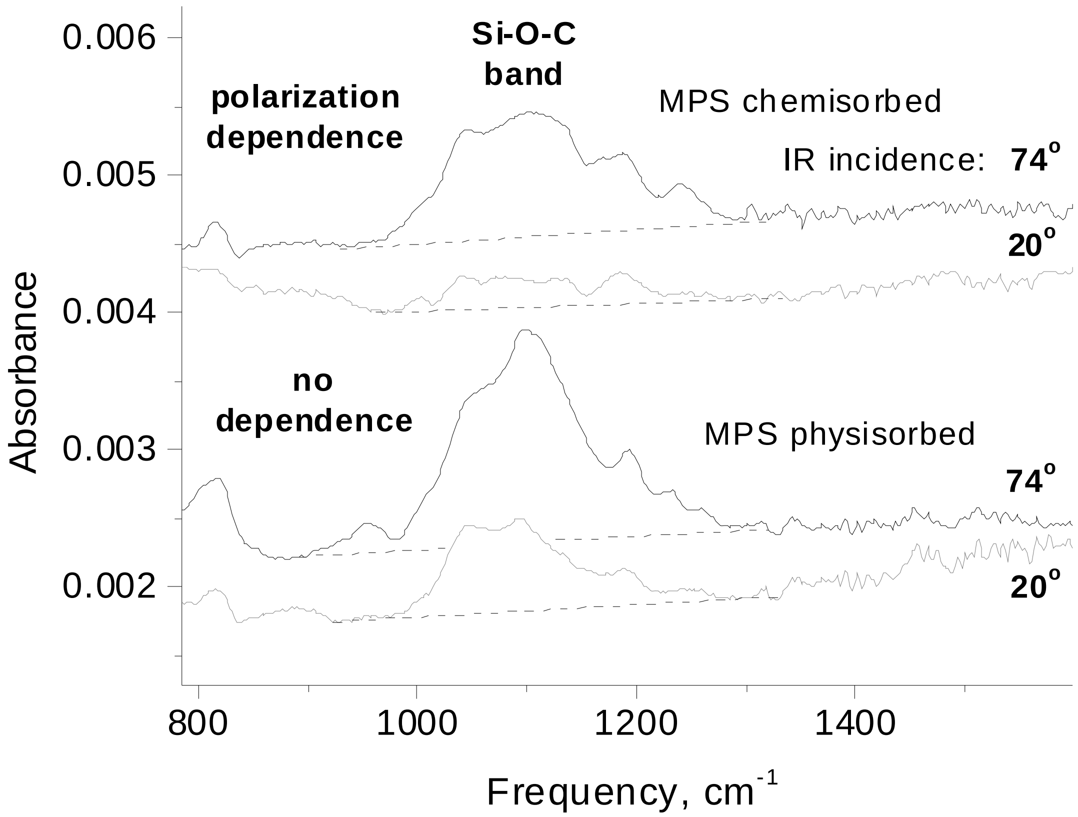

Figure 4.6. Polarization study of chemisorption of MPS to a maleimide surface.
This study suggests that MPS Si–O–C bonds are perpendicular to surface when MPS is covalently bound to the surface. Spectra of MPS chemisorbed and referenced to a PMPI-terminated surface at IR angles of incidence 20° and 74° (top spectra) and MPS physisorbed and referenced to a silicon oxide surface at IR angles of incidence 20o and 74o (bottom spectra). Only 24% of IR incident at an angle near normal (20°) to the surface is absorbed (of absorption at 74°) suggesting polarization dependence of the Si–O–C band (~900-1288 cm^{-1}) for chemisorbed MPS. In contrast, 43% of IR incident near normal is absorbed (of absorption at 74°) suggesting no polarization dependence for physisorbed MPS.

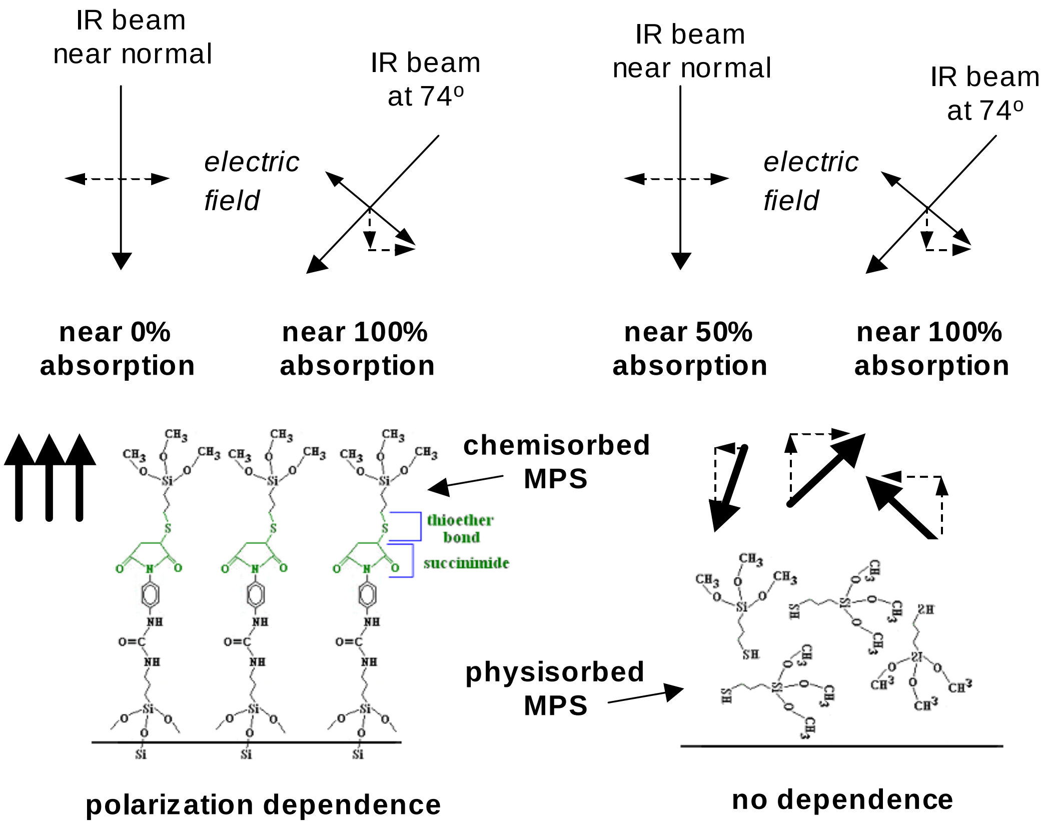
IR beam near normal
IR beam at 74°
electric field
IR beam near normal
IR beam at 74°
electric field
near 0% absorption
near 100% absorption
near 50% absorption
near 100% absorption
chemisorbed MPS
thioether bond
succinimide
physisorbed MPS
polarization dependence
no dependence

Scheme 4.2. Polarization dependence.
When the IR beam is near normal incidence to the surface, its electric field is almost entirely parallel to the surface. Here, only components of chemical bonds parallel to the surface can absorb IR. With most bonds perpendicular to the surface, little is absorbed (left). With bonds in both orientations, parallel components (~50%) are absorbed (right). When the IR beam is at a 74° angle to the surface, its electric field has both parallel and perpendicular components and can absorb both components of chemical bonds. Molecules on both the left and right side have bonds whose components are aligned with the electric field in this case.

4.4.4 Test molecule (APTES) chemical attachment to the maleimide-terminated surface

Figure 4.7 is a comparison between the features of amine and sulfhydryl chemical attachment to the surface. Top and bottom spectra are for the attachment of APTES (amine) and MPS (sulfhydryl) to the maleimide-terminated surface, respectively. Both spectra exhibit a maleimide carbonyl shift at ~1720 cm^{-1} to a lower frequency of a few wavenumbers (cm^{-1}) shown in differential form. Another change in both spectra is the loss of the maleimide C–H alkenyl out-of-plane bending mode at ~835 cm^{-1}. Only the bottom spectrum exhibits a band at 816 cm^{-1}.

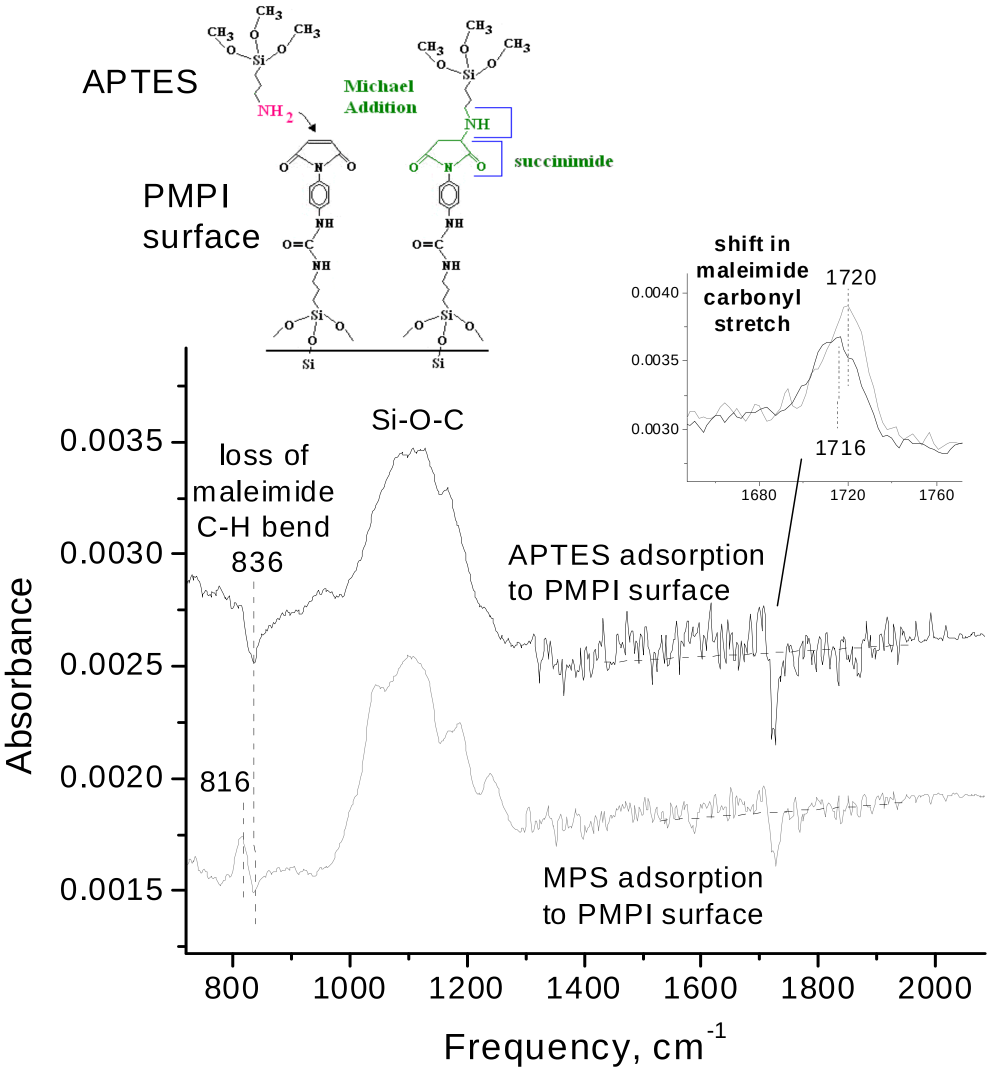

Figure 4.7. Comparison of amine (APTES) and sulfhydryl (MPS) chemical attachment to the maleimide surface.

The top and bottom spectra show the chemical attachment of APTES and MPS to the maleimide surface, respectively and are referenced to respective PMPI-terminated surfaces. Both spectra exhibit a shift in the maleimide carbonyl at ~1720 cm^{-1} and loss of the maleimide alkenyl C–H out of plane bending mode at 836 cm^{-1}. The main difference between the spectra is that only the MPS spectrum exhibits an IR band at 816 cm^{-1}. **Inset:** Shift in maleimide carbonyl stretch before and after APTES adsorption to the PMPI surface. Spectra are referenced to the APS-terminated surface that PMPI is attached to.

Figure 4.8 **a** shows the spectrum of an scFv antibody fragment [15] (from the binding region of the Fab fragment) attached to the maleimide surface, most likely through the primary amines of lysine or arginine residues at the surface of the fragment. Amide bands at 1664 and 1530 cm^{-1} are observed, indicating the presence of protein at the surface. Additionally a number of negative IR bands are present at 1030 and 1151 cm^{-1}, due to loss of APS Si-O-Si bands and at 1238, 1315 and 1720 cm^{-1} due to loss of maleimide bands. Figure 4.8 **b** shows the spectrum of a maleimide surface exposed to PBS for 18 h and exhibits the same negative IR bands as in Figure 4.8 **a**. Figure 4.8 **c** shows the spectrum of APTES in anhydrous solvent adsorbed to the maleimide surface for comparison with the spectra in **a** and **b**. To clarify IR features at 1720 cm^{-1}, the inset of Figure 4.8 (upper right corner) shows the maleimide carbonyl band before and after exposure to protein in PBS, PBS alone or APTES in anhydrous solvent, corresponding to spectra in **a**, **b** and **c**, showing both loss of and shift in the maleimide carbonyl stretch. It is noted that negative bands at 824 cm^{-1} in spectra **a** and **b** may be distinguished from the negative band at 837 cm^{-1} in spectrum **c.**

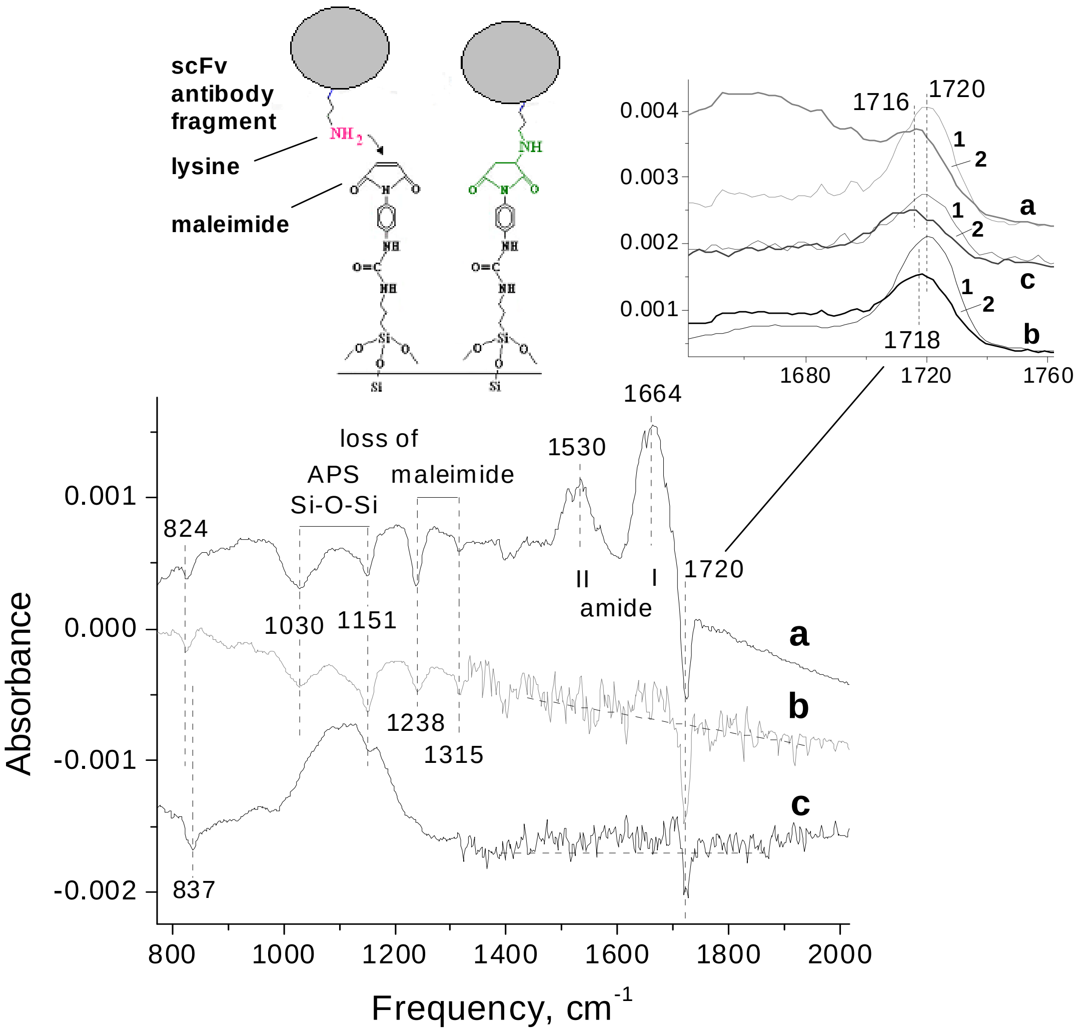

Figure 4.8. Comparison of protein fragment and amine-terminated small molecule (APTES) attachment to maleimide-terminated surfaces.

Spectra of scFv antibody fragment adsorbed and referenced to a maleimide-terminated surface (a), maleimide surface exposed to PBS (aqueous solution) for 18 h and referenced to the pre-exposed maleimide surface (b), and APTES in anhydrous solvent adsorbed and referenced to the maleimide-terminated surface (c). Inset: Spectra of maleimide carbonyl (~1720 cm^{-1}) before (1) and after (2) exposure to a, b, and c as indicated. All spectra are referenced to the APS-terminated surface to which maleimide is attached.

4.5 Discussion

4.5.1 PMPI attachment to the amine-terminated surface

The adsorption steps for protein attachment to the silicon oxide surface are analyzed sequentially, beginning with maleimide (PMPI) attachment to aminosilanized (APS) surfaces. In a number of other studies [2, 16-18], maleimide is attached to amine-terminated surfaces via heterobifunctional crosslinkers with a succinimide ring on one end and a maleimide on the other. Due to the possibility of either moiety reacting with amines [1], bifunctional surfaces likely result, with both maleimide and succinimide termination, rather than purely maleimide termination. In this study, the near complete disappearance of the isocyanate (N=C=O) stretching mode at 2275 cm^{-1} (Figure 4.1, top spectrum) suggests (by negative correlation with the bottom spectrum) that PMPI has reacted with APS almost entirely through its isocyanate moiety, leaving the maleimide olefin ring intact. Appearance of amide I, II and III bands indicates the formation of the urea bond between PMPI and the APS-terminated surface, further supporting reaction through the isocyanate moiety. Other features of the maleimide ring present in both chemisorbed and phsysisorbed spectra of Figure 4.1 further suggest that the maleimide ring remains intact after the surface reaction. Together, these spectra features confirm that the isocyanate and not the maleimide has reacted with the amine-terminated surface. After chemisorption of PMPI to the surface, two schemes for attachment of protein to the maleimide surface are investigated, attachment via sulfhydryl and via amine moieties.

4.5.2 Ellipsometry of maleimide-terminated films.

Based on the size of molecules from which number of monolayers is calculated and the linear increase in film thickness with molecular adsorption times, most APS/PMPI films formed are believed to be multilayers (Figure 4.2 and Table 4.1).

Observing fold increase in APS and PMPI absorbance areas with increasing total film thickness, as the film becomes thicker, the amount of APS increases at a greater rate than the increase in PMPI (Figure 4.4). Hence, film growth is due more to growth in APS than PMPI and there is a greater proportion of APS to PMPI in the film at greater film thickness. PMPI increases by fewer fold than APS because it cannot polymerize to the extent that APS can, since its reaction with the terminal amine of APS should be essentially self-terminating. In contrast, APS likely polymerizes with increase in adsorption time.

The observed increase in PMPI that does occur with increasing film thickness may be due to both increasing film roughness and possible PMPI dimerization [1]. Ellipsometry reports average film thickness, but does not account for film roughness. As more APS adsorbs to the surface, it is possible that its surface area increases due to roughness and formation of islands, providing more available amines for PMPI to attach to. Although PMPI cannot polymerize extensively to form multilayers, it may dimerizes in solution and attach to the amine surface via amine-maleimide addition [1].

4.5.3 Test molecule (MPS) chemical attachment to the maleimide-terminated surface

First, we examine sulfhydryl attachment chemistry, used for orienting antibody fragments at a surface, in which a reducing agent activates a sulfhydryl moiety at the end of the fragment. Here, a sulfhydryl-bearing small molecule, MPS, is used in place of sulfhydryl-modified protein. Features of the middle spectrum in Figure 4.5 indicate chemisorption between MPS and the maleimide-terminated surface. Upon attachment of MPS to the surface, the maleimide alkenyl out of plane C-H bend at 832 cm^{-1} disappears due to the change in the maleimide ring to succinimide ring [17]. A band at 818 cm^{-1} appears, partly obscuring the disappearance of the band at 832 cm^{-1}, but this band is identified in spectra of MPS adsorbed to the silicon oxide surface (Figure 4.5) and is thus believed to be due to MPS, although its assignment is not clear. Additionally, the maleimide carbonyl asymmetric stretch centered at 1720 cm^{-1} is red-shifted slightly to 1717 cm^{-1} upon conversion of the maleimide to a succinimide ring, also observed by Xiao et al. [17]. The decrease in the size of this band also suggests that some of the maleimide moieties may be lost in ring-opening side reactions [5, 8]. Similar N-hydroxysuccinimide (NHS)-terminated surfaces are reported by a number of sources to exhibit three bands: two due to succinimide ring carbonyl stretching (asymmetric at 1747 and symmetric at 1789 cm^{-1}) and one due to the NHS ester at 1820 cm^{-1} (Frey, Lahiri, Voicu). While the IR band of the ester is not expected here since the succinimide in this study contains no ester, it is not clear why the maleimide carbonyl at 1720 cm^{-1} does not convert to the succinimide asymmetric stretch near 1750 cm^{-1}. An explanation may be that the ester adjacent to the succinimide in NHS (lacking here) significantly influences the frequency of the succinimide ring carbonyl bands as well.

4.5.4 Polarization dependence of MPS chemical attachment

Further evidence for the covalent attachment of MPS to the maleimide-terminated surface comes from a polarization study of MPS attachment to this surface. For MPS covalently bound to the maleimide-terminated surface (presumably through its sulfhydryl moiety), the Si-O-C region of MPS exhibits polarization dependence (top spectra of Figure 4.6), whereas for MPS physisorbed to silicon oxide, the same region does not exhibit polarization dependence (bottom spectra of Figure 4.6).

Figure 4.6 illustrates polarization dependence as follows (see also Scheme 4.2): For the top spectrum of MPS chemisorbed to the maleimide surface via its S-H moiety with IR at a 74° angle of incidence from the normal to the surface (Brewster angle), the electric field of the IR beam can interact with methoxy groups at all orientations to the surface and the Si-O-C bands are present from ~900-1288 cm^{-1}. In the top spectrum with IR at a 20° angle of incidence, all components of the IR electric field are nearly parallel to the silicon wafer surface, preventing dipoles of moieties perpendicular to the surface from absorbing IR radiation. Hence, the reduction of the MPS Si-O-C region to 24% at this IR angle of incidence suggests that (on average) MPS methoxy groups are oriented mostly perpendicular to the surface. The presence of Si-O-C bands in the 20° angle spectrum at 43% that of the 74° angle spectrum (Figure 4.6, bottom spectra) suggests that MPS methoxy groups are oriented more randomly relative to the surface when MPS molecules are not bound via their sulfhydryl moiety.

It is important to discuss sufficiency of reduction in IR absorption for polarization dependence. First, the orientation to a surface of both molecular bonds and an IR electric field can be equivalently described as the vector sum of components parallel and perpendicular to the surface. For the negative control (random molecule orientation), only about 50% of components of molecular bonds will be oriented parallel to the surface (with the other 50% perpendicular). Hence, when the IR electric field is parallel to the surface, only 50% of molecular bond components can absorb IR. When the IR beam is at the Brewster angle (74° for silicon), the electric field, at an angle to the surface, has both parallel and perpendicular components relative to the surface and can therefore be absorbed by the components of molecular bonds at all orientations. Additionally, IR at the Brewster angle is transmitted maximally to the detector, further increasing the intensity of IR absorption bands. Thus, randomly oriented molecular bonds can exhibit a 50-60% reduction in IR absorption when the IR electric field is angled nearly parallel to the surface. Substantially more than 50% reduction in absorption is necessary to suggest polarization dependence.

The polarization dependence of MPS Si-O-C modes (with bond components mostly perpendicular to the silicon surface) for MPS adsorbed to the maleimide-terminated surface suggests that MPS molecules in this environment are more restricted than molecules randomly adsorbed to a surface. Covalent attachment of MPS to the surface at a single location (the sulfhydryl moiety) is a reasonable explanation for such restriction of molecule orientation.

4.5.5 Test molecule (APTES) chemical attachment to the maleimide-terminated surface

Since sulfhydryl-activated protein fragments may also contain primary amines on their surface (from lysine and arginine residues), it is of interest to study surface attachment via amine-maleimide addition. Although this mechanism is reported to be much slower than sulfhydryl-maleimide attachment [3], side reactions between primary amines and maleimides are still possible [1, 8]. Xiao et al. observed the attachment of peptide bearing a sulfhydryl and an amine at either end to maleimide-terminated surfaces, so either end may have reacted with the surface [17, 18]. To clarify the mechanism, in this study, APTES is attached to the maleimide surface as a test molecule with only primary amines as the surface-reactive moiety. This attachment yields a similar spectrum to that of sulfhdryl attachment (Figure 4.7). The top spectrum of Figure 4.7 (for APTES attachment) shows disappearance of the maleimide alkenyl out of plane C-H bend at 837 cm^{-1} and a small red-shift in the maleimide carbonyl asymmetric stretch from 1720 cm^{-1} to 1716 cm^{-1} upon conversion of the maleimide ring to a succinimide ring. Different from MPS attachment, no band is present at 816 cm^{-1} for APTES adsorption to the maleimide surface and hence this feature may aid in distinguishing spectral features of amine and sulfhydryl attachment. Other than this spectral feature, spectra of amine and sulfhydryl attachment to maleimide surfaces are very similar and hence for molecules with both amine and sulfhydryl groups it may be difficult to distinguish the extent of attachment of each moiety using FTIR alone.

4.5.6 Protein fragment adsorption to the maleimide-terminated surface

While amide I and II bands in spectrum **a** of Figure 4.8 indicate that protein is adsorbed to the maleimide surface, indication of protein chemical attachment to the surface is not as clear. Comparison between the spectrum of protein adsorption (spectrum **a**) and that of a maleimide-terminated surface exposed to aqueous solution (PBS) (spectrum **b**) suggests that some maleimide and APS moieties are removed from the surface due to attack by water. Negative IR bands in spectra **a** and **b** at 824 and 1720 cm^{-1} occur at nearly the same frequencies as negative bands due to maleimide conversion to succinimide in spectrum **c**. However, the difference in frequency between negative bands at 824 cm^{-1} in spectra **a** and **b** and 837 cm^{-1} in spectrum **c** (and for MPS in Figure 4.7) may indicate whether the maleimide was lost due to attack by water (824 cm^{-1}) or converted to succinimide (837 cm^{-1}).

Observation of the maleimide carbonyl band before and after exposure to protein in PBS, PBS alone or APTES in anhydrous solvent (Figure 4.8 inset, **a**, **b** and **c**, respectively) shows that both loss and shift of this band occur to some degree in all cases. APTES adsorption shows the most pronounced shift and PBS the least, suggesting that molecular attachment causes band shifting whereas rinsing with aqueous solvent causes band loss (and a small 2 cm^{-1} shift, likely due to uncertainty in the data). Whether or not significant band shift is observed for protein adsorption is unclear, as the protein amide I band is adjacent to the maleimide carbonyl and may affect its frequency position. While it is likely that protein is attached to the surface via reaction of primary amines with maleimide, there may be too few reaction sites on the surface of the proteins for significant IR absorption. In contrast, the APTES molecule is small enough to react with far more sites on the maleimide surface than protein can and hence the IR absorptions of its reaction with the surface are perceptible. Hence, adsorption of test molecules to the maleimide surface in anhydrous solvent serves the dual purposes of preventing degradation by water and increasing the IR signal by increasing the quantity of surface reaction sites. This method boosts the number of protein-surface chemical reactions to perceptible levels, permitting observation of biochemical covalent attachment that would otherwise be imperceptible due to sparseness of reaction sites and solvent interference. If a suitable anhydrous solvent is chosen that does not denature protein, it may also be possible to adsorb protein to the surface in the absence of water to directly observe chemical reaction of its moieties with the surface, however sparseness of reaction sites may still be an issue.

4.5.7 Identification of shift in the maleimide carbonyl band: comparison with biotin ureido carbonyl shift

In contrast to the putative shift in the biotin ureido carbonyl mode upon protein adsorption in Chapter 3, the shift in the maleimide carbonyl frequency upon conversion of maleimide to succinimide in thioether attachment of amine or sulfhydryl to the ring is directly observable using test molecules in place of protein. In the absence of interfering protein bands, the shift is distinguishable from band loss by the rise in the leading part of the differential band in the differential spectrum (e.g., Figure 4.8 spectrum **c**) or by direct observation of the shift in the carbonyl band center between spectra before and after attachment of a small molecule to the maleimide (e.g., Figure 4.8 inset). Since the shift in the carbonyl is due to covalent attachment of a sulfhydryl or amine to the maleimide ring, replacement of protein by a test molecule bearing the same moiety was possible. Hence, there is less uncertainty in the identification of band shift in this chapter compared with that in Chapter 3. In Chapter 3, it is impossible to test the effect of binding of the biotin ureido carbonyl in the SA cleft without the protein itself. If, as mentioned in Chapter 3, the shift in the biotin ureido is due to a non-specific interaction with protein, it may be possible to test this hypothesis by adsorbing a small molecule to the biotinylated surface (possessing no IR bands in the protein region) that could hydrogen bond or interact electrostatically with the biotin ureido.

With the observation of the shift in the maleimide carbonyl band, some band loss is also observed superimposed on the shift as evidenced by the decreased area of the band after attachment of the small molecule (or in the differential spectrum, that the negative part of the differential is larger than the positive part). Therefore, loss of maleimide by other mechanisms is also likely, possibly due to trace amounts of water in the anhydrous solvent that the test molecules are solvated in. The confirmation of both shift and loss features simultaneously attests to the complexity of the system and the difficulty of determining the origin of such features. In the case of the biotin ureido carbonyl dip, both loss and shift mechanisms may be simultaneously occurring as well.

It is also important to note that in spectra where protein attaches to the maleimide surface, even with multiple attachment sites, there may not be enough of a signal to detect the attachment and observe a frequency shift. The size of the protein is far bigger than the maleimide it attaches to, making even multiple points of attachment on each protein to the surface relatively sparse.

4.6 Conclusions

The IR spectra in this study have indicated that the expected chemical attachments have taken place at each step in the adsorption process for the chemical attachment of protein to the surface. Spectra confirm that the isocyanate moiety of PMPI has reacted with the terminal amine group of the APS-terminated surface and urea linkage has replaced APS amino and PMPI isocyanate groups. The small molecule model has been shown to be successful for characterization of two types of chemical attachment of protein to maleimide-terminated surfaces, via sulfhydrl and amine moieties. Protein attachment to the surface itself did not yield clear IR bands indicative of chemical attachment, possibly because such bands may be obscured by bands due to water degradation of the APS and maleimide, and interference by protein bands at frequencies 1700 cm^{-1} and lower. Furthermore, due to the size of the protein compared with maleimide moieties, there may be too few bonds formed between the protein and surface to be detected. In contrast, the small size of the test molecules allows them access to far more reaction sites at the surface, and anhydrous solvent significantly reduces interference due to attack of water on the surface. The lack of protein chains and residues also eliminates interference due to their IR bands. The polarization study of the attachment of MPS to the maleimide surface has shown that this small molecule has bonds oriented perpendicular to the surface. Such restriction of orientation further suggests chemical attachment to the surface, as physisorbed molecules adsorb to the surface in random orientations. Since the reactive moieties of these small molecules are the same as in the protein-surface reaction, we can be confident that the relevant chemical reactions have been properly characterized.

4.7 References

1. Jin, L., A. Horgan, and R. Levicky, *Preparation of End-Tethered DNA Monolayers on Siliceous Surfaces Using Heterobifunctional Cross-Linkers.* Langmuir, 2003. **19**: p. 6968-6975.
2. Xiao, S.-J., M. Textor, and N.D. Spencer, *Covalent attachment of cell-adhesive, (Arg-Gly-Asp)-containing peptides to titanium surfaces.* Langmuir, 1998. **14**: p. 5507-5516.
3. Glaser, A.N., *In the Proteins*, H. Neurath and R.L. Hill, Editors. 1976, Academic Press: New York.
4. Oh, S.J., S.J. Cho, C.O. Kim, and J.W. Park, *Characteristics of DNA Microarrays Fabricated on Various Aminosilane Layers.* Langmuir, 2002. **18**(5): p. 1764–1769.
5. Shen, G., A. Horgan, and R. Levicky, *Reaction of N-phenyl maleimide with aminosilane monolayers.* Colloids and Surfaces B: Biointerfaces, 2004. **35**: p. 59-65.
6. Kusnezow, W., A. Jacob, A. Walijew, F. Diehl, and J.D. Hoheisel, *Antibody microarrays: An evaluation of production parameters.* Proteomics, 2003. **3**: p. 254-264.
7. Peluso, P. and OTHERS, *Optimizing antibody immobilization strategies for the construction of protein microarrays.* Analytical Biochemistry, 2003. **312**: p. 113-124.
8. Shen, G., M.F.G. Anand, and R. Levicky, *X-ray photoelectron spectroscopy and infrared spectroscopy study of maleimide-activated supports for immobilization of oligodeoxyribonucleotides.* Nucleic Acids Research, 2004. **32**(20): p. 5973-5980.
9. Ombelli, M., D.M. Eckmann, and R.J. Composto, *Biomimetic Dextran Coatings On Silicon Wafers: Thin Film Properties And Wetting.* Mat. Res. Soc. Symp. Proc., 2003. **734**: p. B10.7.1-B10.7.6.
10. Chabal, Y.J. and H.G. S., *Handbook of Semiconductor Wafer Cleaning Technology*, W. Kern, Editor. 1993, Noyes Publications. p. 433-495.
11. Parker, S.F., *Vibrational spectroscopy of N-methylmaleimide.* Spectrochimica Acta Part A, 1995. **51**: p. 2067-2072.
12. Demirel, G., M. Cakmak, T. Caykara, and S. Ellialtıoglu, *Chemisorption of 3-Aminopropyltrimethoxysilane on Si(001)-(2 x 2).* Journal of Physical Chemistry C, 2007. **111**: p. 15020-15025.
13. *PMPI (N-[p-Maleimidophenyl]isocyanate)*. Thermo Scientific - Pierce Protein Research Products [cited; Available from: http://www.piercenet.com/Objects/View.cfm?type=ProductFamily&ID=02030332.
14. Shigemitsu, Y., K. Komiya, N. Mizuyama, and Y. Tominaga, *Reaction of functionalized maleimides with versatile nucleophiles. Synthesis, electronic spectra and molecular orbital study.* Dyes and Pigments, 2007. **72**: p. 271-284.
15. Jung, S. and A. Plückthun, *Improving in vivo folding and stability of a single-chain Fv antibody fragment by loop grafting.* Protein Engineering, 1997. **10**(8): p. 959-966.

16. MacBeath, G., A.N. Koehler, and S.L. Schreiber, *Printing Small Molecules as Microarrays and Detecting Protein−Ligand Interactions en Masse.* Journal of the American Chemical Society, 1999. **121**: p. 7967-7968.
17. Xiao, S.-J., S. Brunner, and M. Wieland, *Reactions of Surface Amines with Heterobifunctional Cross-Linkers Bearing Both Succinimidyl Ester and Maleimide for Grafting Biomolecules.* Journal of Physical Chemistry B, 2004. **108**: p. 16508-16517.
18. Xiao, S.-J., M. Wieland, and S. Brunner, *Surface reactions of 4-aminothiophenol with heterobifunctional crosslinkers bearing both succinimidyl ester and maleimide for biomolecular immobilization.* Journal of Colloid and Interface Science, 2005. **290**: p. 172–183.

CHAPTER 5: SURFACE ACOUSTIC WAVE STREAMING REMOVAL OF NON-SPECIFICALLY BOUND PROTEIN ON PROTEIN MICROARRAY SURFACES

Norman Lapin[1]*, Darren W. Branch*[2]*, Igal Brener*[2]
[1]*Department of Biomedical Engineering, Rutgers University, 617 Bowser Road, Piscataway, NJ, USA 0890.*
[2]*Microsensor Science and Technology Department, Sandia National Laboratories, Albuquerque, NM, USA 87185*

5.1 Abstract

Protein microarray technology is a burgeoning field, spawned from the success of the DNA microarray. This new field, however, presents new challenges not present in DNA technology, including the efficient removal of protein that binds to the microarray surface non-specifically. This study investigates the use of surface acoustic wave streaming (SAWS) for the mechanical removal of non-specifically bound protein. Here, a SAWS device is integrated with a microfluidic channel to remove non-specifically bound and fouled protein from the surface of antigen microarrays. We demonstrate that both *in situ* acoustic desorption of protein and *in situ* image data collection of fluorescence from protein microarray surfaces on which such desorption occurs are feasible in an enclosed SAWS device-microfluidic integrated system. It is further shown that acoustic desorption of protein can be quantified in terms of power dosage applied to the device and that system characteristics for non-specifically bound protein removal can be extracted based on fluorescence intensity thresholding.

5.2 Introduction

As scientists have reached a deeper understanding of the human genome and its products, it is becoming clear that these products, proteins, are more complex, diverse in function and orders of magnitude more abundant than the genes that encode them [1, 2]. Protein interaction networks are thus of key importance to the understanding of cellular networks and the propagation of disease. Considering the number of combinations of possible protein-protein and protein-drug interactions for a given system, the challenge of protein analysis is compounded by additional orders of magnitude and complexity. Hence, the focus of scientific research has shifted from the study of genomics to that of proteomics. This shift has produced an urgent need for new devices with high throughput and multiplexing capabilities.

Amongst the most promising tools available to researchers to meet the above challenges are protein and antibody microarrays [1, 3]. These arrays are composed of microspots of proteins or protein-interacting molecules patterned on a solid support by a spotting robot. When the surface is exposed to a solution of multiple proteins, different proteins in the solution will bind specifically at cognate locations with complementary active sites. This technology will be critical for innovations and advances in drug discovery, protein-based therapeutics, clinical diagnostics, environmental monitoring and development of national security technologies [3].

A prevalent type of microarray is the antibody microarray, in which antibodies raised against various proteins are covalently bound to the microarray surface and bind only to their antigen partners when exposed to a multiplexed solution of antigens. For antigen microarrays, the phase of the components are reversed with antigen bound at the surface and antibody in solution.

To maximize its high throughput and multiplexing functionality, a protein microarray hosts microscopic protein spots that are situated in dense registration on an open surface. In this arrangement, the entire array is vulnerable to protein fouling and cross-binding when exposed to multiplexed protein solutions. Non-specific binding (NSB) and biofouling of protein to bioassay and biosensor surfaces are considered by some to be the most formidable of the challenges to protein microarray development (based on [4]). NSB proteins attach to one another or to the interface with weak interactions at non-site specific locations. NSB of protein to assay surfaces can manifest as cross reactivity, increasing the rate of false positive readings [2]. Biofouling, a more generalized accumulation of proteins and biological materials on surfaces, decreases assay sensitivity adding noise to a binding signal by increasing background signal intensity. Biofouling can block binding sites causing false negatives, as evidenced by reduction in signal intensity with decreased partial concentration of specific antigen in complex protein mixtures [5]. Furthermore, protein that is non-specifically bound to an antibody-functionalized surface decreases the rate and amount of antigen that can bind specifically [6].

To mitigate the problem of protein fouling, the assay surface can undergo extensive washing and rinsing. However, the stronger the washing agent (e.g., detergents or high salt concentration rinses), the more likely the protein will be denatured. For this reason, the efficacy of this step is quite limited. An alternate solution for the removal of NSB protein is by acoustic streaming. Surface acoustic wave streaming (SAWS) can be generated at the surface of a piezoelectric material by application of a time-varying electrical potential resulting in the propagation of mechanical waves along the surface. This phenomenon is the result of the inverse piezoelectric effect in which application of an electric field produces mechanical strain. Devices fabricated on 128° YX $LiNbO_3$ propagate Rayleigh waves, generating retrograde elliptical motion at the interface. When Rayleigh devices are placed in a fluid, the mechanical waves dissipate within a few wavelengths as the energy “leaks” into the fluid. This energy is converted into longitudinal (compression) waves that travel away from the surface into the fluid at an angle determined by the ratio of the velocity of the Rayleigh wave at solid-air and solid-liquid interfaces. The energy of the longitudinal waves is capable of desorbing biomolecules from the surface, and can be tuned to desorb nonspecifically bound protein only, below the energy of desorption for specific binding (SB) interactions.

Meyer et al. used quartz crystal resonators (QCR) to generate shear waves for the removal of NSB protein from the QCR surface [7]. This process generates bulk waves in the material, requiring 14 W of input power to desorb protein from a relatively large device surface. Cular *et al.* reduced protein fouling at sensor surfaces using interdigital transducers (IDTs) to generate SAWS [8]. These devices require less power, on the order of milliwatts. In these studies, protein desorption took place within a bead of liquid applied on an open device surface.

In this study, a surface acoustic wave streaming (SAWS) device is integrated with a microfluidic channel to remove NSB and fouled protein from the surface of antibody microarrays. The fluid-enclosed aspect of this setup is a necessary characteristic of compact, portable, high-throughput devices. There are several specific advantages to device enclosure. Constant contact with fluid prevents protein at the surface from drying out that can lead to denaturation [2, 9]. The enclosed system also allows for continuous fluid flow during acoustic cleaning. The flow of buffer removes acoustically desorbed antibody, antigen and other particles, carrying them away from the vicinity of the microarray surface before they can readsorb. An additional feature of this setup is a glass bottom wall in the microfluidic channel through which the microarray surface is imaged *in situ* using an inverted microscope.

To compensate for power loss to the gasket retaining the fluid, a bidirectional acoustic horn IDT was patterned on the device surface (Scheme 5.1). The acoustic horn traps acoustic waves generated at the IDT and guides them down a narrowing path along the surface, compressing them laterally and increasing the energy density of the waves.

The goal of this study is to assess the energy necessary to desorb various types of non-specifically attached protein without disrupting the specifically adsorbed patterns of protein. The energy applied to the surface is quantified in terms of power dose applied to the SAWS device through a signal generator and amplifier less what is dissipated due to power reflection at the device and damping by the fluidic system. The net power dose is then correlated with the amount of protein removed from the device surface in terms of decrease in fluorescence intensity of the labeled protein. Regions where protein is initially attached to the surface for sensing binding partners (the microarray spots or squares) are called “sensing regions”. The background areas, where no sensing molecules are present are called “nonsensing regions”. This study assesses and quantifies the efficacy of protein removal by surface acoustic waves in each of these regions on the surface of the protein microarray within the microchannel.

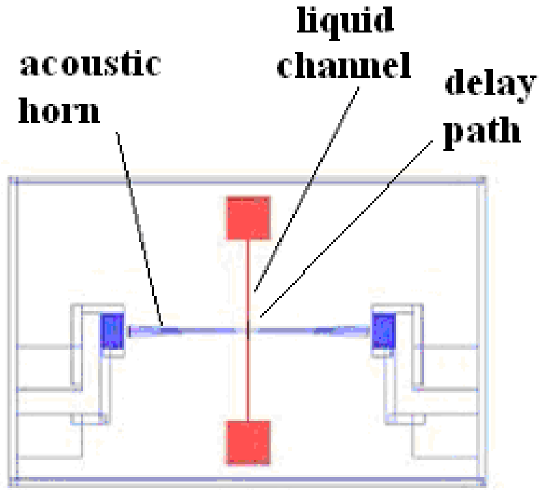

Scheme 5.1. Bi-directional acoustic horn IDT SAWS device.
IDT with acoustic horns is patterned on the device surface (blue). SAWs travel in two directions across the delay path from one acoustic horn to the other. A microfluidic liquid channel (red) is overlaid on the SAWS device to carry away protein removed from the surface by the SAW.

5.3 Experimental Methods

This section will explain how SAWS devices have been integrated with a microfluidic system to carry away protein as it is desorbed from the SAWS device surface. IgG protein was initially patterned in a microarray format on the surface of the SAWS device. The device was then assembled into a fixture that provided electrical power to the SAWS device and formed the microfluidic channel.

5.3.1 Surface preparation

To clean the surface for silanization, 128° YX lithium niobate ($LiNbO_3$) electrode (IDT)-patterned SAWS devices were rinsed thoroughly with acetone, followed by methanol, isopropanol and deionized (DI) water, then dried under a stream of nitrogen gas. Subsequently, the devices were placed in an Ultraviolet-Ozone Cleaning System

(UVOCS Inc.) for 15 min to remove any remaining contaminants. The SAWS devices were then submerged in a 1% v/v solution of 3-glycidoxypropyltrimethoxysilane (GPTMS; SigmaAldrich, St. Louis, MO) in toluene for 30 minutes (Scheme 5.2). The reaction was terminated by rinsing in toluene, followed by sonication for 5 minutes to remove excess organosilane. The devices were then rinsed with methanol and dried under a nitrogen stream. Finally, the wafers were treated for one hour at 120 °C to complete the hydrolysis reaction.

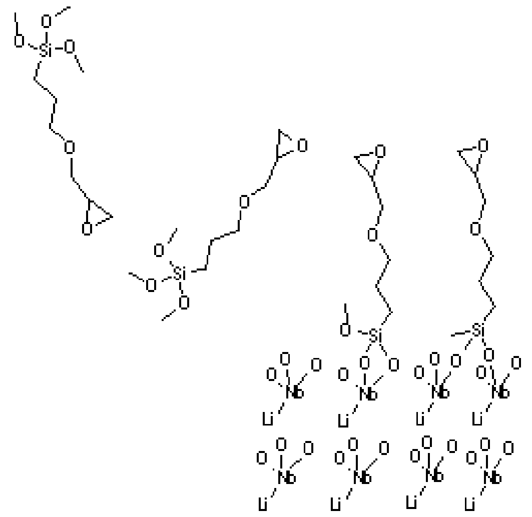

Scheme 5.2. Reaction of GPTMS with the lithium niobate surface.

5.3.2 Fluorescent Labeling of Proteins

Fluorescent dyes Alexa Fluor 488 (green) and Alexa Fluor 594 (red) (Molecular Probes (Invitrogen), Eugene, OR) were selected to label a 2 mg/ml solution of goat anti-mouse IgG and a 1.8 mg/ml solution of mouse anti-rabbit IgG, respectively (as an antigen-antibody pair) for antigen arrays, as described previously [8, 10]. In addition, both Alexa Fluor 350 (blue) and Alexa Fluor 488 were used to fluorescently label bovine serum albumin (BSA) for general fouling experiments. All protein solutions were maintained at pH 7.4. After labeling reactions and collection of labeled protein into vials were completed (protocol according to the Alexa Fluor protein labeling kit), absorbance of each protein solution was measured on a Beckman Coulter DU 800 Spectrophotometer. The absorbance values obtained were used to calculate protein concentration (mg/ml) and degree of fluorescence labeling (moles of dye/mole of protein) (see Introduction, Section 1.4.2). Stock concentrations were diluted as necessary for desired concentration in experiments. Stock and diluted protein solution were kept in the dark at all times except during aliquotting.

5.3.3 Protein patterning of the surface for formation of antigen arrays

5.3.3.1 Photoresist patterning and protein adsorption

A microarray pattern of 40 x 40 μm square wells was formed from AZ5214 photoresist using a photolithographic technique. Photoresist was spun onto the surface of the silanized lithium niobate SAWS devices for 30 s at 3000 rpm. The uniform coating of photoresist formed on the surface was subsequently soft-baked for 60 s at 90 ^{o}C. A custom-fabricated dark field emulsion mask aligner was then placed over the SAWS device with the microarray pattern positioned at the center of the device in the delay path between the surface-patterned acoustic horns. The mask-covered device was exposed to UV light for an optimized time of 32 s. The device was subsequently developed for 50 s in a 1:5::400K developer:DI water solution with mild agitation to ensure uniform development. Immediately following development, devices were rinsed in DI water with mild agitation for 1 min to terminate the development reaction.

To pattern protein on the surface, a volume of 3–6 µl of 0.2 mg/ml Alexa Fluor 594-labeled mouse anti-rabbit IgG (*the antigen*) was delivered to the photoresist-patterned region in the delay path at the center of the SAWS device between the acoustic horns. In the square wells of the pattern, where photoresist was absent, the antigen adsorbed to the GPTMS-functionalized surface (presumably by covalent attachment via amide bonds formed between primary amines of protein lysine and arginine residues and the epoxide ring of the GPTMS molecule, Scheme 5.3). The device was sealed inside a humidity chamber and kept in the dark for 45 minutes to allow the attachment to take place. After adsorption, the surface was immediately rinsed 3× with 1 ml phosphate buffered saline (PBS). The devices were then rinsed with acetone followed by a 10 s DI water rinse to remove the photoresist leaving a pattern of IgG squares covalently attached to the surface (sensing regions). The devices were again rinsed with PBS and DI water and dried under a nitrogen stream. The background or nonsensing region of the surface was subsequently blocked by adsorption (and covalently attachment) of 1 or 10 mg/ml BSA for 30 min using a similar procedure to that for antigen adsorption.

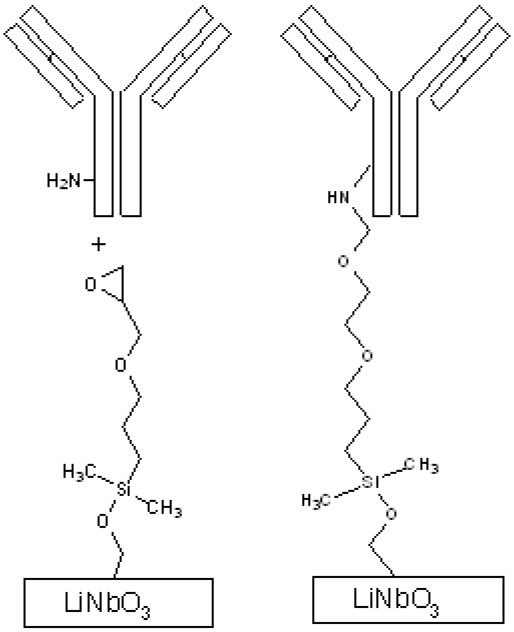

Scheme 5.3. Reaction of primary amines of lysine and arginine residues of protein (antigen) with surface-bound GPTMS.
Taken from [8].

5.3.3.2 Microarray Spotting (Alternative method)

A microarray printer, ArrayIt SpotBot®2 (TeleChem International, Sunnyvale, CA) was used to apply protein solution spots to the SAWS device surface. A 5×5 array of spots was applied in the region between the acoustic horns with center-to-center spacing of ~200 µm between spots. After air drying, each spot area was ~ 150 µm × 150 µm.

5.3.4 Protein adsorption to antigen array surfaces

To assess the ability of SAWS devices to remove NSB protein while preserving the native function of the remaining protein, protein was adsorbed to the antigen array on the device surface. For specific binding experiments, 0.4 mg/ml Alexa Fluor 488-labeled goat anti-mouse IgG (*the antibody*) was pipetted onto the antigen-patterned surface and incubated for 60 min following a similar procedure to that of section 5.3.3.1. To avoid excessive protein fouling in the microchannel and to simplify the experiments, all adsorption steps were performed *ex situ*. However, to approximate microchannel conditions, a solvent-cleaned glass cover slip was placed over the drop of antibody solution immediately after pipetting. The cover slip was then removed for the PBS rinse step. Other proteins applied to the patterned surface were Alexa Fluor 488 and Alexa Fluor 350-labeled BSA for control experiments of total NSB and protein fouling.

5.3.5 Verification of Film Thickness

To verify the thickness of the silane film, GPTMS was adsorbed to oxide terminated-silicon wafers. The average thickness of GPTMS was determined by ellipsometry on an EL X-01R Ellipsometer (Micro Photonics Inc., Allentown, PA).

Layer	Thickness (nm)	Surface Coverage
SiO2	2.76 ± 0.15	n/a
GPTMS	1.55 ± 0.19	~ 2 monolayers*

* Calculation based on [8].

5.3.6 Microfluidic Setup

Two pieces of fabricated polycarbonate (Regal Plastics Supply Co., Albuquerque, NM) with a depression for the SAWS wafer and microchannel machined out of one piece, were screwed together to form a fixture sandwiching the SAWS device (Scheme 5.4). Electrical test probes (AlphaTest Corp., Mesa, AZ) in the opposite side of the fixture made contact with the SAWS device terminals via silver epoxy painted around the edges from one side of the device to the other. A PDMS gasket fit into a grove around the microchannel was designed with a compression fit interfering by 0.005” (0.13mm).

PBS was delivered to the microchannel through microfluidic PEEK™ tubing (tubing inlet: ID=0.030“,OD=1/16”; outlet: ID=0.040“,OD=1/16”) from a 50 ml syringe mounted on a Harvard Apparatus PHD 2000 Programmable Syringe Pump (Harvard Apparatus, Holliston, MA). Microchannel dimensions: square cross-section, height = 0.51 mm, width = 0.79 mm, length = 9.74 mm. Teflon tape was wrapped around the microfluidic fittings at the inlet and outlet of the fixture to keep the system from leaking. The protein patterned lithium niobate SAWS device formed the top wall of the channel, while a glass plate sealed over a hole machined through the polycarbonate microchannel walls formed the bottom transparent wall, through which both excitation and emission light could penetrate. PBS was passed continuously through the microchannel at a rate varying primarily from 30 – 50 μl/min. The continuous flow removed protein desorbed from the surface through waste tubing continuously as acoustic cleaning took place.

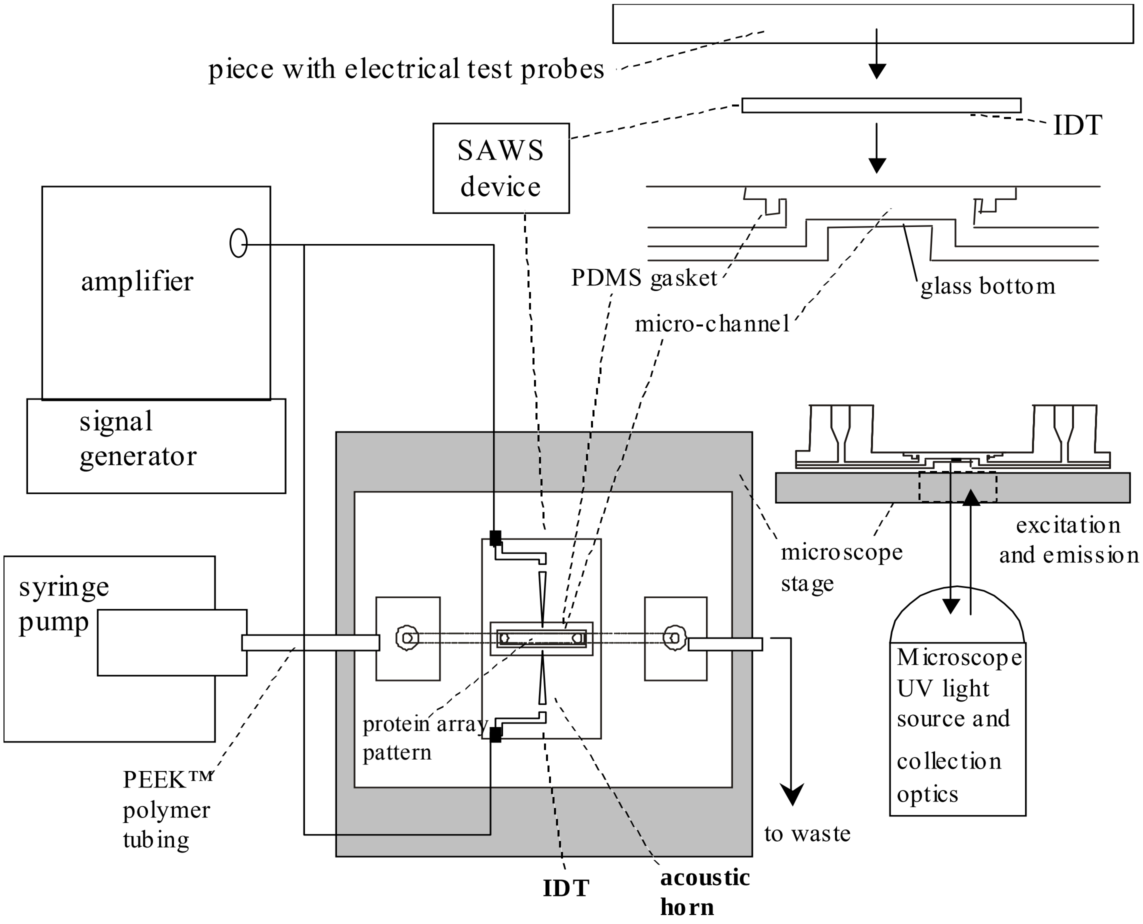
piece with electrical test probes
IDT
SAWS device
amplifier
PDMS gasket
glass bottom
micro-channel
signal generator
microscope stage
excitation and emission
syringe pump
Microscope UV light source and collection optics
protein array pattern
PEEK™ polymer tubing
to waste
IDT
acoustic horn

Scheme 5.4. Integrated Microfluidic-SAWS device setup.
After placing the PDMS gasket into the grove in the fabricated polycarbonate piece, the SAWS device is placed IDT-side down into the depression in the polycarbonate.

5.3.7 SAWS Device Design and Integration with Microfluidic Channel

Delay-line Rayleigh SAWS devices were fabricated from 128° YX $LiNbO_3$ wafers with an electrode pattern of 40 double split finger pairs per interdigital transducer [8]. IDTs were separated by approximately 120λ and operated at a center frequency near 97 MHz.

To localize acoustic excitation in the central region of the fixture, a bi-directional acoustic horn IDT was used as shown in Scheme 5.1. The acoustic horns were designed to compress the Rayleigh waves laterally by a factor of four. The tips of the acoustic horns came within several microns of the PDMS gasket at the center of the microchannel on each side of the channel, focusing the energy at the center of the delay path.

The SAWS device enclosed in the fixture was characterized on an Agilent E8358A PNA Series Network Analyzer (Agilent Technologies, Inc, Palo Alto, CA). The power delivered to the SAWS devices was determined by measuring S-parameters S21 and S11 for the network. The insertion loss ranged from -28.3 to -33.8 dB when the microchannel was dry. Upon entry of liquid into the microchannel, the insertion loss dropped to between -40 and -50 dB. Return loss (reflected power) ranged from -10 to -20 dB.

The SAWS fixture was mounted on a microscope stage, connected via microfluidic tubing to the syringe pump and connected via cables and a power splitter to a Hewlett Packard 8656B signal generator (Hewlett Packard, Shropshire, UK) and an EVI 420A, 20W RF amplifier (Scheme 5.4).

5.3.8 Imaging

Acoustic desorption experiments were conducted under dark conditions. Image data was collected with a Roper Scientific Cool Snap ES® CCD camera coupled to an Olympus® IX-70 inverted microscope at 200× magnification. Images of both covalently attached red-labeled mouse anti-rabbit IgG (antigen) and secondarily adsorbed green-labeled goat anti-mouse IgG (or green or blue-labeled BSA) were collected *in situ* at 15 min intervals, with SAWS power turned off, and fluid flowing using Semrock Brightline® TXRED-4040B (red) and FITC-3540B (green) filter sets, respectively.

Shutter exposure time was optimized for dynamic range at the start of each experiment for each filter individually, avoiding intensity saturation, and remained constant per filter for the duration of each experiment. The exact time of light exposure was recorded for every image collected, usually between 5 and 15 s, and this data was applied to the photobleaching correction as compounded time in the exponential photobleaching term.

Images appearing in the text have been adjusted in intensity as necessary for ease of viewing. However, quantitative data collection from these images was performed without any enhancement of intensity. The original images were very low in intensity due to the low quantity of fluorophores present in near-monolayers of labeled protein at device surfaces.

5.3.9 Image Data Processing

All image capture and processing was performed with MetaMorph® software version 6.3r2 by Universal Imaging Corporation. For each series of images collected for a given desorption experiment, location and size of selected regions in which fluorescent intensity was measured were kept constant with respect to the microarray pattern. Average, standard deviation, maximum and minimum intensity data were collected for each region. “Sensing” and “nonsensing” representative regions were selected based on uniformity of intensity. Intense specks of agglomerated protein were avoided.

5.3.9.1 Background and photobleaching corrections

To improve the accuracy of fluorescence quantification, background and photobleaching corrections were applied to the data. Dynamic background fluorescence was measured for each image at regions near the adsorbed protein where no protein was present. For each image, background intensity varied from region to region. As desorption of NSB progressed, in some cases background intensity exceeded final NSB intensity values. In those cases, an average of other background values was used as an estimate to ensure that all intensity values would be positive. Background subtraction primarily had the effect of shifting the curves along the intensity axis, but did not significantly alter the shape or slope of the desorption curves.

After background subtraction, a photobleaching correction was applied to the fluorescence intensity data. In the photobleaching experiments, fluorescently-labeled protein was exposed to UV excitation light and fluorescent intensity recorded at various time points as photobleaching occurred. Time constants τ, for photobleaching were determined by fitting an exponential curve to the data for each dye-conjugated protein: ($\tau = 454.5$ s for Alexa Fluor 488-labeled IgG, and 34.5 s for Alexa Fluor 594-labeled IgG. The latter time constant, however, was found to be unreliable.)

In the SAWS desorption experiments, exposure of fluorescently-labeled protein to UV excitation light for imaging time t was compounded over time and average region intensities were multiplied by the appropriate exponential term, $e^{t/\tau}$ to compensate for intensity loss due to photobleaching. Certain data did not require a photobleaching correction (where stated) when it was possible to sufficiently minimize exposure to excitation light during imaging such that no significant photobleaching took place.

5.3.9.2 Normalization of fluorescence intensity

Initial fluorescent intensity of regions varied with each trial. The variations in intensity might have been due to changes in the amount of light scattered by the SAWS device, PDMS gasket and polycarbonate frame each time they were assembled. Therefore, to capture the dynamic range of different trials on a single plot, for each trial, fluorescence intensity was normalized to the maximum intensity of all regions measured before starting acoustic desorption (Figure 5.1).

5.4 Results

5.4.1 Definitions for device characterization and evaluation of device efficacy

To characterize SAWS device function and evaluate its efficacy, certain definitions are helpful. Power dose (in mW*s) is chosen to describe energy input into the system in order to account for energy expended over time. The power dose necessary to remove a “sufficient” amount of NSB protein is defined as the minimum dosage at which no "off-pattern" (non-sensing) regions exhibit fluorescence intensity (within one standard deviation of their mean values) above the threshold intensity. A “sufficient” amount is that below the lowest specific binding intensity after SAWS operation. The threshold intensity for sufficient NSB protein removal is defined as the average intensity of both sensing and non-sensing regions at the power dose at which fluorescence intensity stops decreasing in all regions. It is assumed that at the point at which fluorescence intensity can decrease no further, no more protein can be removed from the surface. The use of averaging prevents the threshold from being affected by the crossing of any sensing and non-sensing region intensity values. In this study, such crossing of values did not occur. The fluorescence threshold and minimum power dosage are taken as characteristic values of the system for the given type of protein adsorption. The threshold intensity for removal of NSB protein is also used to threshold images.

5.4.2 Removal of non-specifically bound antibody from antigen-patterned surfaces

Figure 5.1 shows fluorescence intensity of microarray patterned regions normalized to maximum initial intensity of all selected regions versus SAWS device power dose in mW*s applied to the surface in acoustic desorption of protein. Prior to operation of the SAWS device, we first observe that initial fluorescence intensity at sensing regions is higher than that at non-sensing regions (Figure 5.1**a**). A fluorescent image of the microarray surface before protein removal is shown in Figure 5.2 and a thresholded image in Figure 5.3. The initial desorption rates are similar for all regions measured (~ 5% decrease / 100 mW*s). We then see that as power dose increases, fluorescence intensity of all regions (sensing and non-sensing, on-pattern and off-pattern respectively) decreases until intensity levels of all regions reach a minimum (Figure 5.1**b**), thresholded image in Figure 5.4). The intensity threshold, based on fluorescence intensity values at final power dosage, occurs at about 17% of maximum fluorescence. (For thresholding images, this normalized value is converted back to an absolute intensity per image and photobleaching and background corrections reversed.) The power dosage for "sufficient" NSB removal (the dosage at which intensity just dips below the threshold) occurs at ~1080 mW*s (Figure 5.1**c**, thresholded image in Figure 5.5). Average final intensity of sensing regions was about 22% of initial maximum intensity, about 3× the average final intensity of non-sensensing regions, near 7% initial maximum intensity.

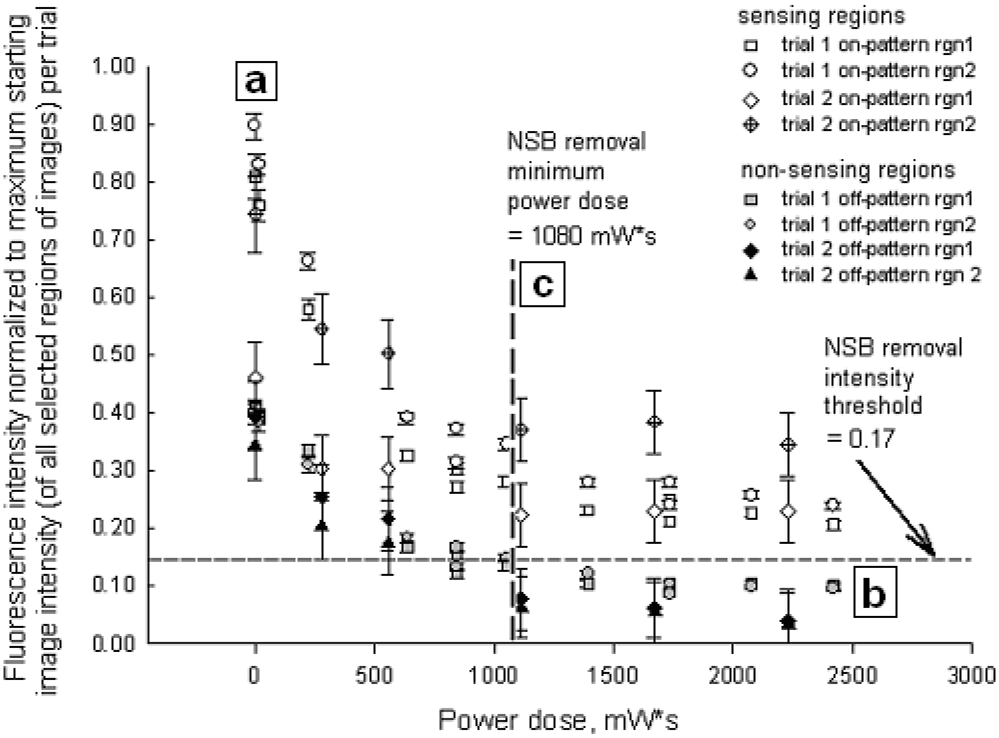

Figure 5.1. Fluorescence intensity of Alexa Fluor 488-labeled antibody (normalized to maximum initial intensity of all regions per trial) vs acoustic cleaning power dose (mW*s). Power dose and antibody intensity on sensing regions (light symbols) and non-sensing regions (dark symbols) at initial value (**a**), final value (**b**), and minimum power dose to remove "sufficient" NSB protein = 1080 mW*s (**c**). Acoustic desorption trials, n=2 and regions/trial (sensing and non-sensing), n=2 each type. Background and photobleaching corrections have been applied to the data prior to normalization.

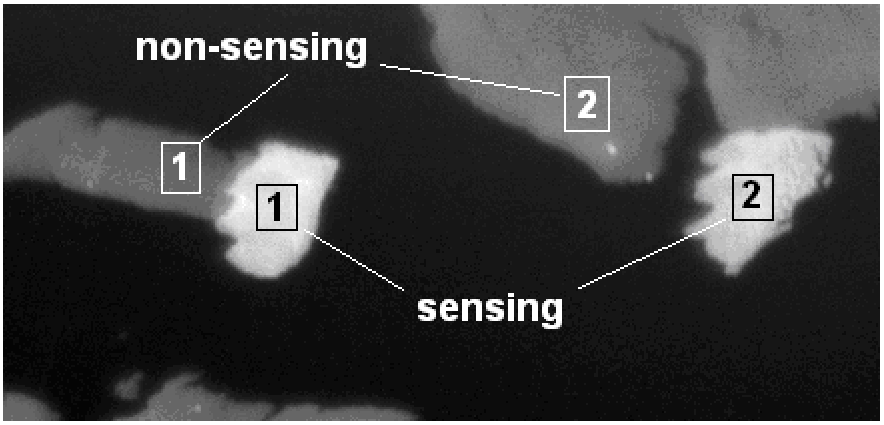

Figure 5.2. Representative fluorescence intensity image of labeled-antibody adsorption. Alexa Fluor 488-labeled antibody adsorbed to sensing (antigen-patterned) regions (1 and 2) and non-sensing (non-patterned) regions (1 and 2), corresponding to Figure 5.1**a** (prior to power dosing by SAWS device). Intensity adjusted for ease of viewing.

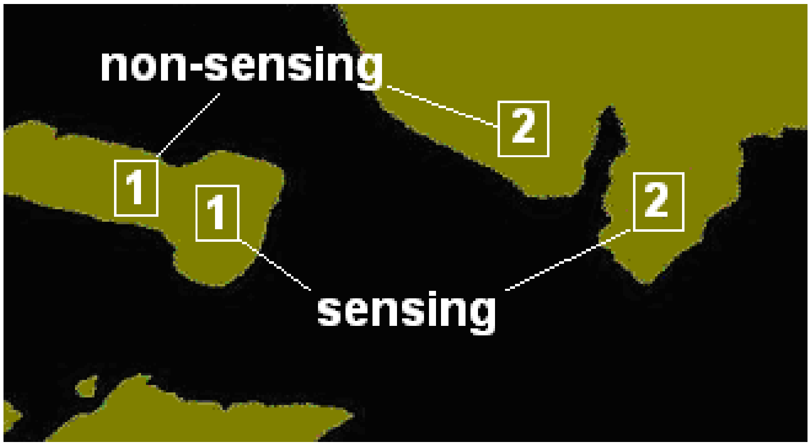
non-sensing
1
1
2
2
sensing

Figure 5.3. Representative thresholded image of fluorescent intensity of antibody adsorbed to antigen array prior to acoustic desorption, corresponding to Figure 5.1**a**.

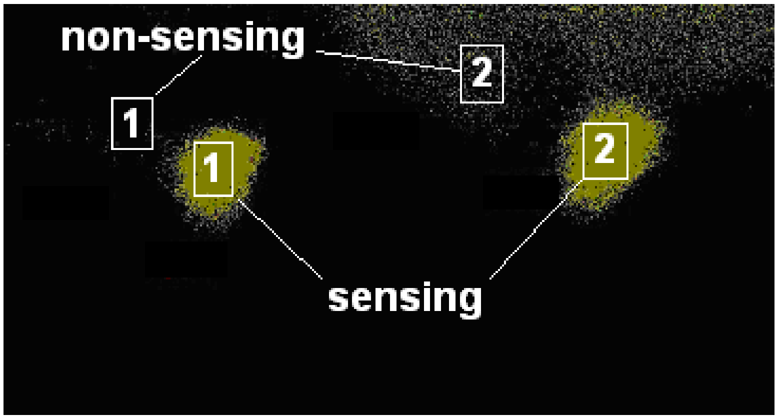
non-sensing
1
1
2
2
sensing

Figure 5.4. Representative thresholded image of fluorescent intensity of antibody adsorbed to antigen array at final acoustic desorption power dose, corresponding to Figure 5.1**b**.

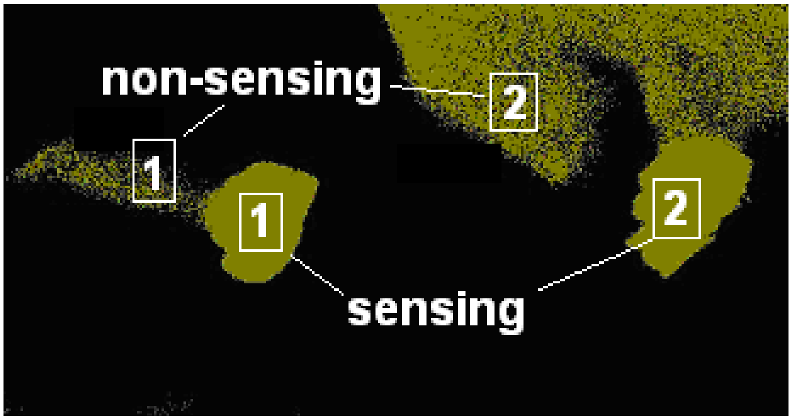
non-sensing
1
1
2
2
sensing

Figure 5.5. Representative thresholded image of fluorescent intensity of antibody adsorbed to antigen array corresponding to Figure 5.1**c**.
at minimum acoustic desorption power dose necessary for “sufficient” NSB protein removal.

5.4.3 Control Experiment: Removal of general protein fouling from the microarray surface

To assess the binding and removal of protein with no specificity to the microarray surface (as compared with specifically bound protein), Alexa Fluor 350 (blue)-labeled BSA was adsorbed to the antigen array surface. Figure 5.6 shows normalized fluorescence intensity versus SAWS device power dose applied to the microarray surface. There was a slight, but not significant, initial intensity difference between BSA adsorbed to sensing versus non-sensing regions. We observe that as power dose increases, fluorescence intensity of BSA on all regions does not decrease significantly in intensity. Since no significant intensity decrease occurred, no photobleaching correction was applied to the data. Background regions with no protein present were difficult to distinguish from regions with protein present and hence no background correction is applied.

To test the possibility that blue-labeled BSA binds covalently to the background (non-sensing) regions, unlabeled BSA blocker was increased from 1 mg/ml in the first experiment to 10 mg/ml in a second experiment (data not shown). There was no significant changes in this experiment, hence, covalent attachment is unlikely the reason for failure to remove the blue-labeled BSA from the surface.

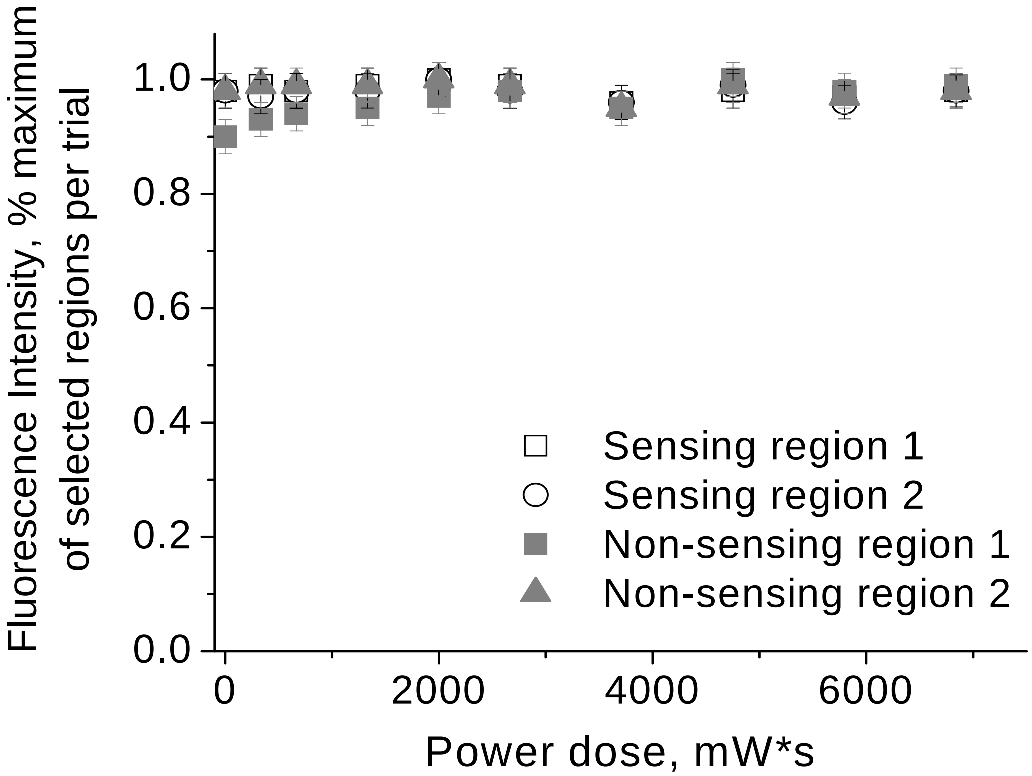

Figure 5.6. Fluorescence intensity of nonspecifically bound protein (Alexa 350 labeled BSA). In contrast with non-specifically bound antibody, fluorescence does not decrease with acoustic power dose delivered to surface. Due to minimization of photobleaching and difficulty distinguishing background, no photobleaching or background corrections were applied to the data.

5.4.4 Control Experiment: Acoustic cleaning on covalently bound protein

As a control experiment, the SAWS device was run with antigen (mouse IgG) covalently bound to the surface only (the microarray without target protein present), to demonstrate that covalently bound protein is not removed by SAWS. Fluorescent intensities of nonsensing regions contained no fluorescently labeled protein. These regions were thus used as background fluorescence and subtracted from sensing region intensity values to get net fluorescence intensity for the covalently bound protein. Fluorescence intensity in sensing regions remains constant with increasing power dosage (Figure 5.7).

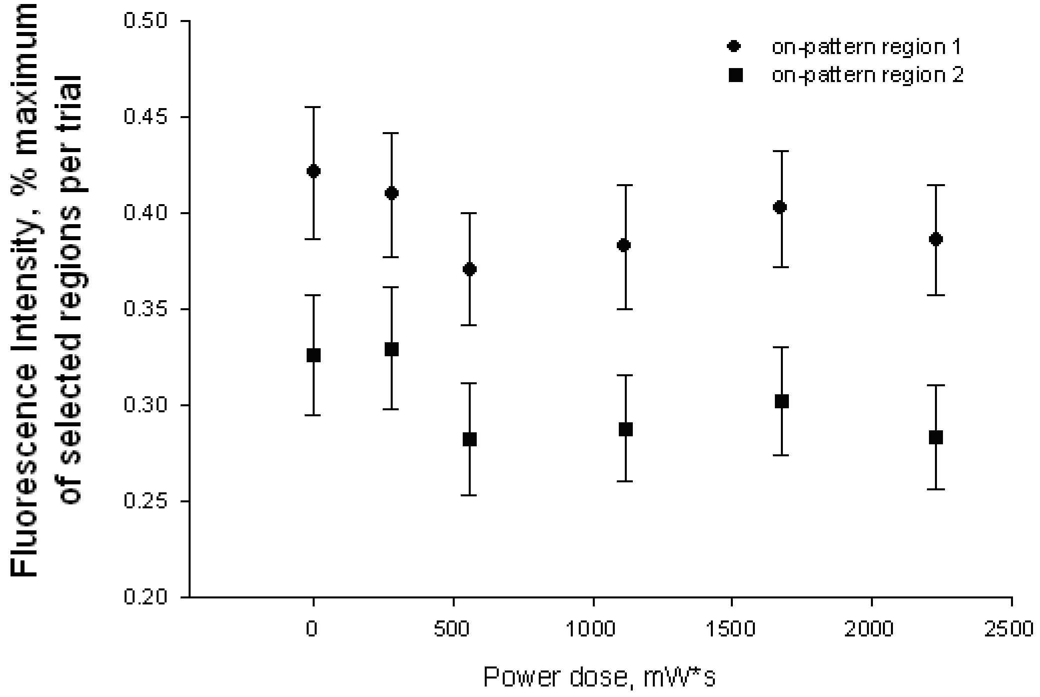

Figure 5.7. Fluorescence intensity of covalently attached antigen (Alexa Fluor 594-labeled mouse IgG) vs SAWS device power dose (mW*s). Fluorescence intensity does not decrease with acoustic power dose delivered to surface. Due to minimization of photobleaching, photobleaching correction was not applied.

5.5 Discussion

5.5.1 Removal of non-specifically bound antibody from antigen-patterned surfaces

That initial fluorescence intensity at sensing regions is higher than that at non-sensing regions is likely because less protein is removed from sensing regions after the rinse step, prior to measurement under the microscope. This observation is in accordance with the fact that specific binding (at sensing regions) is substantially stronger than non-specific binding (at non-sensing regions).

The relatively uniform and steep decrease in fluorescence intensity across sensing and non-sensing regions alike is likely due to removal of multilayers of protein from the surface at all regions. Equal removal rates from both region types are in accordance with multilayer removal, since the adsorbed protein desorbs from non-specific attachment to self-similar protein in both regions.

The final intensity values of the non-sensing regions after background and photobleaching corrections (performed on data of Figure 5.1) likely reflect the amount of NSB protein that remains adhered to the surface that could not be removed by SAWS. The remaining intensity in the sensing regions should be mostly due to antibodies specifically bound to antigen at the surface and possibly some NSB protein that could not be removed as well. Clearly more fluorescence remains in the sensing regions than non-sensing regions and the intensity difference between these regions is mostly likely attributed to the specific binding of antibodies to sensing region squares of the antigen array. It is notable that all four final non-sensing region intensities measured are found to be below the threshold value and all four sensing region final values, above the threshold. Hence, there is strong segregation between behavior of protein removal on sensing versus non-sensing regions.

A concern in quantifying protein removal by SAWS with *in situ* image collection is the extent to which photobleaching affects the accuracy of NSB protein removal, even after applying a correction factor. Photobleaching is expected to occur equally at both sensing and non-sensing regions, since both regions are equally exposed to excitation light intensity during image collection (e.g., Figure 5.2). Hence, the observed difference in fluorescence intensity between these regions is independent of photobleaching and of the accuracy of the photobleaching correction, applied to all data.

5.5.2 Control Experiment: Removal of general protein fouling from the microarray surface

Upon adsorption of blue-labeled BSA to the antigen array, we observe little difference between initial fluorescence of BSA in sensing and non-sensing regions in accordance with the lack of specificity of BSA to either the antigen squares or the non-sensing region. A slight difference in fluorescence between these regions might be attributed to a difference in surface environments, since mostly IgG exists on sensing regions while BSA is present on non-sensing regions prior to adsorption of blue-labeled BSA. After operation of the SAWS device and little change in BSA fluorescence, it seems that the secondarily adsorbed BSA is much more difficult to remove from the antigen array surface than antibodies. Some possible reasons for this tight binding may include denaturation or coagulation of the protein at the surface. However, it is less likely that the secondarily adsorbed BSA is interacting primarily with the background BSA, since it that case, it would be removed from the antigen squares, which likely contain far more IgG than BSA. Another possibility is that the secondarily adsorbed BSA is hardly present at the surface at all, since its initial fluorescence intensity at the surface is about one third that of labeled IgG initial intensities. In that case, most of the secondarily adsorbed BSA may have been removed by rinsing prior to acoustic desorption, leaving only a small amount of remaining BSA strongly bound to the surface.

Furthermore, it is possible that at such small intensity values, background fluorescence dominates and is difficult to separate from labeled-protein fluorescence.

5.5.3 Ceiling on protein removal for this setup

It has been suggested previously [8] that specifically bound protein can be removed at power dosages higher than those necessary to remove NSB protein. Therefore, selective removal of specifically bound protein for regeneration of microarray surfaces may be possible by modulation of power dosage applied to the surface. In this study however, the range of power that could be applied to the SAW device surface was constrained by the microfluidic fixture setup. Sufficient pressure was necessary to prevent leakage of liquid through the polycarbonate fixture/PDMS gasket/Lithium Niobate wafer sandwich that could otherwise short circuit the IDT. However, increased contact area of the gasket with the surface over devices used in *ex situ* experiments increased device insertion loss, decreasing the ability of the device to transmit power to the microarray surface. Furthermore, the input power to the SAWS chip had a ceiling of 320 mW (-12.7dBm), above which the device cracked. This may in part be due to concentration of the power density by the acoustic horn. At insertion loss values at pressures necessary to prevent leakage (~-30dB, a 1000 fold reduction in signal amplitude) a maximum of ~1.3 mW was available for acoustic desorption. Such small values were observed to be below the power threshold (related to the activation energy of desorption) necessary to remove specifically bound protein, regardless of dosing time.

5.6 Conclusions

This study demonstrated that *in situ* acoustic desorption and image data collection of protein microarrays are feasible in an enclosed SAWS device-integrated microfluidic system. The ability to combine these aspects is important for portability and high throughput in the development of next generation microarray systems.

It was further demonstrated that acoustic desorption can be quantified in terms of fluorescence intensity decrease with power dose and that characteristic values of the system can be identified for protein desorption. Such characteristic values could potentially be a means of estimating power dosage requirements of specific systems. For antibody desorption from sensing and non-sensing regions of antigen microarrays, we achieved good separation between final intensity values between region types. The characteristic values are of further use in thresholding fluorescent images to highlight critical desorption levels.

While success was achieved with antibody desorption, interestingly, we found that BSA was not possible to remove at the SAWS power levels available. Due to necessity of a tight seal to prevent leaks between the microchannel and the SAWS device in the present microfluidic setup, the amount of power capable of being transmitted to the microarray surface was decreased compared with *ex situ* SAWS device operation.

5.7 References

1. Glokler, J. and P. Angenendt, *Protein and antibody microarray technology.* Journal of Chromatography B, 2003. **797**: p. 229-240.
2. Mitchell, P., *A perspectie on protein microarrays.* Nature Biotechnology, 2002. **20**: p. 225-229.
3. Kambhampati, D., ed. *Protein Microarray Technology*. 2004, Wiley-VCH Verlag GmbH & Co. KGaA: Weinheim.
4. Kusnezow, W., A. Jacob, A. Walijew, F. Diehl, and J.D. Hoheisel, *Antibody microarrays: An evaluation of production parameters.* Proteomics, 2003. **3**: p. 254-264.
5. Haab, B.B., M.J. Dunham, and P.O. Brown, *Protein microarrays for highly parallel detection and quantitation of specific proteins and antibodies in complex solutions.* Genome Biology, 2001. **2**(2): p. research0004.1–0004.13.
6. Chen, Z. and A. Sadana, *An analysis of antigen-antibody binding kinetics for biosensor applications utilized as a model system: influence of non-specific binding.* Biophysical Chemistry, 1996. **57**(2-3): p. 177-187.
7. Meyer, G.D., J.M. Moran-Mirabal, D.W. Branch, and H.G. Craighead, *Nonspecific binding removal from protein microarrays using thickness shear mode resonators.* Sensors Journal, IEEE, 2006. **6**(2): p. 254- 261.
8. Cular, S., D.W. Branch, V.R. Bhethanabotla, G.D. Meyer, and H.G. Craighead, *Removal of Nonspecifically Bound Proteins on Microarrays Using Surface Acoustic Waves.* Sensors Journal, IEEE, 2005. **8**(3): p. 314-320.
9. MacBeath, G., A.N. Koehler, and S.L. Schreiber, *Printing Small Molecules as Microarrays and Detecting Protein−Ligand Interactions en Masse.* Journal of the American Chemical Society, 1999. **121**: p. 7967-7968.
10. Bourdon, C.J., D.W. Branch, G.D. Meyer, and H.G. Craighead, *Active mixing in microchannels using surface acoustic wave streaming on 128 YX LiNbO.* Proposed for publication in Journal of Microelectro Mechanical Systems, 2005.

CHAPTER 6: INFRARED SPECTROSCOPIC CHARACTERIZATION OF GENIPIN-INDUCED CHANGES IN COLLAGEN GELS

This chapter is adapted from part of:
Genipin-induced changes in collagen gels: Correlation of mechanical properties to fluorescence, Harini G. Sundararaghavan, Gary Monteiro, Norman A. Lapin, Yves J. Chabal, Jennifer R. Miksan, and David I. Shreiber, J. Biomed. Mater. Res. A, 87A(2): 308-320, 2008.

6.1 Abstract

Fourier transform infrared spectroscopy (FTIR) was used to characterize and monitor the crosslinking reaction between collagen and the crosslinker, genipin in real-time *in situ* and over extended time *ex situ*. Infrared bands in the spectrum of collagen gel exposed to genipin appear at 1104 and 1370 cm^{-1} and are assigned to the C–N stretch of the tertiary nitrogen of genipin-crosslinked collagen. The band at 1370 cm^{-1} is much smaller than other bands in the spectrum, likely due to the sparseness of crosslinks compared with genipin molecule, much of which is likely uncrosslinked, diffused in the collagen gel. An understanding of such crosslinking reactions at the molecular level can aid in the development of tissue replacements that rely on the tuning of mechanical properties for optimization of performance.

6.2 Introduction

Controlled crosslinking of collagen gels plays an important role in tissue engineering as well as cell and tissue mechanics. In order to design artificial replacement tissues, it is desirable to control the mechanical properties of biomaterials.

Collagen is found extensively throughout the body and is widely used as a biomaterial scaffold. Controlling the extent of collagen crosslinking is a useful way to control the properties of collagen gels. Collagen can be made denser by increasing the concentration of collagen monomers in solution prior to self-assembly, but investigated more often is crosslinking by addition of a chemical.

Lysyl oxidase [1, 2] and transglutaminase [3, 4] are enzymes that naturally crosslink tissues *in vivo*, but their use on a large scale is expensive. Treatment of gels with aldehydes is often performed, but these chemicals are cytotoxic. Ribose can also be used to crosslink collagen, but this method takes a long time unless toxic concentrations are used. Ultraviolet light has been used to crosslink gels as well, but can degrade cellular DNA. An alternative is genipin, an extract of the fruit of *Gardenia Jasminoides*, which crosslinks cellular and acellular tissues [5] and is non-toxic to cells at low concentrations [6].

Genipin crosslinks gelatin through nucleophilic attack of the C3 atom of genipin by primary amines of lysine and arginine residues [7]. In this reaction, a tertiary nitrogen atom is embedded in the six-membered ring of the genipin molecule in place of an oxygen atom. A similar reaction with the lysine and arginine residues present in collagen is expected.

Upon crosslinking with collagen, genipin-crosslinked collagen turns blue [8]. The crosslinks also emit fluorescence at 630 nm when excited at 590 nm [9]. The fluorescence emitted is proportional to the degree of crosslinking.

In this work, we examine the effects of exposure to genipin on acellular collagen gels. In particular, we examine the molecular changes that occur to collagen during genipin crosslinking using FTIR *ex situ* for long-term exposure to genipin and *in situ* in real-time, during short time initial exposure of the collagen gel to genipin. Collagen is monitored with FTIR using attenuated total reflection geometry (ATR), as infrared (IR) light is almost entirely absorbed in transmission geometry. In ATR geometry, the collagen gel trapped on one side of a beveled-edged silicon wafer is probed by an evanescent wave formed within two μm of the surface outside the wafer by IR light that reflects completely within the wafer. Subtraction of the spectra of liquid water additionally aid in elucidating the IR spectrum of genipin-crosslinked collagen.

Through this study, we have gained an understanding of the evolution of IR spectra of genipin-mediated collagen crosslinking with time, which in turn provides an understanding of the effects of genipin crosslinking of collagen at the molecular level. Such an understanding can be useful in assisting in the design of bioartificial tissues for a wide range of tissue systems.

6.3 Materials and Methods

The reaction between genipin and collagen was monitored in situ using FTIR for up to 4.5 h in an attenuated total reflection (ATR) geometry (Figure 6.1). A type I collagen solution was pipetted onto a silicon plate (~1 cm × 1.5 cm) with the longer side beveled at a 45° angle for entry and exit of the IR beam. The plate was sandwiched between two pieces of Teflon® with the top piece hollowed out to contain the collagen. The ATR setup was maintained at 37 ^oC in a nitrogen-purged Magna-IR 760 FTIR Spectrometer (Thermo Electron Corporation, Waltham, MA) to facilitate self-assembly of the collagen. After self-assembly, a solution of 10 mM genipin was deposited on top of the collagen and allowed to diffuse into the gel to the silicon–collagen interface. Only the highest concentration of genipin was studied with FTIR to see the most exaggerated response to crosslinking. The infrared beam entered the silicon wafer and was reflected internally (~8 × in the top face) creating an evanescent wave that probed a depth of ~2 μm above the surface of the silicon wafer into the collagen gel. Spectra for collagen crosslinked with 10 mM genipin for 12 h (with genipin solution equilibrated throughout the gel as described earlier), and then rinsed extensively with PBS to remove all free genipin, which represents the most extreme condition characterized rheometrically and fluorimetrically, and the spectra for a pure 10 mM genipin solution were similarly acquired. Spectra from untreated type I collagen gels served as the reference for the crosslinked collagen, while the spectrum from water was used as the reference for the genipin solution.

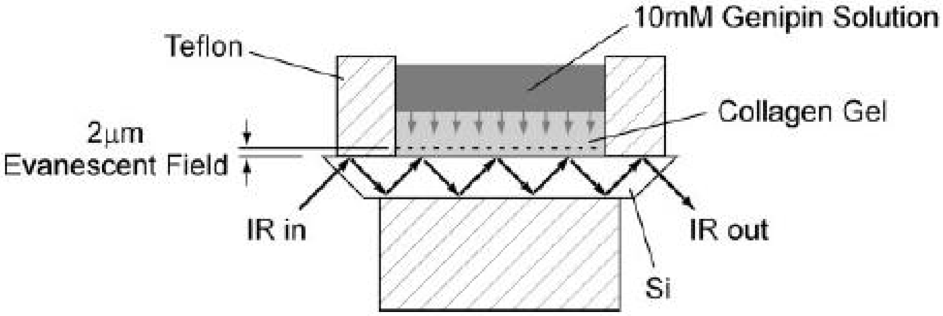

Figure 6.1. ATR setup showing genipin deposition for time-resolved study.

Genipin solution (10 mM) is deposited on top of and diffuses through the collagen gel. A 2 μm region of the collagen gel is probed by the IR evanescent field during genipin-mediated crosslinking. The genipin solution (10 mM) and collagen crosslinked with genipin for 12 h are probed in a similar way.

6.4 Results

The FTIR spectra of 10 mM genipin, ‘‘fully’’ genipin-crosslinked collagen (exposure to 10 mM genipin for 12 h and extensively rinsed of free genipin), and collagen during *in situ* crosslinking with 10 mM genipin are presented together in Figure 6.2. The spectrum of the genipin solution is dominated by three modes at 990, 1080, and 1635 cm^{-1}, assigned to the ring C–H out-of-plane bend [10], ring C–H in-plane bend [10], and C=C double bond ring stretch modes [10, 11] of the core of the genipin molecule, respectively. The absorption at 1080 cm^{-1} may also include the C–O stretch mode of the primary alcohol on the genipin molecule [10, 11]. Additionally, the C–O–C asymmetric stretch and the CH_3 bend of the methyl ester are observed at 1300 and 1443 cm^{-1}, respectively. The 12 h crosslinked collagen spectrum features these modes, as well as bands at 1104 and 1370 cm^{-1} that are believed to be vibrational modes related to the formation of new bonds between genipin and the primary amines of lysine, hydroxylysine, or arginine residues in collagen. The band at 1370 cm^{-1} is assigned to the C–N (ring) stretch of the tertiary aromatic amine [10, 12] of the crosslinked genipin nitrogen iridoid [13] that is bound covalently to the collagen. The broad, flat appearance of the crosslinking band at 1370 cm^{-1} in the 12 h spectrum is likely due to the flanking of two genipin molecule modes at 1360 and 1395 cm^{-1} (unassigned). The band at 1104 cm^{-1} is assigned to the C–N stretch of the tertiary nitrogen with the adjacent aliphatic carbon atom present in lysine or arginine residues [10, 14]. An absorption near 1104 cm^{-1} is also present in the unreacted genipin molecule as a shoulder to the absorption at 1080 cm^{-1}. It is assigned to the vibrations of both the cyclic ether and secondary alcohol on the six-membered ring of the genipin molecule. When genipin reacts with collagen, both of these moieties are removed. Furthermore, the band at 1104 cm^{-1} in the 12 h crosslinked spectrum is significantly stronger than the corresponding band in the spectrum of pure genipin (relative to the band at 1080 cm^{-1}), suggesting that this absorption band is mostly associated with modes formed as a result of crosslinking.

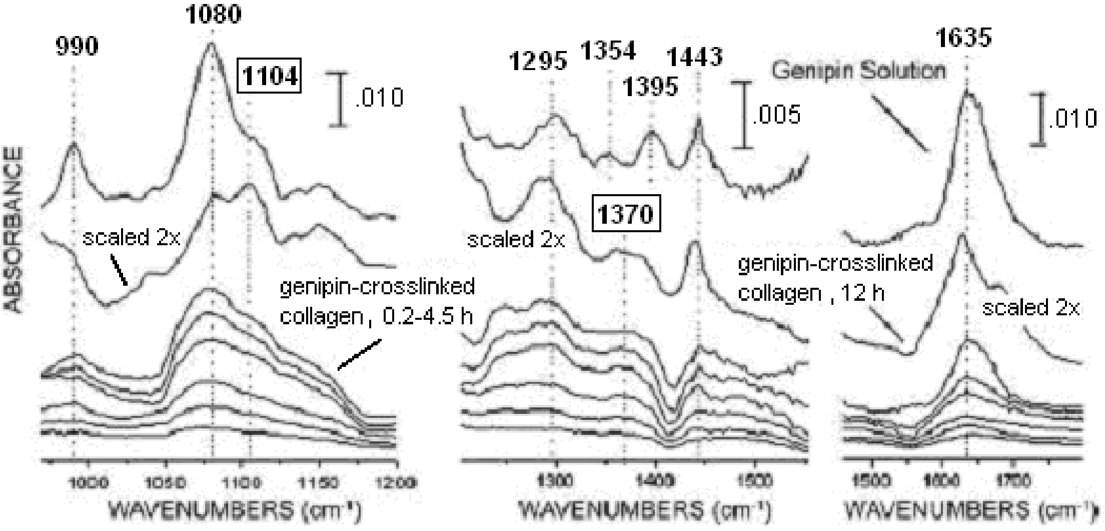

Figure 6.2. IR absorbance spectra of genipin and genipin-crosslinked collagen.
IR absorbance spectra of 10 mM genipin referenced to a spectrum of pure water (top); collagen after 12 h of crosslinking with 10 mM genipin and extensive rinsing, referenced to a spectrum of uncrosslinked collagen (second from top, scaled 2×) and collagen crosslinked with 10 mM genipin *in situ*, 0.2, 0.4, 0.8, 1.7, 3.1, and 4.5 h after adding genipin, referenced to the initially genipin-free collagen gel (bottom). Several spectral features that are present in the genipin solution alone, and/or the crosslinked and rinsed collagen are seen to evolve during the *in situ* crosslinking.

To better identify the origin of features present in the spectrum of 12 h crosslinked collagen, the changes in the collagen spectrum were monitored *in situ* during the first 4.5 h of crosslinking (Figure 6.2, bottom spectra). In this time-resolved experiment, spectral features were expected to increase due to: (1) diffusion of genipin into the region probed by the IR beam (the bottom surface of the collagen gel); and (2) crosslinking of collagen, leading to the appearance of new vibrational modes due to bonds formed during crosslinking. The *in situ* time-resolved spectra show the growth of several bands that are present in both crosslinked collagen and genipin, such as modes at 990, 1080, 1443, and 1633 cm^{-1}. In addition, the beginning of the growth of a band centered near 1370 cm^{-1} is observed. This feature is only seen in crosslinked collagen.

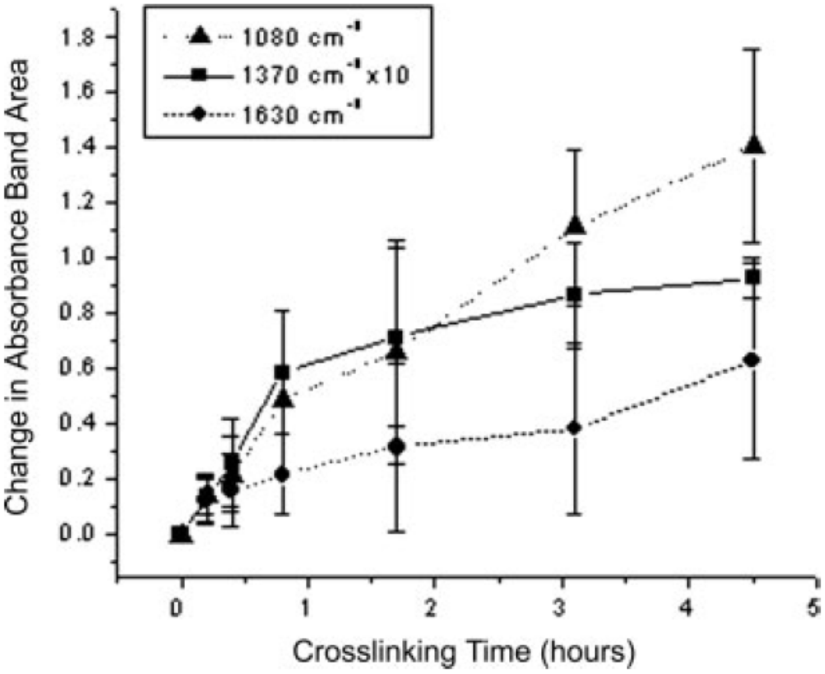

Figure 6.3. Changes in absorbance band areas versus crosslinking time for some of the highlighted bands in Figure 6.2: two genipin bands (triangle, 1080 cm^{-1} and circle, 1630 cm^{-1}), and a new genipin-to-collagen crosslinking feature (square, 1370 cm^{-1}). To allow all spectra to be viewed on a common plot, values of smaller band areas were scaled by a constant, as indicated in the inset. Crosslinking time began (at t = 0) when genipin reached the bottom of the collagen gel at the interface with silicon. Error bars combine two sources of errors: (1) baseline selection for area calculations, and (2) reproducibility of runs. End point area values of each band for different runs were normalized to a common value due to variation in absolute absorbance area possibly caused by variation in collagen density among samples.

Figure 6.3 summarizes the time dependence of several absorbance features. Because of the proximity of the various genipin molecule and crosslinking bands, calculated band areas may include components of smaller bands adjacent to the dominant spectral feature. The 1080 cm^{-1} band area (spanning 1040–1180 cm^{-1}) likely includes the growth of a number of other smaller bands possibly including the crosslinking feature at 1104 cm^{-1}, although it is too small to contribute substantially to band area. The feature at 1370 cm^{-1} is adjacent to genipin bands as stated earlier, and all are included in the area calculation (band complex spanning 1344–1414 cm^{-1}). To facilitate comparisons between trends in band growth, area absorbance values of the weaker band at 1370 cm^{-1} were scaled by a constant (indicated in the inset). Band area growth also differed in absolute value from run to run. Therefore, final *in situ* values (t = 4.5 h) of absorbance band areas amongst runs were normalized to a common value for each band, respectively. Similar increasing monotonic trends were observed for change in absorbance of genipin bands at 1080 and 1630 cm^{-1}; however, the growth of the crosslinking band at 1370 cm^{-1} appeared to slow down within several hours. Indeed, the small area of the crosslinking band at 1370 cm^{-1} and its apparent slowing in growth are likely due to the relatively small number of genipin-to-collagen crosslinks in the gel that can form compared with the amount of genipin that diffuses to the region. A description of the modes marked in the spectra of Figure 6.2 is shown in Figure 6.4.

6.5 Discussion

The colorimetric and fluorimetric properties of the crosslinked collagen are associated with molecular changes produced during crosslinking. In our study, the FTIR spectra include features at 1104 cm^{-1} (C–N stretch) and 1370 cm^{-1} (C–N stretch), that are neither characteristic of genipin nor collagen alone, and are, therefore, presumably associated with the crosslinked collagen and, perhaps, the color/fluorescence changes. The *in situ* FTIR demonstrated temporal changes in these features that paralleled the early changes in stiffness and fluorescence at 10 mM. However, due to limitations in the FTIR setup, the *in situ* spectroscopy could only be performed for ~4.5 h before evaporation began to introduce inconsistencies in the results, and a true correlation of stiffness-to-fluorescence-to-spectroscopy was not obtained. Interestingly, Touyama et al. examined the intermediate pigment changes that occur upon reaction of genipin with methylamine. Brownish-red intermediates were associated with 2-methyl-4-carbomethoxy-2-pyrindine derivatives, which had a spectroscopic feature at 1630 cm^{-1} [11, 15]. We also observed a peak at ~1630 cm^{-1} in the rinsed, crosslinked collagen, which is shifted slightly to the left of a corresponding peak at ~1635 cm-1 in the genipin solution. This shift may be artifactual due to water vibrational peak subtraction and/or due to double bonds, which contribute to the 1630/35 cm^{-1}, being slightly affected due to their proximity to the covalent bonding upon crosslinking and subsequently causing a small 5 cm^{-1} shift for the average of all double bonds.

6.6 Conclusions

In this study, the IR vibrational modes of genipin and genipin-crosslinked collagen have been identified *in situ* for short time initial exposure of the gel to genipin as well as *ex situ* for longer-term exposure to genipin. Spectra of *in situ* short time and *ex situ* longer-term exposures were similar in band position, but with some differences. Bands at 1104 and 1370 cm^{-1} are believed to be associated with crosslinking, as the band at 1370 cm^{-1} is neither present in the spectrum of collagen nor genipin alone, and the band at 1104 cm^{-1} is larger in proportion to other bands than when observed in genipin or collagen alone (suggesting that it may be a new band present in the same region as other bands for genipin or collagen). Specifically, these bands are both assigned to the C–N stretch of the tertiary nitrogen of the crosslinked six-membered ring of genipin and may perhaps be associated with the color and fluorescence changes in the collagen gel upon crosslinking with genipin.

While other bands in the spectrum of real-time genipin crosslinking of collagen increased monotonically with time, the band at 1370 cm^{-1} reached a plateau within four hours and was much smaller than other bands in the spectrum. The relatively small size and increase in the area of this band is likely due to the limited number of crosslinks formed compared with the much larger quantity of bonds due to genipin that diffused into the collagen gel.

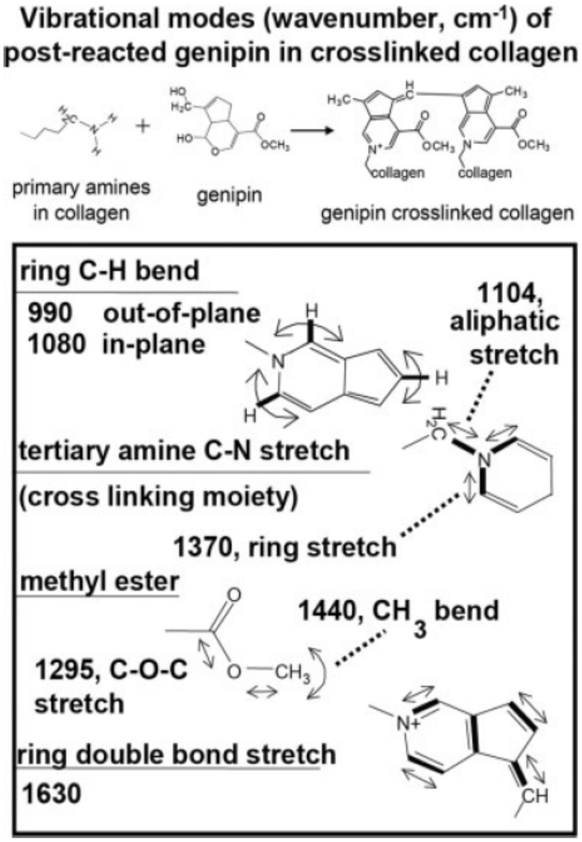
Vibrational modes (wavenumber, cm-1) of post-reacted genipin in crosslinked collagen
primary amines in collagen
genipin
genipin crosslinked collagen
collagen
collagen
OCH3
ring C-H bend
990 out-of-plane
1080 in-plane
1104, aliphatic stretch
tertiary amine C-N stretch
(cross linking moiety)
1370, ring stretch
methyl ester
1440, CH3 bend
1295, C-O-C stretch
ring double bond stretch
1630

Figure 6.4. Description of the modes marked in the spectra of Figure 6.2.

6.7 References

1. Casey, M.L. and P.C. MacDonald, *Lysyl oxidase (ras recision gene) expression in human amnion: Ontogeny and cellular localization.* J Clin Endocrinol Metab, 1997. **82**: p. 167–172.
2. Quaglino, D., C. Fornieri, L.B. Nanney, and J.M. Davidson, *Extracellular matrix modifications in rat tissues of different ages. Correlations between elastin and collagen type I mRNA expression and lysyl-oxidase activity.* Matrix, 1993. **13**: p. 481-490.
3. Piacentini, M., C. Rodolfo, M.G. Farrace, and F. Autuori, *''Tissue'' transglutaminase in animal development.* Int J Dev Biol, 2000. **44**: p. 655-662.
4. Nurminskaya, M.V., B. Recheis, J. Nimpf, C. Magee, and T.F. Linsenmayer, *Transglutaminase factor XIIIA in the cartilage of developing avian long bones.* Dev Dyn, 2002. **223**: p. 24-32.
5. Chang, Y., M.H. Lee, H.C. Liang, C.K. Hsu, and H.W. Sung, *Acellular bovine pericardia with distinct porous structures fixed with genipin as an extracellular matrix.* Tissue Eng, 2004. **10**: p. 881-892.
6. Sung, H.W., R.N. Huang, L.L. Huang, C.C. Tsai, and C.T. Chiu, *Feasibility study of a natural crosslinking reagent for biological tissue fixation.* J Biomed Mater Res, 1998. **42**: p. 560-567.
7. Mi, F.L., *Synthesis and characterization of a novel chitosan-gelatin bioconjugate with fluorescence emission.* . Biomacromolecules, 2005. **6**: p. 975-987.
8. Takami, M. and Y. Suzuki, *Hydrophobic blue pigment formation from phosphatidylgenipin.* J Nutr Sci Vitaminol (Tokyo), 1994. **40**: p. 505-509.
9. Almog, J., Y. Cohen, M. Azoury, and T.R. Hahn, *Genipin-A novel fingerprint reagent with colorimetric and fluorogenic activity.* J Forensic Sci, 2004. **49**: p. 255-257.
10. Socrates, G., ed. *Infrared Characteristic Group Frequencies—Tables and Charts.*, ed. Wiley. 1994: New York.
11. Touyama, R., Y. Takeda, K. Inoue, I. Kawamura, M. Yatsuzuka, T. Ikumoto, T. Shingu, T. Yokoi, and H. Inouye, *Studies on the blue pigments produced from genipin and methylamine. I. Structures of the brownish-red pigments, intermediates leading to the blue pigments.* Chem Pharm Bull 1994. **42**: p. 668–673.
12. Liu, Y.M., C. Jiaa, H. Do, and A. Eltoukhy, *Evaluation of amorphous carbon nitride thin film for magnetic rigid thin film disk by IR spectroscopy.* IEEE Trans Magn, 1997. **33**: p. 3106–3108.
13. Fujikawa, S., Y. Fukui, and K. Kunimasa, *A spontaneous reaction product between genipin and glycine.* Tetrahedron Letters, 1987. **28**: p. 4699-4700.
14. Butler, M.F., N. Y.F., and P.D.A. Pudney, *Mechanism and kinetics of the crosslinking reaction between biopolymers containing primary amine groups and genipin.* J Polym Sci Part A: Polym Chem, 2003. **41**: p. 3941–3953.
15. Touyama, R., K. Inoue, Y. Takeda, M. Yatsuzuka, T. Ikumoto, N. Moritome, T. Shingu, T. Yokoi, and H. Inouye, *Studies on the blue pigments produced from genipin and methylamine. II. On the formation mechanisms of brownish-red*

intermediates leading to the blue pigment formation. Chem Pharm Bull, 1994. **42**: p. 1571-1578.

CHAPTER 7: CONCLUSIONS

In this work, we have primarily employed infrared spectroscopy to characterize molecular layers and chemical bonding in various biosensor platforms and monitored surface features that change in response to varying environmental conditions. We have also explored the use of several additional methods and techniques for surface characterization including ellipsometry, fluorescence and infrared polarization techniques.

For the molecular layers of each platform, we have identified a number of characteristics of surface attachment using infrared spectroscopy. In Chapter 2, biotin covalent attachment to the APS surface has been characterized through disappearance of NHS moieties of the biotin derivative biotin-NHS from 1740–1820 cm^{-1}, and the formation of amide bonds apparent in amide I and II vibrational bandss at ~1650 and 1530 cm^{-1} respectively. In Chapter 4, maleimide chemical attachment to the APS surface has been characterized through disappearance of the isocyanate band at 2275 cm^{-1} and formation of urea bonds, identified from the appearance of urea amide I, II and III bands. Both sulfhydryl and amine chemical attachment to maleimide surfaces were identified through disappearance of the of the maleimide alkenyl C–H out of plane bending mode and a slight red-shift in the maleimide carbonyl asymmetric stretching mode. In the biotin-streptavidin system of surface attachment, biotin-streptavidin non-covalent attachment was associated with a dip near 1716 cm^{-1} putatively identified as a red-shift in the biotin ureido carbonyl stretching mode upon interaction of the biotinylated surface with streptavidin and/or aqueous solvent used in protein adsorption and the following rinse step.

In Chapter 6, a bulk rather than surface study, covalent attachment between the small crosslinking molecule, genipin and the primary amines of lysine and arginine residues of collagen was identified by the appearance of bands at 1104 and 1370 cm^{-1}. The band at 1370 cm^{-1} is not present in either collagen or genipin alone (and the band at 1104 cm^{-1} appeared larger in proportion to other bands than for genipin or collagen alone). Both bands are assigned to the C–N stretch of the tertiary nitrogen present in genipin-crosslinked collagen. The relatively small size and slow growth of the band at 1370 cm^{-1} in real-time studies of collagen crosslinking by genipin are in accordance with the probability that relatively few crosslinks are formed upon genipin diffusion into the collagen gel.

Polarization studies of MPS attachment to the maleimide-terminated surface suggested that molecular orientation of MPS was restricted upon covalent attachment to this surface. This study lent further evidence to the chemical attachment of this small molecule to the maleimide surface.

Infrared features of certain chemical and biomolecular layers were monitored throughout subsequent adsorption steps and found to respond to various environmental factors during these process steps. We found that the stability of APS films varies with pre-silanization atmospheric moisture and that subsequent features of biotin attachment are dependent on APS stability. Features of the biotin layer attached to the APS surface changed with solvent used in biotinylation. When water was used as a solvent, the frequency of the biotin ureido carbonyl stretching mode was red-shifted and the biotin ureido band at 1250 cm^{-1} was larger than when anhydrous DMF was the solvent. Since water is known to attack the silane surface to which the biotin is attached, these spectral changes may be indicative of disorder of the biotinylated film. The dip at 1716 cm^{-1} upon protein attachment to the biotinylated surface and/or rinsing seemed to be present more often and under different conditions when anhydrous DMF was used as a solvent in biotinylation instead of water.

Additional surface characterization was conducted using ellipsometry and fluorescence measurements. Combining ellipsometry with infrared absorption area measurements, a relative measure of APS and PMPI components in film polymerization and multilayer formation was assessed. As expected, we found that the content of APS increased with increasing film thickness at a greater rate than the content of PMPI in the film, due to the greater extent of APS polymerization compared with PMPI dimerization. At microarray surfaces where antibodies were specifically and non-specifically adsorbed to covalently bound antigen and background regions, fluorescence quantification of fluorophore-labeled antibodies was successful in indicating sufficient SAWS power dose to remove nonspecifically bound protein.

Clearly, through identification of surface characteristics by infrared spectroscopy, ellipsometry and fluorescence measurements, surface layers have been monitored and observed to respond to a variety of environmental conditions and adsorption steps. The ability to monitor the initial steps of biosensor surface formation may be useful in observing response of the system at the molecular level to tuning of processing conditions. With characteristics indicative of molecular level changes through iteration of process parameters, changes in biosensor surface layers may then be correlated with improvements in function and accuracy of bioassays and biosensors.

Curriculum Vita

NORMAN A. LAPIN

EDUCATION

05/2009	Ph.D. Biomedical Engineering The Graduate School – New Brunswick, Rutgers University New Brunswick, New Jersey
02/1998	B.S. Mechanical Engineering Department of Mechanical and Aerospace Engineering State University of New York at Buffalo Buffalo, New York

EXPERIENCE

Internship 2005	Sandia National Laboratories Microsensor Science and Technology Department Albuquerque, New Mexico
Product Engineer 1998 – 2001	Ford Motor Company / Visteon Corporation Allen Park, Michigan
Study Abroad 1996 – 1997	Beijing Polytechnic University Beijing, China

PUBLICATIONS

“Infrared Characterization of Biotinylated Silicon Oxide Surfaces, Surface Stability, and Specific Attachment of Streptavidin”, N. Lapin and Y. Chabal, *Journal of Physical Chemistry Part B*, Accepted, 2009.

“Attachment of Streptavidin-Biotin on 3-aminopropyltriethoxysilane (APTES) Modified Porous Silicon Surfaces”, S. Singh, N. Lapin, P. Singh, M. Khan and Y. Chabal, *International Conference on Transport and Optical Properties of Nanomaterials Conference Proceedings*, Accepted, 2009.

“Genipin-induced changes in collagen gels: Correlation of mechanical properties to fluorescence”, H. Sundaraghavan, G. Monteiro, N. Lapin, Y. Chabal, J. Miksan, and D. Shreiber, *Journal of Biomedical Materials Research Part A*, 87A(2): 308-320, 2008.